AN ABSTRACT OF THE THESIS OF

Barbara Zennaro for the degree of Master of Science in Marine Resource Management presented on February 17th, 2006
Title: Correlations of Sea Surface Height and Solid Earth Tides with Seismicity in the Equatorial Pacific Ocean: a GIS Approach

Abstract approved:

Redacted for Privacy

Robert Duncan

In the equatorial Pacific Ocean, earthquakes are used as an indicator of tectonic stress for normal faults in the Galapagos Spreading Center, transform faults along the East Pacific Rise and thrust faults in the Middle American subduction zone. Linkages between seafloor tectonic processes and oceanographic and lunar conditions were explored using time-series cross-correlation analyses on two different time scales.

Data for earthquakes in the eastern tropical Pacific study area are obtained using the hydrophone arrays of the NOAA-VENTS Program. Hydroacoustic monitoring (listening to underwater sounds) provides scientists with a detailed dataset that includes even small earthquakes, starting as low as magnitude 0.6, that are not perceived by land-based seismographs. Data for sea surface heights (SSH) consist of two different datasets. On a moon's quarter time scale, SSH data used to investigate the influence of the earth tide and changes in oceanic conditions were remotely acquired by the altimeter on board the TOPEX/Poseidon (T/P) satellite. SSH data used to investigate the influence of the ocean tides were obtained from the Tidal Model Driver (Padman and Erofeeva 2003), that predicts SSH for locations every hour. The Geographic Information System (GIS) was used for the visual display of the data and to compute basic descriptive statistics. A lab-book was created for the educational-outreach section of this work, explaining step by step how GIS has been used.

Significant results show correlations between normal faults and ocean tides and between the thrust fault and earth tides. Also, the Quebrada and the Discovery transform faults show high correlation of earthquake events, suggesting that at such temporal and spatial resolution, the plate moves as a rigid block.

Correlations of Sea Surface Height and Solid Earth Tides with Seismicity in the Equatorial Pacific Ocean: a GIS Approach

by
Barbara Zennaro

A THESIS

submitted to

Oregon State University

in partial fulfillment of
the requirements for the
degree of

Master of Science

Presented February 17, 2006
Commencement June 2006

Master of Science thesis of Barbara Zennaro presented on February 17, 2006

APPROVED:

Redacted for Privacy

Major Professor, representing Marine Resource Management

Redacted for Privacy

The Dean of College of Oceanic and Atmospheric Sciences

Redacted for Privacy

Dean of the Graduate School

I understand that my thesis will become part of the permanent collection of Oregon State University libraries. My signature below authorizes release of my thesis to any reader upon request.

Redacted for Privacy

Barbara Zennaro, Author

ACKNOWLEDGEMENTS

The acknowledgment is that only and unique page that is able to give a soul to all the work done in these three years. If I were Dante, these were my Virgilio and my Beatrice that helped me to find the right path once I was lost. I would like to thank my mom, to make me coming here and simply for being my mother. Irma Delson and Bob Duncan, to help and support me when I thought I could not make it. Bob Dziak, to welcome me in Newport and to support and understand me. Joe Cone for always being there to teach me anything I wanted to learn. Maria Jose and Tyson, for sharing with me adventures all over the world in the past 7 years. Biniam, for being my big brother! To Otto for always being there for me, gracias! To Corvallis, that for the second time in my life gave me something so big and important. Thanks to my fellows at the International Cultural Student Program, Paty, Samudra, Ai, Preeti and the geo grads for being so nice. Thank you to Ally and her family that always welcomed me in their houses. Thanks to Nick Piasas and Joe Haxel and again Otto Gygax for the support in running my data analysis. To so many people that I cannot mention them all! Also, I would like to thank all the awards and scholarships and Fellowships that helped me financially throughout these years: the International Cultural Scholarship Program, the Laurel Scholarship, the Warren W. Denner Memorial Graduate Student Fellowship Award, the Keith H. Wrostad Memorial Fellowship in Geophysics Award, the HMSC Housing Scholarship, the Markham Award and the Chipman-Downs Memorial Fund Award

And finally, Thanks to Paul, for being next to me all these years, and especially for taking me in American Samoa. With love.

TABLE OF CONTENTS

TABLE OF CONTENTS (Continued)

TABLE OF CONTENTS (Continued)

LIST OF FIGURES

LIST OF FIGURES (Continued)

LIST OF FIGURES (Continued)

LIST OF TABLES

1. INTRODUCTION

This research investigates the linkages between seafloor tectonic processes and oceanographic and lunar conditions by using two datasets that have recently become available. Previous researchers (Kasahara et al. 2001; Vidale et al. 1998; Wilcock 2001) have investigated the role that changes in sea surface height (SSH), such as those that occur during ocean tides, have in triggering earthquakes and hydrothermal activity. My research is aimed at expanding these findings to a longer temporal and larger spatial scale. The research examines the role and the impact that lunar phases and changes in sea surface height (SSH) due to moon tides and seasonal to annual changes in oceanographic conditions, have on crustal processes at three different kinds of plate boundaries located in the eastern tropical Pacific, over a period of six years. The research was conducted on two different time scales. The first time scale is based on the four cycles the moon undergoes every month and is meant to explore the influence that earth tides and changing oceanic conditions have on the marine crust. The second time scale looks at daily variation in SSH due to ocean tides and it is meant to explore the influence of hourly changes in SSH with marine earthquakes.

Data for earthquakes in the eastern tropical Pacific study area are obtained using the hydrophone arrays of the NOAA/Vents Program. Hydroacoustic monitoring (listening to underwater sounds) provides scientists with a detailed dataset that includes even small earthquakes, starting as low as magnitude 0.6, that are not perceived by land-based seismographs. Data for sea surface heights consist of two different datasets. SSH data used to investigate the influence of the earth tide and changes in oceanic conditions are remotely acquired by the altimeter on board the TOPEX/Poseidon (T/P) satellite which is able to detect changes in SSH due to El Niño and La Niña with a high level of accuracy every 10 days. SSH data used to investigate the influence of the tides are obtained from the Tidal Model Driver (TMD), a model created at Oregon State Univeristy by Padman and Erofeeva (2003) that predicts SSH for given locations every hour.

A geographic information system (GIS) was used for the visual display of the data and to compute basic descriptive statistics. A lab-book was created for the educational-outreach section of this work, explaining step by step how GIS has been used. The goal is to create a new document available on line at http://oregonstate.edu/~zennarob/indice where scientists and students may repeat the GIS procedures used in the research and improve their GIS skills. Most of the inferential statistics were acquired using routines written in Matlab.

1.1 BACKGROUND

Mankind has long been influenced by the cycles of the moon. In ancient time, sailors noticed its correlation with ocean tides. Today, scientists recognize its role in crustal deformation during earth tides. These two different kinds of tides affect the seafloor in different ways. Earth tides cause compression and dilatation of the ocean crust and are known to be a possible mechanism responsible for triggering marine earthquakes by deforming the crust (Stein 1999). Ocean tides are responsible for changes in SSH and therefore they alter the total pressure exerted by the water column on the seafloor: this variation may be too small to initiate earthquakes themselves, but they may trigger earthquake activity when imposed on slowly increasing tectonic stress (Glasby and Kasahara 2001).

Stress caused by the moon's gravitational pull can be up to an order of magnitude higher beneath the ocean than those found in the continents because of the effects of loading by ocean tides (Wilcock 2001). For this reason, earthquakes occur more frequently at low tide, when the extensional stresses are maximum in all directions, suggesting that the decrease in "confining pressure when some weight of the ocean is removed at low tide" would lead to a "reduction in normal stress, which causes faults already very close to their failure point to slip" (Tolstoy et al. 2002; Wilcock 2001).

Other studies have shown the existence of low-frequency pulses, called pressure pulses, which have a good correlation with semi-diurnal changes in tidal forces (Kasahara et al. 2001). Stein (1999) suggests that the alteration on shear and normal stresses caused by an earthquake on the surrounding fault causes large changes in seismicity rate.

Therefore, if changes in sea surface height such as the ones caused by tides are in part responsible for earthquake events, do changes in SSH experienced during climatic oscillations such as El Nino or La Nina have a similar effect? What is the influence of earth tides on seafloor volcanic-tectonic processes?

1.2 OCEAN TIDES

Correlations between earthquake recurrence and changes in SSH due to ocean tides have been documented previously. Tidal triggering appears significant for some active volcanoes and mid-ocean ridges (Tolstoy et al. 2002), and several studies report triggering of extensional and thrust earthquakes (Tanaka et al. 2002; Tsuruoka et al. 1995). Yet, strike-slip earthquakes, which are by far the most common, have shown little or no tidal influence (Tsuruoka et al. 1995; Vidale et al. 1998). While solid earth tides induce stresses only up to $5*10^3$ Pa (0.05 bars), water loading builds stresses up to nearly $5*10^4$ Pa (0.5 bars) in ocean basins (Cochran et al. 2004). Thrust and normal faults have relatively larger tidal stress amplitude than strike-slip faults due to a larger influence of the ocean loading component. Tidal stresses may be more influential in subduction zones since these are the areas with large tidal stresses and shallow events under lower confining pressures (Cochran et al. 2004). Tidal stress amplitude decays with depth (Cochran et al. 2004), therefore the expectation would be to find stronger correlation with SSH for shallower earthquakes. The most frequent tidal-triggered events have been on shallow, normal-type faulting along axial ridges, such as Juan de Fuca, perhaps associated with hydrothermal circulation. A study by Cochran et al. (2004) showed a

statistically significant increase in triggering of globally distributed large tectonic events (M>5.5) with increasing tidal stress amplitude.

Stein (2004) suggests that tiny changes may trigger small shocks on faults critically stressed for failure and that tidal triggering does occur beneath some active volcanoes and mid-ocean ridges. Stein also states that the tidal effect is much weaker than earthquake-induced stress change due to other main shocks, and therefore the stress changes due to tidal changes in sea surface height may not be big enough to raise the stress load above the triggering threshold. Tidal oscillation of stress on the crust may also be too brief to nucleate abundant earthquakes.

Kasahara and Sato (2000) and Kasahara (2002) also investigated the correlation between SSH and earthquake events. Their main results show a correlation between the number of earthquakes registered per hour in deep-sea hydrothermal activity and changes in sea level. This suggests that the volcanic swarms in the dataset used may also show a similar correlation, with earthquakes coinciding with low SSH. Those studies also showed the existence of low-frequency pulses having a good correlation with semi-diurnal and diurnal changes in relation to tidal forces (Kasahara and Sato 2000).

Tanaka et al. (2002) have found that earthquakes are triggered by the tides only when the tidal stress adds to or acts in the same direction as, the regional tectonic stress. Nearly all previous studies sought for an increased rate of earthquakes when the tidal stress is high or rising. In a sense, Tanaka et al. (2002) reframed the tidal triggering hypothesis in terms of the tidal stress azimuth rather than its phase.

Wilcock (2001) found that earthquakes occur more frequently near low tides, especially during the lowest spring tide, when the extensional forces are at maximum in all directions. In his research, the highest earthquake frequencies are observed when the tensional stress perpendicular to the ridge axis is near a maximum and when the shear stress driving normal faulting on ridge-parallel faults dipping at 45° is near a minimum.

Vidale et al. (1998) hypothesize that because the rate of stress change caused by earth tides exceeds that from tectonic stress accumulation, tidal triggering of earthquakes could

be expected in the final hours of loading of the fault were at the tectonic rate of rupture. It is also critical that the final loading begins soon after the achievement of a critical stress level.

1.3 EARTH TIDES

Gravitational interactions between the Earth, the Sun, and the Moon are responsible for ocean and earth tides, the latter being the deformation of the crust with oscillatory stresses (Vidale et al. 1998). Earth tides consist of viscous-elastic deformation of the earth surface (Marechal et al. 2002), creating slight bulges on the side facing the Moon and the Sun as the Earth rotates on its axis. Earth tides represent the largest contribution to temporal variations in crustal stress (Vidale et al. 1998) and even though they do not produce a strong motion (shaking), they do alter the stress on faults (Stein 1999). As it happens for ocean tides, when the Moon and the Sun are aligned, their gravitational forces combine and the tidal range is at its maximum. These happen during new and full moons and are called spring tides. Neap tides occur during the first and third-quarter phases of the Moon, when lunar and solar forces act in opposition and the tidal range is at its minimum. The tide goes through a full cycle (a spring and a neap tide) every 14.76 days.

The forces that produce tides are a small fraction of the forces that cause earthquakes, eruptions, and hydrothermal activity (Marechal et al. 2002), but even though the forces are small, they can trigger an event. Shallow (0-40 km in depth) earthquakes are most affected by changes in gravitational pull since they are under lower confining pressure and therefore tidal stress may be proportionately more influential. In subduction zones, ocean loading tends to be largest and low-angle thrust events are most common. Cochran et al. (2004) showed a correlation between the occurrence of shallow, thrust earthquakes and the occurrence of the strongest tides. In strike-slip faults, such as the San Andreas

and the Calaveras fault, Vidale et al (1998) found that there is no clear effect of the tidal stress change on the timing of earthquake rupture initiation.

1.4 EARTHQUAKES AND STRESS

Earthquakes result from a sudden movement of a part of the Earth's lithosphere, typically along faults at plate boundaries where the stress resulting from differential motion of plates exceeds the strength of the brittle rocks. During an earthquake, elastic strain energy accumulated over time is released and radiates seismic waves. Earth material responds to stress, or force/unit area (Yeats et al. 1997). Stress acts in three different dimensions, initiating three principal stresses with different orientation: a vertical stress, and two horizontal stresses, north-south, east-west, and, denoted as σ_1, σ_2 and σ_3 respectively (figure 1). These stresses influence the orientation of the faults: when the vertical stress is stronger than the two horizontal stresses, the fault will be a normal fault. When the horizontal stresses are stronger than the vertical stresses, then the faults will either be transform fault or a thrust fault.

Every time the SSH varies, the total pressure and therefore the total vertical stress (σ_1) exercised on the sea floor also varies. A rock buried in the crust is subjected to the confining pressure of the load of a column of rock and water on top of it, which is accompanied by equal stress acting upward on its base (Yeats et al. 1997). The changes in water column height, therefore, also cause changes in the confining pressure, which may affect the threshold at which an earthquake will happen for a particular zone. When the SSH is lower, the total confining pressure and the vertical stress on the sea floor is lower, while the vertical stress will be higher with higher SSH. Faults that will be affected the most by changes in SSH will be those faults that depend the most on vertical stress, such as thrust and normal faults (in this case study, the spreading centers and the subduction zone).

1.5 EARTHQUAKE RECURRENCE MODELS

The Coulomb fracture criterion predicts the shear stress necessary to cause failure under different confining pressures (Yeats et al. 1997). Based on this insight, there are four different kinds of earthquake recurrence models (figure 2) (Kellogg and Hunter 2000).

In a "perfectly periodic model", earthquakes always occur when the stress level reaches the threshold value that causes the stress to drop to the same low value after each earthquake. All of the earthquakes have the same slip and they are equally spaced in time. This is probably not accurate for the dataset used, since there are earthquakes of varying magnitudes happening at all times.

In a "slip predictable model", the stress always drops to the same level after an earthquake. Once an earthquake has occurred, we know that the slip during the next earthquake will be equal to the plate motion that has subsequently occurred. The longer the time since the last event, the larger the next event will be. It is not possible to apply this model to the dataset, since slip rate caused by earthquakes are unknown.

In a "creep model", the fault moves by a series of creep events and each year the total slip from creep is the same as the amount of relative plate motion. Unfortunately, there is no way to measure the creep in the studied faults, therefore this model cannot be used.

Finally, in a "time predictable model"earthquakes always happen when the stress level reaches a threshold value. The slip during each earthquake is variable, so the stress released after each earthquake is not always the same. Once the slip in one event has been measured, then it is known that the next event will occur when an equal amount of plate motion has occurred. In this model, both increases and decreases in seismicity rate are followed by a time-dependent recovery (Stein 1999).

In three of these models, the magnitude of the earthquakes will determine how much the stress level will be reduced, with smaller earthquakes releasing only a fraction of the accumulated stress. The time predictable model was selected as the best fit for the

hydroacoustic data. Thus sound waves contain information about the location, the timing and the magnitude of the earthquakes, giving an idea of how much stress was relieved.

1.6 THE HYPOTHESIS

It is proposed that changes in SSH may influence the position of the stress threshold line, which fluctuates up and down, following the natural short or long term oceanographic cycles. During periods of high sea surface height, the total pressure of the water column on the sea floor is higher, and the vertical stress σ_1 increases. This increase of vertical stress allows horizontal stresses to accumulate over a longer period of time. When the sea surface height decreases (with lower tides or changing oceanographic conditions), both the confining pressure and the vertical stress σ_1 decrease, leading to more earthquakes (figure 3). As the ocean moves back on forth in an ocean basin, the additional weight of the water acts to load and unload dipping faults (Cochran et al. 2004).

Documented increases in the sea surface height (and therefore pressure) occur regularly during El Niño events in the eastern Pacific Ocean, when warmer (therefore less dense) water coming from the west Pacific, flows eastward toward Central America. Similarly, SSH decreases during cold periods when La Niña occurs, and surface water flows westward, driven by intense Trade Winds. The north and the east Pacific are also affected by fluctuation in SSH due to the Pacific Decadal Oscillation (PDO), and a general trend of increasing SSH due to global warming. The change in total pressure for every meter of change in SSH is equal to 10k Pa pressure (Vidale et al. 1998).

Figure 4 is a graphic representation of the statement of the hypothesis. The undulating dotted line represents changes in threshold caused by variation in SSH during spring and neap tides. Unfortunately, only the timing and the magnitude of earthquakes are considered in this model, and the interaction of earthquakes and the lunar time scale are

not taken into account. Stein (1999) states that when stress change is translated into probability, earthquakes interaction should be considered.

1.7 THE PURPOSE OF THIS STUDY

For those who try to predict earthquakes, it is important to investigate possible links between crustal processes and other parameters. In this research, I will investigate possible linkages between changing oceanographic conditions and earthquake recurrence, specifically if a decrease in SSH acts as a triggering mechanism for the earthquakes.

By conducting a time series cross correlation analysis between SSH and earthquake events, I will be able to identify the presence of a SSH signal that affects the seismicity in the three different kinds of plate boundaries present in the study area. It is important to understand if an how such factors play a role in crustal processes in order to predict with more accuracy earthquakes and earthquake hazards.

1.8 EXPLORING THE USE OF GIS FOR MARINE SEISMICITY RESEARCH

GIS is a powerful tool for both graphic representation of data and for spatial analysis in many different fields. GIS technology allows the display of geographic information keeping it linked to a set of attributes, such as location, timing and magnitude of each individual event.

GIS was used in this research to divide the whole dataset into sub-datasets for each seismic zone and to calculate descriptive statistics for earthquake occurrence in each dataset. As a product of the research procedure, a beginner's GIS manual was created to enable scientists to perform fast and accurate analysis of their seismic data.

INTRODUCTION: FIGURES

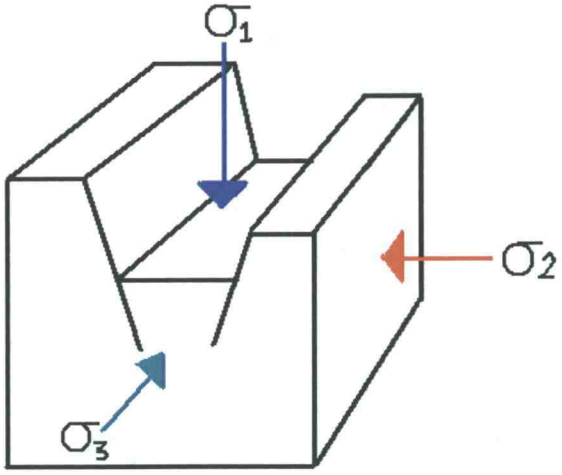

Figure 1: Stress on a cube. σ_1 is the horizontal stress and σ_2 and σ_3 are the two horizontal stresses.

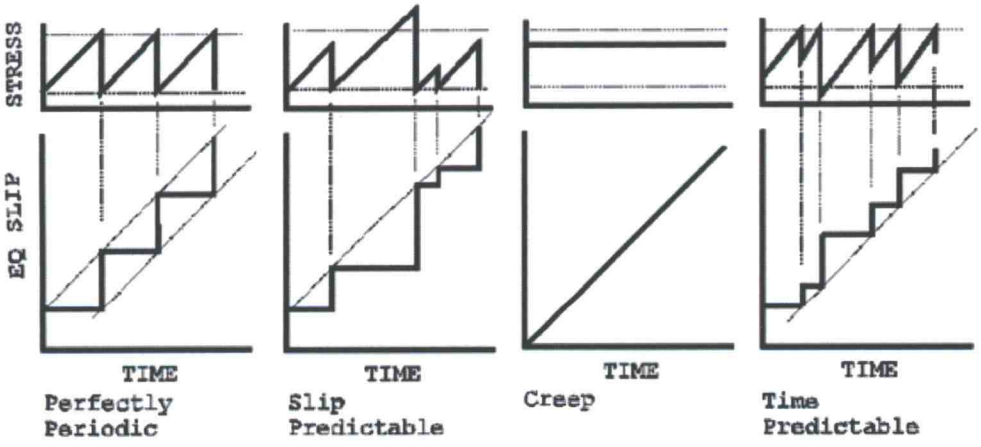

Figure 2: The graphs above illustrate four idealized models of earthquake recurrence for a fault that bounds two plates that are in steady motion with respect to each other (Kellogg and Hunter 2000).

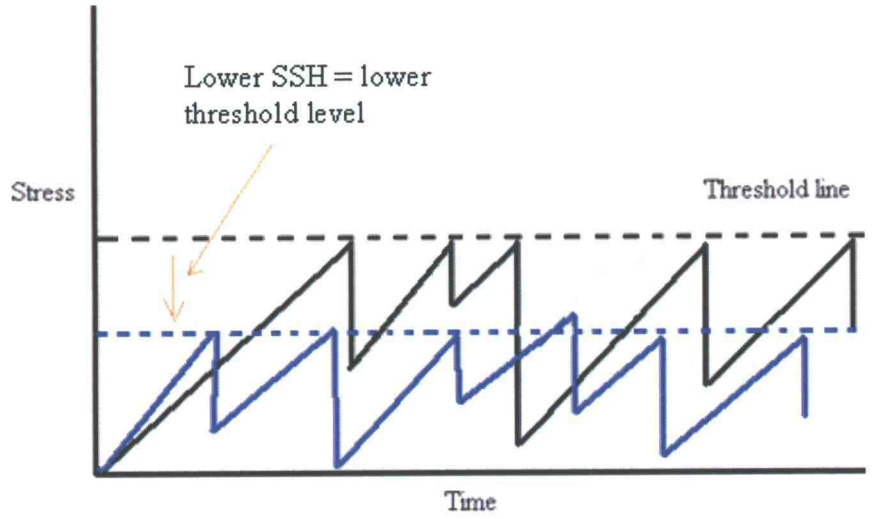

Figure 3: Fluctuations in threshold line position due to variation in SSH.

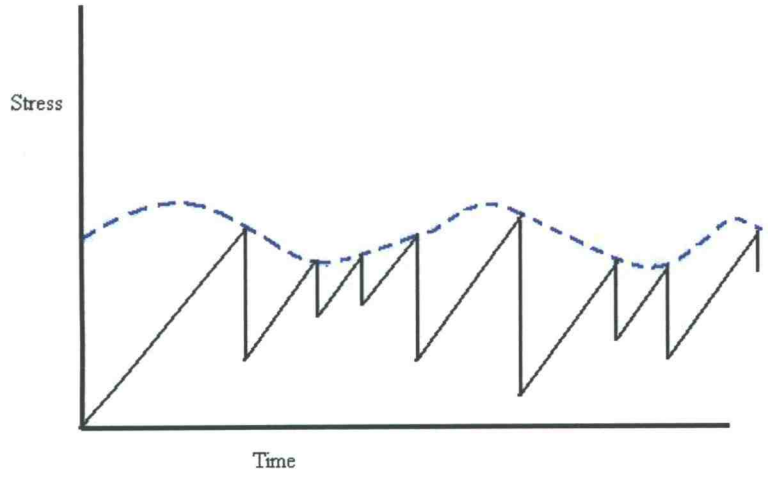

Figure 4: Time predictable model as hypothesized in the research. The threshold line fluctuates up and down as a result of changing oceanographic and lunar condition.

2. LITERATURE REVIEW

The following chapter describes in detail the study sites and all the processes, both atmospheric-oceanic and tectonic, that occur in the study area. It also explains the advantages and the improvement on the data set gained by choosing such study area.

2.1 THE STUDY AREA: EASTERN TROPICAL PACIFIC

The tropical Pacific is by far the largest of the three tropical oceans and it is subjected to a self-sustained air-sea coupled oscillation on interannual time scales, which is the basis for the El Nino Southern Oscillation (ENSO). From an oceanic point of view, the equatorial Pacific is divided into a pool of warm water in the west and a tongue of cold water in the east. The cold region is due to wind driven upwelling off the coast of Peru, while the warm pool is due to the warming of stable waters, pushed westward by the Trade Winds. Periodically, the Trade Winds weaken causing the cessation of the upwelling in the eastern tropical Pacific and causing eastward movement of the warm water stored in the warm pool in the western Pacific. This phenomenon is called the El Niño Southern Oscillation. The warm pool is characterized by sea surface temperatures (SST) among the warmest in the world, and because of its size, it is the world's most important source of heat into the atmosphere and to higher latitudes in the Pacific Ocean.

The study area is located in the Eastern Tropical Pacific between 20° north and south of the equator and westward of the coasts of Central and South America extending seaward for approximately 20° longitude (figure 5). Here, the seafloor has two active spreading centers: the East Pacific Rise (EPR) running north to south between longitudes 105° and 110°, and the Galapagos Spreading Center (GSC), perpendicularly intersecting the EPR about 2° north of the equator and running eastward toward the coast of Central America.

The East Pacific Rise (EPR) is a long, fast spreading center (>100 mm/yr – full rate, Curewitz and Karson 1998), trending south from the southern coast of the northern

American continent. It lies about 200 km west of the coast of Peru. Fast-spreading ridges are inherently advantageous for conducting integrated time-series studies of ridge processes due to the probabilities of observing accretionary events (e.g., episodes of cracking, intrusion, or eruption) in any 10 yr time period (Haymon and Cormier 2000). Fast spreading ridges are usually characterized by a 2-10 km wide flank and a 200-400 m axial high flanked by smooth abyssal hill terrain.

The Galapagos Spreading Center (GSC) is a relatively short, east-west trending spreading center which lies almost exactly on the equator and forms a triple junction at its intersection with the EPR. Eastward, it passes north of the Galapagos island and into the Gulf of Panama. It is an intermediate spreading center (40-65 mm/yr), whose axial topography is particularly sensitive to small changes in spreading and magma supply, governed by the presence of the nearby Galapagos hotspot (Canales et al. 1997).

Both the EPR and the GSC are formed by the upwelling of hot magma that cools and solidifies as lithospheric plates as newly formed oceanic crust moves down the flanks of the ridge (Perfit and Chadwick 1998). The two ridges separate three oceanic plates in a triple junction (figure 5): on the west side of the EPR, the Pacific plate moves to the west; on the eastern side of the EPR, to the north of the GSC, the Cocos plate moves 32 mm/yr to the east-north, subducting beneath Central America. To the south of the GSC, the Nazca plate moves 34 mm/yr to the east and then subducts beneath South America.

The area of interest for this research was chosen for three main reasons. First, it includes all three types of plate boundaries: spreading, subduction and transform motion. These different plate boundaries are characterized by various kinds of faults and earthquake mechanisms and may respond differently to changes in sea surface height. Second, the area is acoustically monitored by the NOAA/PMEL hydrophone arrays; these hydrophones are able to detect smaller ($M<4$) and therefore more numerous earthquakes than land-based seismic networks, giving a more accurate picture of the earthquake activity (Dziak et al. 2004). Third, the area is affected regularly by changes in

oceanographic conditions and SSH such as the ones happening during El Niño and La Niña regimes, as well as tidal cycles.

2.2 PLATE BOUNDARIES

The study site includes examples of all three types of plate boundaries and different kinds of faulting (figure 6): divergent or extensional margins (normal faults at oceanic spreading ridges) are located where plates move apart and new ocean crust is created; conservative margins (strike-slip faults) are found where plates slide past one another without construction or destruction of the plate and are commonly found connecting segments of spreading ridges in the oceans; convergent or destructive margins (thrust faults, subduction zone) are formed when the denser and therefore heavier oceanic plate subducts beneath the lighter continental plate.

On the EPR, spreading rates vary from north to south. Using the GSC as a natural break, the study area was divided into two different zones: zone 1 in the north (0°, +20°) includes all the boundaries along the Cocos plate, including the GSC in the southern portion, two transform faults (Clipperton and Siqueros) on the western side and the middle American on the north-eastern side. Zone 2 is the southern part of the EPR (0°, -20°) and includes five transform faults (Quebrada, Discovery, Gofar, Yaquina and Wilkes) on the Nazca-Pacific plate boundaries. Such a division in zones makes it possible to compare the seismic behavior of slow versus fast spreading ridges segments affected by a similar change in SSH.

Strike-slip faults along the EPR are a rich source of information because of the occurrence of deep (running as deep as 25 km) and strong earthquakes, and variability because of the difference in the spreading rate between the southern and the northern part of the EPR. Earthquakes are caused by the plates mostly sliding past each other laterally, producing less sinking or lifting of the ground than normal and thrust faults. These transform faults are oriented at right angles to the spreading ridge axis running on the

east-west axis, therefore the stress that influence these faults the most is the east-west stress (σ_1). Seismicity on these offsets is due to one plate moving in the opposite direction with respect to the other plate, with earthquakes occurring along the fault's plane. These faults are usually short (~100 km long) with shallow earthquakes (M<7) on the young crust where the maximum size is proportional to the fault's length (Yeats et al. 1997). Very fast spreading centers produce smaller earthquakes than slower spreading centers because transform faults at fast-spreading ridges occur in younger and warmer (and thus, weaker) brittle lithosphere (Yeats et al. 1997).

In general, fast spreading ridges produce wide transform zones where shear is accommodated by multiple, closely-spaced, strike-slip faults (Fortes 1999). These faults have thicker crust than ridges and therefore tend to have larger earthquakes.

Normal faults develop in spreading centers (extensional margins) in which the maximum compressive stress is vertical (σ_2) and are represented by the EPR and the GSC. Here the crust is too thin and hot to generate large earthquakes, and since the brittle-plastic transition happens only a few kilometres below the surface, the zone is unable to store much elastic strain energy (Yeast et al. 1997).

Thrust faults occur in the Middle American Trench subduction zone. Thrust faults are reverse faults that dip 45° or less. In reverse faults, the minimum stress is vertical (σ_1) and the maximum principal compressional force is the horizontal stress ($\sigma_{2,3}$). However, the vertical stress may decrease or increase the amount of frictional resistance of the subducting plate, therefore influencing the occurrence of earthquakes (figure 7).

There are four general types of earthquakes associated with subduction zones: shallow interplate earthquakes caused by failure of the interface between the downgoing slab and overriding plate; shallow earthquakes caused by deformation within the upper plate; earthquakes at a depth of 40-700 km within the downgoing oceanic slab; earthquakes seaward of the fault, caused mainly by flexing of the downgoing plate, but also by compression of the slab (Yeats et al. 1997).

2.3 REGIONAL SEISMIC ANALYSIS -ZONE 1

EPR and Cocos and Pacific Plates

In zone 1, the EPR separates the Cocos plate from the Pacific plate and it includes two right-lateral transform faults (Orozco and Siqueros) and one left-lateral transform fault (Clipperton). The spreading rate of the EPR in zone 1 varies from 74 mm/year in the upper portion next to the Orozco fault, to 110-120 mm/year near the Siqueros fault. Also, between 2° N and 4° N there is the Galapagos microplate, whose seismicity was not included in the present study. Over the approximately 4000 km spanned by this plate boundary, the morphology of the axial region varies remarkably little (Macdonald et al. 2004).

2.3.1 GALAPAGOS SPREADING CENTER

Spreading ridges are found at relatively shallow depth, around 2.5 km beneath the sea surface, and their elevation relative to the deeper surrounding seafloor is due to the thermal expansion of the hot material beneath the ridge, as indicated by the small gravity anomalies over them. Spreading ridges are characterized by shallow, low-magnitude earthquakes that are caused by extensional forces. The Galagaos Spreading Center's (GSC) spreading rate is intermediate, ~65 mm/yr (Floyd et al. 2002) and it is a classic example of an interactive hotspot-ridge system (Morgan et al. 1978). The influence of the Galapagos hotspot on the nearby Galapagos Spreading Center (GSC) can be readily observed in along-axis variations in bathymetry, gravity, geochemical anomalies, as well as in the off-axis relics of seafloor depth and residual gravity anomalies (Canales et al. 2002). The Galapagos hotspot is located ~170 km south of the GSC, beneath Isla Fernandina. The eastern portion of the GSC is offset by several large transform faults and for this reason this area will not be considered.

2.3.2 CLIPPERTON AND SIQUEROS TRANSFORM FAULTS

The Clipperton transform fault exhibits large variations in elevation, having a large uplifted block in the middle of the faults, creating a change in elevation of 1500 m (Fortes 1999). The Clipperton (10°15'N) and the Siqueros (89°5'N) transform faults (figure 8) represent two contrasting modes of transform tectonics; since they move in opposite directions, changes in spreading direction cause compression across the Clipperton fault and extension across the Siqueros fault (Carbotte and Macdonald 1992; Pockalny et al. 1997). Clipperton offsets the ridge axis by 85 km to the right with a slip rate of approximately 101 mm/yr, while Siqueros offset is 140 km to the left with a slip rate of 107 mm/yr (Pockalny et al. 1997). The area is magmatically and tectonically active and the dataset includes two volcanic swarms in 1998 and 2001 in Siqueros.

While the Siqueros fault is made up of multiple transform segments separated by intra-transform spreading centers (Gregg et al. 2004), the Clipperton fault is a single fault segment that has undergone tectonic compression during the last 0.5 Ma and has the lowest hydroacoustically recorded seismicity rate of the six faults. Based on earthquakes recorded in the Harvard CMT catalogue, however, the Clipperton fault has had the highest amount of cumulative energy released of the six transforms between 1976 and 2004. The last large magnitude (M_w) 6.6 earthquake occurred in May 1995, immediately preceding the deployment of the NOAA hydrophone array. One possibility for the recent low seismicity rate is that the Clipperton transform fault is in a seismic quiet period as demonstrated by Gregg et al. (2004), and as also evident in the data used in this research.

Between the Clipperton and the Siqueros faults, the 325 km-long ridge axis spreads at a full rate of 110 mm/yr and maintains a minimum depth in the range of 2500-2600 m, making this one of the more shallow sections of the EPR. North of Clipperton and south of Siqueros, the EPR axial height is deep, narrow and triangular.

2.3.3 MIDDLE AMERICAN SUBDUCTION ZONE

The subduction zone in the study area is the Middle American Trench, which is part of the "Ring of Fire", a volcanic arc that includes over 75% of the world's active and dormant volcanoes, stretching from New Zealand, along the eastern edge of Asia, north across the Aleutian Islands of Alaska, and south along the coast of North and South America (figure 9). The eastern section of the ring is the result of the Nazca and the Cocos plates being subducted beneath the western end of the Caribbean and South American plates. The Middle American Trench extends northwest-southeast for more than 2,700 km from central Mexico to Costa Rica, with a maximum depth of 6,669 m (Manea et al. 2003). The subducted ocean floor warms in the upper mantle and becomes somewhat more elastic as it is pushed deeper beneath the continental lithosphere. In the offshore thrust zone where the brittle rock from the oceanic plate meets the opposing rock of the continental shelf, mechanical stress builds. This "locked" zone stores energy that is ultimately released as an earthquake.

Earthquakes on subduction zones are usually larger and deeper than strike-slip fault earthquakes; they have shorter recurrence intervals than those earthquakes along inland active faults, and the normal-thrust nature of the fault can cause tsunami waves.

It is important to understand the mechanisms that may trigger earthquakes in these areas since much of the population lives along the coasts. Past destructive tsunamis include: Colima 1900 and 1932, Oaxaca 1931, 1965 and 1978, and most recently the well studied 1992 earthquake that caused a tsunami in Costa Rica (Odias 1998). Seismic wave analysis of the 1992 event indicated that this event was much shallower than other typical subduction-zone earthquakes (Manea et al. 2003). Analysis of the seismological record showed the fault motion of this earthquake to be unusually long in duration and occurring in the top 10 km of oceanic crust - a depth much shallower than that of typical subduction-zone earthquakes (Aki 1992).

In the Middle American Trench (MAT), the young (< 25 Ma) lithosphere of the Cocos plate subducts underneath the Caribbean plate at a rate of ~80 mm/yr (DeMets

2001), with obliquity varying due to changes in the strike of the fault, from essentially zero in southern Costa Rica to more than 15° in Nicaragua (La Femina et al. 2002). In general, oblique, shallow subduction at a high rate of convergence, which occurs along the greater portion of the Middle America, results in northwest-trending crustal block motions that parallel the coast. However near Nicaragua most of the crustal motions are made by "bookshelf" faulting. Earthquakes included in these datasets may therefore be due to the subduction zone and also, in the case of the ones located farthest inland, to northeast-striking left lateral faults in Nicaragua (La Femina et al. 2002).

2.4 REGIONAL SEISMIC ANALYSIS - ZONE 2

EPR and Nazca and Pacific Plates

In zone 2, the EPR divides the Pacific plate from the Nazca plate. Here, the Pacific and the Nazca plates spread apart at 125-152 mm/yr, the fastest rate of the entire mid-ocean ridge system (DeMets et al 1994). The ridge is defined by a linear high, 5-15 km wide and rising 300-500 m above the surrounding seafloor (Haymon and Cornier 2000), partitioned by five left-lateral transform faults (figure 10): the Quebreda, the Discovery, the Gofar, the Yaquina and the Wilkes transform faults.

2.4.1 QUEBRADA, DISCOVERY, GOFAR TRANSFORM FAULTS

The Quebrada, Discovery and Gofar transform faults are located close to each other and exhibit similar seismic behavior. McGuire et al. (2005) showed that these transform faults have a low number of earthquakes and high aftershock rates compared to continental strike-slip faults. McGuire et al. (2005) also suggested that these faults are excellent locations to gain a better understanding of the physics of earthquake rupture and fault failure. While all three faults routinely generate small earthquakes, only the

Discovery and Gofar faults have large earthquakes. "The lack of large events at Quebrada means that 99% of the plate motion across this fault occurs aseismically, whereas about half of the plate motion across the Discovery fault occurs in earthquakes". This "difference in fault coupling is important both for understanding the strength of plate boundaries and for understanding what makes a fault capable of producing an earthquake". However, in the dataset I examined, Quebrada does not show lower seismic rates compared to Discovery and Gofar.

The Quebrada, Discovery, and Gofar transform faults all consist of multiple transform segments separated by intra-transform spreading centers. These transforms have undergone tectonic extension during the last 0.5 Ma and they each exhibit relatively high seismicity rates during the hydrophone monitoring period. Siqueros, Discovery and Gofar faults show moderate seismic moment release for the last 28 years (Gregg et al. 2004).

2.4.2 YAQUINA, WILKES TRANSFORM FAULTS

The Yaquina transform is a 30 km long fault composed of several fragments (Gregg et al 2004). It appeared to have a low moment release for the last 28 years and it is thought to be a hybrid transform/non-transform offset (Lonsdale 1983). The Wilkes left-lateral transform fault offsets the East Pacific Rise about 200 km, of which only 100 km are seismically active. Kureth and Rea (1981) suggest that some event, other than a shift in the Nazca-Pacific pole of rotation, occurred 0.9 m.y. ago to change Wilkes fault behavior.

2.5 OSU/NOAA AUTONOMOUS HYDROPHONE ARRAY

In May 1996, the National Oceanic and Atmospheric Administration's Pacific Marine Environmental Laboratory (NOAA-PMEL) deployed six hydrophones along the East

Pacific Rise (EPR) for monitoring low-level seismicity. The hydrophones are moored to the sea floor and by being autonomous they represent an excellent strategy for monitoring remote areas of the world's oceans. Two hydrophones each are located at six grid points (10°N, 95°W; 0°N, 95°W; 10°S, 95°W; 10°N, 110°W; 0°N, 110°W; 10°S, 110°W). The instruments are collected and replaced every 6-12 months and are able to continuously record sound (from 1-110 Hz pass band) in the ocean coming from any direction. At the time of recovery, a NOAA research vessel collects the hydrophones and the data which are then processed on land. Computer software can then automatically associate and locate common events using a process called triangulation (NOAA/PMEL 2005), by combining the arrival time and the arrival bearing on several arrays whose geographic location is known. The amplitude of the events is also an indicator of their magnitude. The hydrophones are suspended in the SOFAR (SOund Fixing And Ranging) channel, a channel in which, for its temperature and pressure properties, sound waves (T-waves) get trapped and can therefore travel for very long distances (Fox et al. 2001).

The set of hydrophones represents a notable improvement in the quality of data regarding marine earthquakes: with the ability to record the events directly in the sea rather than from land-based stations, it is possible to detect smaller earthquakes whose energy is usually dissipated before arriving at land-based stations, and to provide more accurate source locations than land based seismic networks. Also, the instruments offer a long-term, relatively low cost alternative to ocean-bottom seismometers and they allow for observation of the velocities of primary waves travelling at or just below the Moho (Pn velocities) and mantle/core phases arriving at normally inaccessible deep-sea locations (Dziak et al. 2004).

In choosing the EPR as my area of interest, I benefited by having the OSU/NOAA autonomous hydrophones surrounding the area. Data regarding location, magnitude and timing of earthquakes are very accurate with limited sources of error.

2.6 PRESENCE OF PERIODIC EVENTS

In the eastern tropical Pacific, there are year-to-year and several-year oscillations of climate that are associated to the ocean-atmosphere interactions. These oscillations are clearly visible due to their sea-level signature (order 10 cm) from satellite data regarding sea surface height (SSH) and sea surface temperature (SST). They consist of a singular set of equatorial waves that propagate eastward (equatorial Kelvin waves) or westward (equatorial Rossby waves) at a much faster phase speed than the mid latitude Rosby waves. The most important oceanographic changes that affect the SSH and SST of the study site are El Niño Southern Oscillation (ENSO), La Niña, and the Pacific Decadal Oscillation.

El Niño/Southern Oscillation (ENSO) is an irregular oscillation involving both the atmosphere (Southern Oscillation) and the ocean (El Niño). It follows a relatively well-known sequence that occurs after the Indonesian atmospheric low pressure and the Peruvian atmospheric high pressure weakens, causing a declining in strength of the southeast Trade Winds. This shift in the position and intensity of the atmospheric pressure, and therefore of the winds, dramatically alters the structure and the physics of the ocean and its currents in the Pacific Ocean (see figure 12). In normal circumstance, the SSH near Indonesia, western Pacific Ocean, is a few tens of centimetres higher than the one in the area of interest because of the pull up caused by the Trade Winds (Segar 1998).

When El Niño occurs, the horizontal pressure change within the equatorial Pacific atmosphere is too weak to balance the sea surface slope. As a consequence, warm surface water flows toward the east with no deflection along the equator (where there is no Coriolis effect) in the form of a long wavelength wave. About nine months after the event starts (Segar 1998), the wave reaches the study area causing an increase in SSH. Once the wave hits the coast of Peru, stopping the upwelling system, it divides in two Kelvin waves that flow along the coast, respectively south and north. Figure 12 shows the effects of El Niño and La Niña on the study area. El Niño usually disrupts normal winter

conditions throughout the Pacific Ocean, starting around September and lasting until May or June (Wolter and Timlin 1993).

Figure 13 represents the situation during El Niño: higher than-average SSHs are red and white; below average are blue and purple; average is green. The oscillation set in motion by El Niño sometimes appears to overshoot as the system recovers (Segar 1998). The trade winds become stronger and the water near Indonesia becomes warmer, while water temperatures near Peru get colder (Segar 1998) (figure 14). This condition increases the upwelling along the coast of Peru and results in a cold tongue of denser water moving westward. During these conditions, SSH is lower than average. The dataset in this study includes two La Niña events, in 1995-1996 and in 1998-1999 (strong).

The "Pacific Decadal Oscillation" (PDO) is a long-lived El Niño-like pattern of Pacific climate variability. While the two climate oscillations have similar spatial climate fingerprints, they have very different behavior in time. Two main characteristics distinguish PDO from El Niño/Southern Oscillation (ENSO): first, 20th century PDO "events" persisted for 20-to-30 years, while typical ENSO events persisted for 6 to 18 months; second, the climatic fingerprints of the PDO are most visible in the North Pacific/North American sector, while secondary signatures exist in the tropics - the opposite is true for ENSO. Several independent studies find evidence for just two full PDO cycles in the past century: "cool" PDO regimes prevailed from 1890-1924 and again from 1947-1976, while "warm" PDO regimes dominated from 1925-1946 and from 1977 through (at least) the mid-1990's. As shown in the figures (modified from T/P images), zone 1 and 2 are similarly affected by changes in SSH due to El Nino and La Nina. The dataset includes one strong El Niño event in 1997-1998.

Seasonal variations in SSH are also due to storms and hurricane activity, that disturb the sea surface as well as the oceanic crust. They typically start in May and last until October (figure 15).

LITERATURE REVIEW: FIGURES

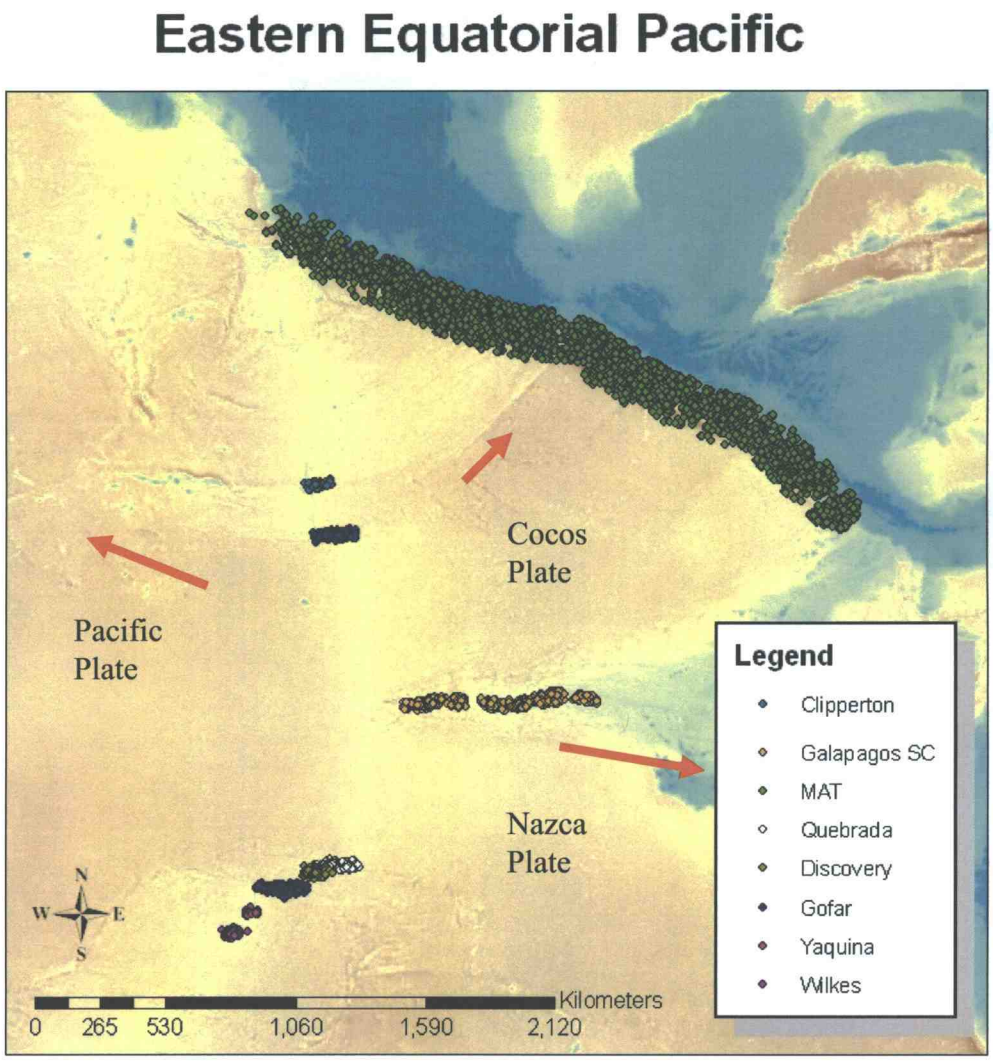

Figure5: The study area with dataset representative of the three plate boundaries. Red arrows indicate the direction of the plate movement.

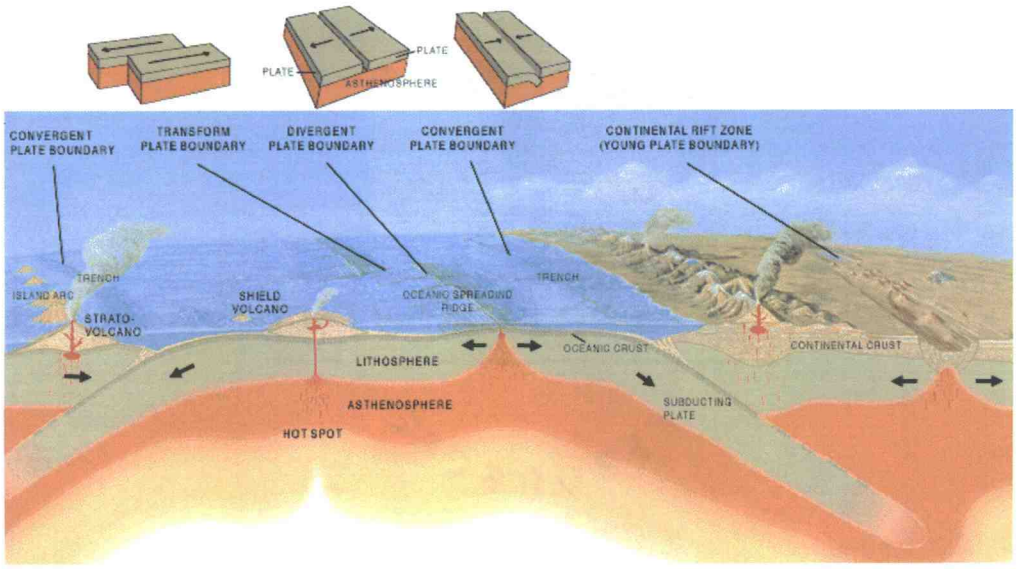

Figure 6: Different kinds of plate boundaries (USGS 2004)

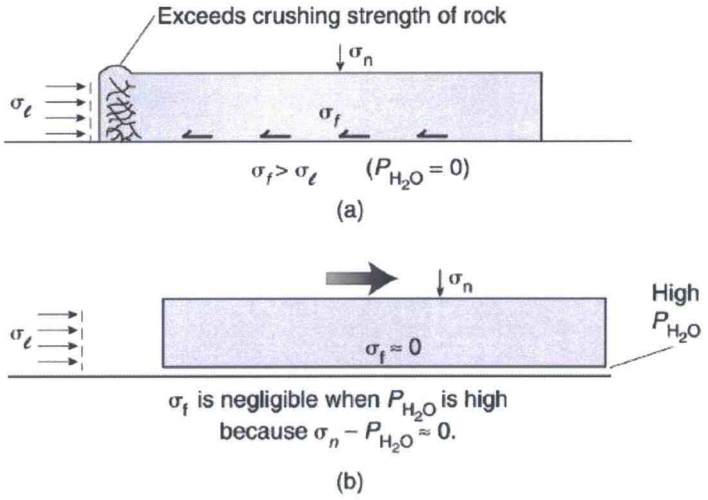

Figure 7: Stress on a thrust fault. By decreasing the amount of frictional resistance, the thrust sheet can move under very small applied load. σ_l is the stress resulting from horizontal loading, σ_f is the frictional resistance, σ_n represents the pore pressure (Van der Pluijm and Marshak 2004).

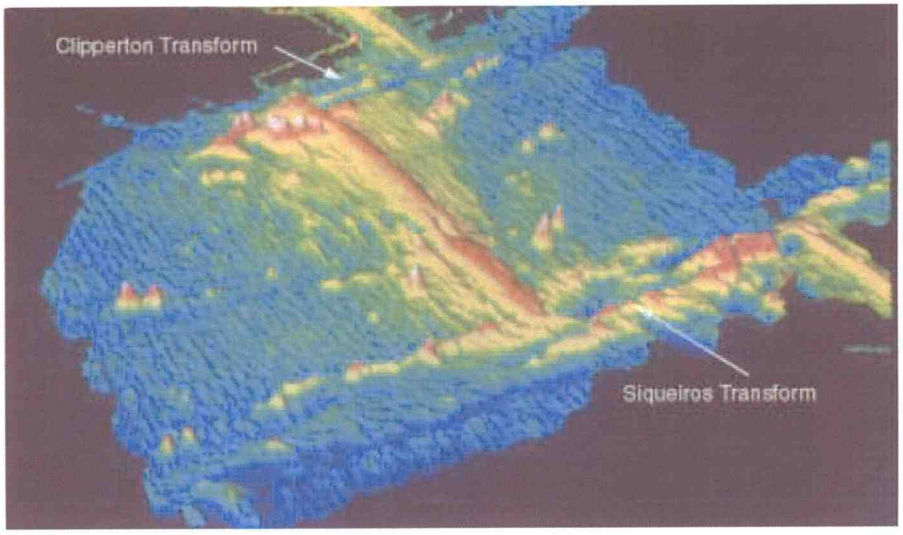

Figure 8: Topography of the Clipperton and the Siqueros fault (McDonald et al. 1992).

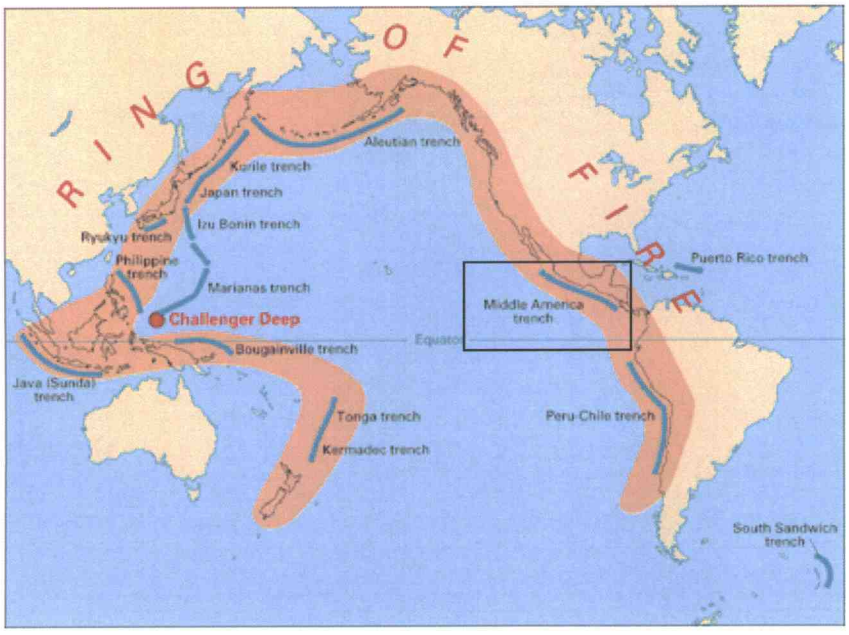

Figure 9: The ring of fire (USGS 1999) and the position of the Middle American Trench.

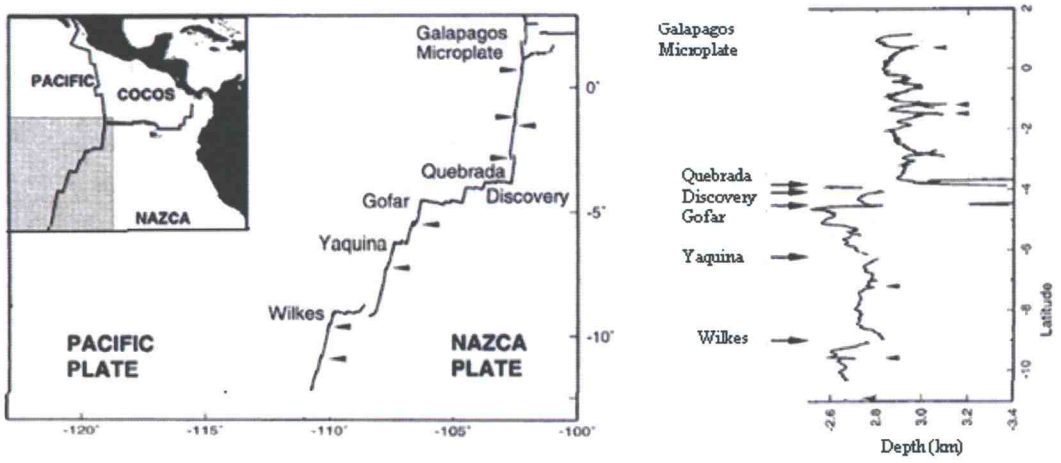

Figure 10: the study site in zone 2 and depths of faults (Adapted from Cornier 1997).

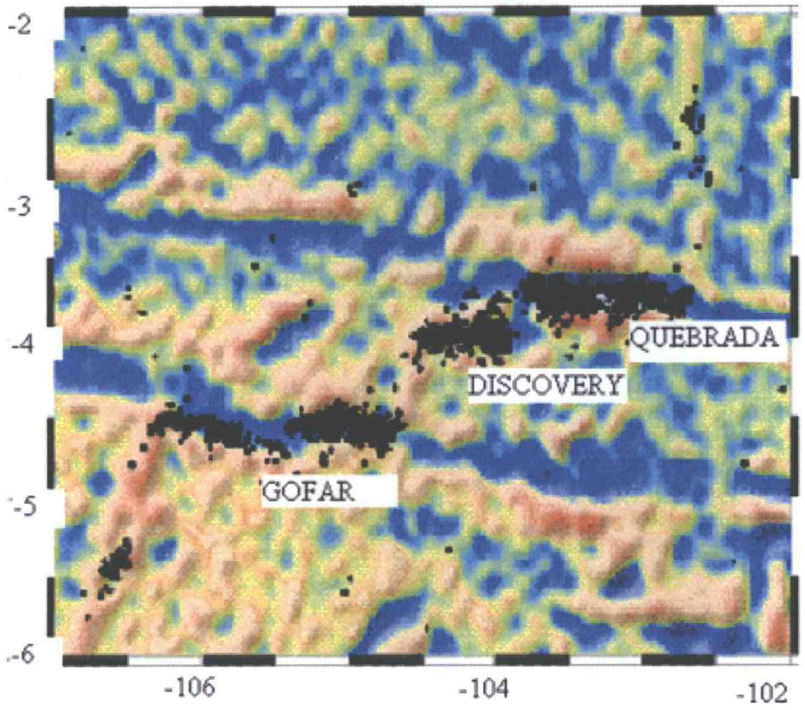

Figure 11: The Quebrada, the Discovery and the Gofar transform faults (McGuire 2005).

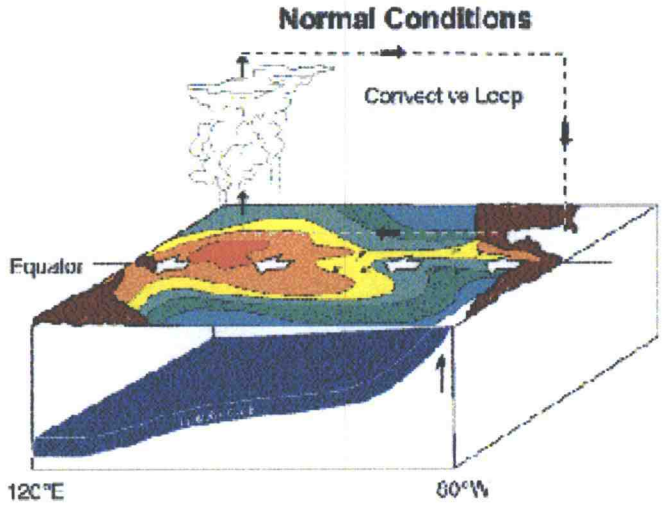

Figure 12: Oceanic and atmospheric conditions during El Nino (Niwa Science 2006)

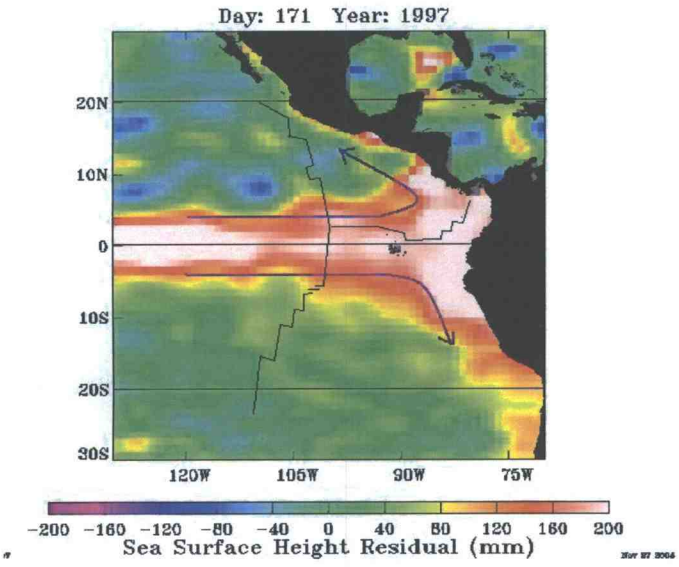

Figure 13: Sea surface height residual during El Niño (Adapted from T/P webpage)

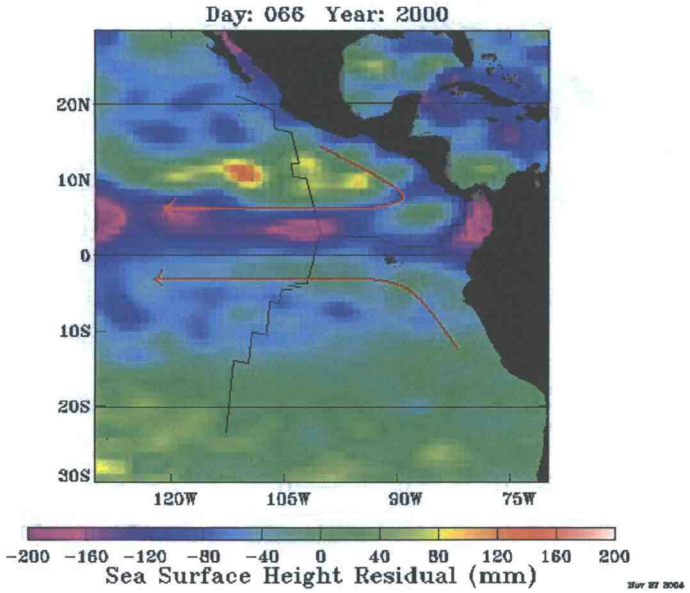

Figure 14: Sea surface height residual during La Nina (Adapted from T/P webpage)

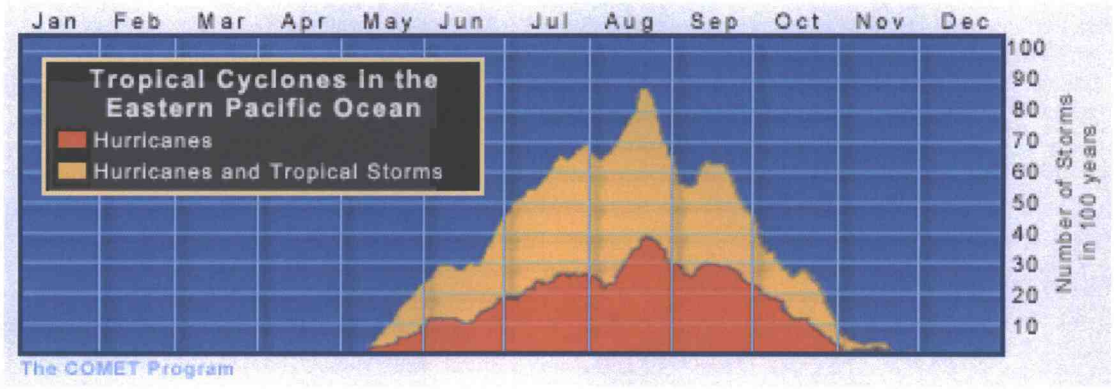

Figure 15: Tropical cyclones in the Eastern Pacific Ocean (COMET 2006)

3. METHODOLOGY

This chapter is divided into four parts. The first section describes the earthquake and the sea surface elevation datasets, explaining the source, the use and the possible sources of error for each dataset. In the second section, the choices of time scales used are described and justified. The third section describes descriptive statistics, in particular how GIS was used in this study. In the last section, the methods used for inferential statistics, which include time series autocorrelation analysis, time series cross correlation analysis and variance spectrum analysis, are described. There are three main factors identified in this research as possible sources of earthquake triggering: the weight of the water column overlying the fault; the influence of earth tides responsible for crustal deformation on moon's quarter time scale; the influence of ocean tides responsible for sea level change on an hourly time scale. These last two factors are isolated by choosing an appropriate time scale, while the weight of the water column is given by the SSH datasets.

3.1 DATASETS

Three datasets were used jointly in this research. The following sub-chapter describe for each data set how it was obtained, what it looks like and what are the possible source of errors. The data set include earthquake data set that was used for both the analysis on the lunar time scale and the ocean time tide, and two data set describing changes in SSH, one that would consider changes due to different oceanic conditions on a lunar time scale, and the other that would consider changes due to daily ocean tides

3.1.1 EARTHQUAKE DATA

Earthquakes have been used in this research as an indicator of tectonic activity. Earthquakes happen in the lithosphere when there is a rupture within the brittle rocks

caused by accumulated stress and they are present in different plate boundaries: spreading centers, transform faults and compressional (subduction) zones.

Description

Data regarding earthquake events (time, magnitude and location and calculation errors) for the study area in the eastern equatorial Pacific were obtained from the NOAA-PMEL catalogue, available on the Vents website (NOAA, accessed in 2005). These data occured from May 1996 to October 2002 and were obtained by hydrophones able to monitor low level seismicity by recording acoustic energy coming from earthquakes and other sources, such as whales, boats etc. (*T*-phases), radiated into the water column.

A "T-phase" or "T-wave" is an acoustic phase (sound) from an earthquake that travels through the ocean. T-phases propagate very efficiently in the low-velocity SOund Fixing and Ranging (SOFAR) channel (from 400 to 1600 m water depth) and can travel very long distances without attenuation. The arrival times can be used to locate precisely where the energy entered the SOFAR channel. By recording T-waves, the hydrophones are able to detect much smaller and more distant earthquakes than the seismographs on land. In fact, sound propagates incredibly more in water, compared with sound propagated through rock which is attenuated especially in crustal materials (figure 16).

Because earthquakes occurring on the EPR and GSC are typically low magnitude, use of hydrophones to exploit the low attenuation properties of the sound channel is necessary in order to detect earthquakes from these remote areas. The slow sound velocy properties of the SOFAR channel, combined with a good azimuthal distribution of the hydrophones relative to the EPR and GSC, allow minimization of timing and therefore earthquake location errors. The standard errors in this area are estimated to be ± 2 km, $\pm$ 10 s for the southern/northernmost faults (the Wilkes and the Siqueiros Faults) and are slightly smaller for the faults located in the center of the array (Fox et al. 2001).

The hydrophone array measures sound pressure in decibels (db), a logarithmic scale used to measure the amplitude of a sound, and the typical value for marine earthquakes is around 210 db (Dziak 2001). Values in decibels were subsequently converted to body-

waves magnitude (m_b), using the relationship for the East Pacific earthquakes created by Fox et al. (2001):

$$SL = 7.84\ (m_b) + 195.83$$

where SL is the earthquake's source level, or sound pressure in decibels.

The dataset was inserted into a working GIS station where earthquakes on spreading centers, faults and subduction zones were easily isolated into new layers from the rest of the dataset. Data regarding earthquakes for each seismic zone were then grouped twice, following different time scales: earthquakes were grouped and counted every 7.48 days to follow the cycles given by changing earth tides; earthquakes were also grouped and counted every hour, to explore the influence of hourly changes in sea surface height produced by ocean tides. Table 1 shows, for each fault in the study area, the number of events recorded, maximum earthquake magnitude and the direction of motion in each seismic zone. The whole dataset consists of a total of 19,039 events, of which 5,879 are located on transform faults, 2,990 come from the Galapagos Spreading Center and 10,170 are earthquakes due to the Middle American subduction zone. Figures 17 and 18 are graphic representations of the whole earthquake dataset in which each point represents an event. The entire dataset was divided into two different zones, north and south of the Galapagos Spreading Center, respectively.

Sources of error

Sound waves move at a faster speed in water (1500 m/s) than in air (341 m/s), since water is denser. Water temperature may affect the speed of sound (sound in warmer water travels faster than in colder water) and some errors are possible calculating the exact location and timing of events; nevertheless, considering the large temporal and spatial scale upon which the research is focused, small errors in location and timing can be ignored.

Moreover, the software can occasionally miscalculate or merge different events, therefore to reduce this kind of mistake and to eliminate any source of background noise that could interfere with the correct positioning of the events, all events with magnitude

smaller than 0.6 were not considered. In this way, errors were significantly reduced in the dataset used in this research.

3.1.2. SSH FROM SATELLITE

Data regarding changes of SSH with time were obtained from the altimeter (Advanced Very High Resolution Radar, NOAA AVHRR) mounted on the TOPEX/Poseidon (T/P) satellite. Satellites orbiting around the Earth allow us to get information about a geographic area *remotely,* from a distant point of view. The science of getting information about an area without being in direct physical contact with the object is called Remote Sensing. In this research, remote sensing has been used to obtain information about the height of the sea surface on those areas of the ocean above the faults studied.

The T/P satellite was launched in 1992 as a joint project between Centre National d'Etudes Spatiales (CNES-France) and the National Aeronautics and Space Administration (NASA-USA) to map the ocean surface topography. Originally designed to last 3 to 5 years, T/P is still providing valuable ocean altimetry data over 12 years later, becoming the longest running earth-orbiting radar mission. T/P uses radar altimeters to measure sea-surface topography over 90% of the Earth's ice-free oceans (from 66°N to 66°S), providing useful information used in various fields on different spatial and temporal scales, from studies on ocean dynamics (Ray et al. 2004) to studies on the seasonal to interannual (i.e. ENSO) variability in the Equatorial Pacific. The SSH data are available from NASA JPL web at http://poet.jpl.nasa.gov, ranging from January 1996 to January 2001.

On board the satellite, there are two altimeters: the dual frequency Radar Altimeter from NASA and a Single-Frequency Solid-State Radar Altimeter. SSH measurement from both altimeters are merged and corrected for precise orbits to form a primary data product, the Merged Geophysical Data Record (MGDR). The T/P altimeter satellite has

recently become an integral part of NOAA's operational satellite system for monitoring the oceans (Cheney et al. 1998). The application of satellite radar altimetry offers a method of acquiring level-change information with good accuracy (Fu et al. 1998) providing improved estimates of the three-dimensional oceanic temperature, density, and velocity fields (Gross et al. 1998).

Description

Both gravity (which does not change significantly over hundreds of years) and ocean circulation influence the height of the sea surface. In this research, sea surface height (SSH) is defined as the computed deviation from the mean SSH calculated over a period of 3 years from 1993 to 1996 (Fu and Cazenave, 2001), with tidal and inverted barometric effects removed (Liggett 2003). The height is calculated by the radar altimeter that sends short pulses of microwave energy toward the ocean below. The round-trip travel time of the reflected pulse yields the distance between the spacecraft and the sea surface, while the shape of the reflected pulse is also used to determine wave height and sea surface wind speed (Case 1995).

The satellite provides data of any area of the ocean every 10 days with a footprint size of the altimeter is typically about 3-5 km in diameter, depending on the significant wave height. Measurements are taken approximately 1/sec along track, giving a spacing of about 6 km (CSR/TSGC 1999). The satellite's data suits this kind of research since its accuracy in both the temporal and spatial resolution is very high and therefore it is possible to gain a good picture of large-scale variability of the ocean. Also, the increase in orbit height (1336 km against the 785 of the previous satellites) results in an improvement in the orbit accuracy (table 2).

SSHs were obtained for five different areas: one for the Clipperton and Siqueros transform faults, one for the Middle American Trench, one for the GSC, one for the Quebrada, the Discover and the Gofar transform faults, one for the Yaquina and the Wilkes transform faults. For each area, a time series average value of SSH was obtained with a 10 day temporal resolution. Table 3 describes the bounding coordinates of the

areas overlying the faults. The area chosen for each fault varies depending on the fault lengths, and it is chosen to encompass the total area overlying the faults.

Sources of error & solutions

SSH in the ocean varies on different scales depending on various factors: on smaller spatial scales, wave activity makes the sea surface rough, promoting variable SSH measurements since the backscattered energy is dependent on the wavelength and the depression angle of the wave. But since this research expands on a large study area, such error becomes insignificant. On larger spatial scales, SSH is highly correlated with both the ocean temperature and the mass transport of ocean currents (Fu et al. 1998), and therefore it is important to understand that percentage of the SSH changes is due to thermal expansion and what percentage is due to mass transport, since these two parameters will influence the total pressure exercised on the sea floor in a different way. T/P satellite is also able to monitor changes in Sea Surface Temperature (SST), and can make corrections calculating the rise in SSH due to thermal expansion. The resultant correlated SSH data are therefore not strongly influenced by thermal expansion (Cheney et al. 1998).

Errors in SSH measurements from the satellite are corrected in many different ways. The presence of two channels to receive data allows correction for propagation delays in the ionosphere, reducing a significant error source in the measurement (Case 1995). Also, twice a day, the altimeter automatically undergoes an internal calibration mode. This calibration lasts about 5 minutes and takes place when the altimeter is over land so that useful ocean data are not lost. Also, for the first 5 years of function, the T/P satellite passed directly over a Chevron oil drilling platform (+/- 1 km) every 10 days as it traced its orbit. Direct comparisons of the sea level and ancillary measurement derived independently from the satellite and platform have been used to create a 5-year time series of absolute calibration estimates for the T/P sensors (altimeter and radiometer) and the overall measurement system (Haines et al. 1998).

3.1.3 SSH FROM TIDAL MODEL

Predictions in daily variations in SSH were obtained from the Tide Model Driver (TMD) written by Laurie Padman, Lana Erofeeva and Gary Egbert at Oregon State University (2003). TMD is a Matlab package for accessing the harmonic constituents for the ESR/OSU family of high-latitude tide models, and for making predictions of tide height and currents.

Tidal constants were extracted using all semidiurnal tidal constituents for 4 areas in the study area, two for each zone (table 4). Locations of the predicted tide were chosen in areas with higher seismicity. The tidal model is corrected for load tides (generally, roughly out of phase with the ocean tide); it works jointly with the TPXO6.2 model that is able to account for the deformation of the solid earth due to the added weight of water above it. TPXO6.2 uses radar altimetry data from T/P and has a medium-resolution (1/4° x 1/4° pixel size) (Padman and Erofeeva 2003). The load tide is not the same as the earth's own tidal response to lunar and solar gravitation: the body tide must be estimated separately from solid earth models if required.

Changes in SSH were obtained every hour for each day from 19th May 1996 to 19th October 2002. The data were then paired with earthquake activity of the same period and statistical analysis was made. The TMD resulted in a cost effective method of obtaining data and continuously covers all temporal ranges of the SSH and earthquake data used.

3.2 TIME SCALES

The choice of the time scale is a critical part of this research. Earthquake trigger mechanisms include many different factors, including: atmospheric pressure changes, earth and ocean tides, geomagnetic storms, strain shifts related to distant earthquakes, underground magma movement, and dam-construction-related water weight changes and others. Since the exact cause of the earthquakes in my database is not known, the choice of the right time scale is essential for proper analysis and must include other factors such

as the moon and the sun's gravitational pulls and variation due to daily tides. The following two sub-sections describe and justify the choice of the two time scales used in this research.

3.2.1 EARTH TIDES

A subdivision of the lunar cycle into quarters is necessary to reflect those changes in gravitational pull that are present during transition between spring and neap tides. Effects of the gravitation pull of the moon and the sun on the oceanographic crust are called earth tides. During neap tides, the moon, earth and sun positions form a 90° angle. This happens at every first quarter and third quarter, and under such situations the gravitational pull of the moon and the sun counteract each other by pulling in orthogonal directions (figure 19). During spring tides, the moon, earth and sun are aligned and their forces add together creating stronger tides.

The lunar quarter time scale includes two cycles in which the gravitational pull is increasing (from first quarter to full moon and from third quarter to new moon) and two cycles in which the pull is decreasing (from full moon to third quarter and from new moon to first quarter).

Earthquake data were assembled using a Matlab routine created with the help of Otto Gygax, for each seismic area in groups of 7.3 days each. Moon phases were calculated from a moon phase calculator available on the web (Astronomical Application Department, 2005) for latitude of -110° and longitude +10° (time zone 7). Output data consist, for each time step, of number of events, average magnitude and collection of events. Interpolation was used to obtain the SSH measurement for each lunar quarter time step using a Matlab routine offered by Prof. Nick Pisias. Figure 20 represents the original SSH data (time interval = 10 days) and the new output (time interval = 7.3 days). As expected, some accuracy in the SSH was lost in this process.

Three tests were made in this time scale: cross correlation analysis between number of earthquakes and changes in sea surface height, to seek for possible correlations; cross correlation analysis between faults to see whether faults may behave in a similar way; cross correlation analysis between number and earthquakes and average magnitude, to see if the seismic areas follow the Gutenberg-Richter relationship and therefore the chosen time scale is effective.

3.2.2 OCEAN TIDES

As described in the introduction, changes in SSH have been proven in past research to work as a trigger mechanism for marine earthquakes. In this research, daily variations in SSH due to ocean tides were compared in time series cross correlations and variance spectrum analyses against numbers of earthquakes to verify if results obtained in past research are also correct in the eastern equatorial Pacific study site.

Ocean tides and earth tides do not happen simultaneously. There is a delay in the ocean tide due to the frictional force between the oceans and the atmosphere. Because of the orbital tilt of earth's axis of rotation with respect to the plane of ecliptic, the moon's position remains within 5 degrees of the ecliptic. Therefore, frequency of tides varies with latitude, as shown in figure 21 (Phillips 2006).

In higher latitudes (A), there is only one high tide per day (diurnal tide), because at A' the water opposite the tidal bulge at A is actually *below* mean sea level. At lower latitudes (B), the tidal bulges are different heights above mean sea level, with the tide being higher at a point when it is rotating under B than it is under B' (*mixed tide).* Along the equator (C), the tidal bulge is the same height above mean sea level at both C and C'. Tides will therefore be of approximately the same height (*semidiurnal tide*) (Phillips 2006).

Since the areas studied are located at different latitudes, they will also experience tides with different magnitudes. The disadvantage of this methodology consists of the

fact that in doing this analysis, the earthquake dataset is broken down into smaller units, thereby losing part of the accuracy during the statistical tests. In this hourly time scale, cross correlation analyses between number of earthquakes and changes in SSH were run for each swarm activity detected.

3.2.3 EARTHQUAKE CLUSTERS

Because of the length of the hourly dataset (58,416 hours between 19 May 1996 and 16 October 2002) and the few number of earthquakes in certain seismic zones, there are many hours with zero events. Thus, it has not been possible to run a time-series cross correlation with the whole dataset. In fact, such attempts were unable to show any correlation (figure 22).

Therefore, individual clusters of earthquakes were identified and isolated. Clusters of earthquakes are defined as groups of earthquakes occurring in a short period of time in the same area. Clusters of earthquakes occurring in temporal proximity were isolated by creating spreadsheets (figure 23) and graphs showed the number of earthquakes recorded in each fault for each hour. Dates were identified whenever there was a variation from the mean seismicity (i.e. more then 5 earthquakes per hour). Then earthquakes for those selected dates were projected on a map using ArcGIS to verify if they happened within a certain distance from each other (~15 km radius, as suggested by Boettcher and Jordan 2005). A new layer containing the final cluster of earthquakes was then created and earthquakes were joined with the corresponding changes in sea surface height using a Matlab routine. After this, the cross correlation analysis was run using another Matlab routine. A bathymetry layer was used to locate particular features on the sea floor that may help to identify the source of the cluster. Diagrams showing the number of earthquakes versus time for all seismic areas are available in the appendix.

Clusters of earthquakes identified and analysed are shown for the transform faults (table 5), for the Galapagos Spreading Center and the East Pacific Rise (table 6), and for

the Middle American Trench (table 7), for a total of 33 clusters. Figure 24 shows the location of the selected clusters in the study area, excluding the subduction zone.

There are three main reasons that may explain why earthquakes happen in a specific area in a short time period. Small earthquakes may happen after a stronger earthquake (mainshock-aftershock) and in this case there will be first an earthquake with a greater magnitude followed by earthquakes with smaller magnitude. Earthquakes with smaller magnitude may precede and follow an earthquake with a bigger magnitude (foreshock-mainshock-aftershock). Also, earthquakes with similar magnitude may occur in swarms, especially in volcanic areas. To distinguish among these different categories, the attribute table available in ArcGIS was used to explore the magnitude of the earthquake and to classify the cluster in the three different categories (figure 25). It is important to differentiate between these different earthquakes when exploring the influence of changes in sea surface height on the sea floor. This is especially true in the case of the strike-slip faults, since it is likely that earthquake afterslip overwhelms the small tidal stress changes (Vidale et al., 1998). Even though researchers have found little correlation between earthquakes and tides, correlations between the tides and the eruption have been identified (USGS, 1998).

Time-series cross correlation was finally run for each identified cluster, for the number of earthquake recorded per hours and the changes in sea surface height obtained from the TMD model.

3.3. DESCRIPTIVE STATISTICS

Descriptive statistics involves organizing and summarizing data, and in my research this is carried out by means of the geostatistical analyst in the Geographic Information System (GIS) framework. Descriptive analysis is important to understand the nature of

the data used and includes the creation of graphs, charts and tables, as well as the calculation of various kinds of statistical parameters.

In order to be able to understand the response of the seismic zone to changes in SSH, it is important to understand the behavior of the seismic area. Therefore, a number of statistical tests and correlations were done. It was also used to seek for possible errors in earthquake selection and therefore represents a tool to filter the data before starting with the inferential analysis.

3.3.1. GIS

GIS represents a dynamic to interact with maps. It is possible to easily define the manner in which information is presented, and locations and/or objects can be used to initiate a query or analysis. The components of a GIS include skilled persons, spatial and descriptive data, analytical methods, computer software and hardware, all organized to automate, manage and deliver information through geographic presentation. Within the GIS map, each dataset comes with an attribute table, where each data point has specific coordinates and can also have descriptions of different fields. For example, each earthquake in the dataset not only has a specific location, but it is also described in terms of timing of arrival and magnitude of event.

The GIS is capable of fast simple statistical analysis applied to the geographical and temporal location of the events. For each seismic zone, histograms were made to explore measures of central tendency (mean and median) and standard deviation. The GIS is also capable of providing normal and general QQ plots, Voronoi mapping, semi-variograms and covariance cloud graphs and cross-covariance for small datasets (<300 points).

3.3.2 GIS USES

In this study, GIS was first used to select earthquakes in the seismic areas of interest. Events for each seismic region were identified and isolated in a separate layer so that it was possible to work and carry out descriptive analysis on each sub-dataset separately. Figures 26 and 27 represent the whole dataset before and after the definition of each seismic region. The whole dataset includes many earthquakes outside the transform faults, errors in location and apparent earthquake events caused by distant earthquakes that were grouped together due to the acoustic properties of the water column.

Visually, the GIS is useful in different ways. By using graduated symbols (e.g. circles of different sizes), it is possible to see where the biggest earthquakes occur. In this way, the geographic position is maintained for each event, and it is possible to add another value from the attribute table to the graphic representation of the data. Classification methods allow us to subdivide the data according to the desired criteria: natural breaks classification (find natural clusters of attribute values); defined interval classification (divides a set of attribute values into classes that are divided by precise numeric increments); equal interval classification (takes the range of values and subdivides them into ranges of equal value intervals); quantitative classification (creates classes with equal numbers of features); and standard deviations classification (creates an even number of classes that represent whole or fractional deviation from a mean value).

Statistically, GIS is able to produce a histogram for any of the subsets for any field present in the attribute table. Figure 28 is an example of a histogram created for the Siqueros transform fault to explore the range of earthquake magnitudes. Information given include: the number of earthquakes in the particular dataset (1479), the lowest earthquake magnitude recorded (magnitude 0.7), the highest earthquake magnitude recorded (magnitude 6.3), the mean and median seismicity (magnitude 2.3), standard deviation (0.9), skewness and kurtosis of the histogram (1 and 3.9). By underlining the column containing information about earthquakes with the higher magnitude (from 5.7 to

6.2), it is possible to see simultaneously on the map where these earthquakes happened. This consists of a first description of the seismic structure of the fault.

GIS is also able to calculate normal and general quantile-quantile (QQ) plot. This is a graphical technique for determining if two datasets come from populations with a common distribution. A 45° reference line is also plotted and if the two sets come from a population with the same distribution, the points should fall approximately along this reference line. The greater the departure from this reference line, the greater the evidence for the conclusion that the two data sets have come from populations with different distributions.

Figures 29 and 30 represent two QQ plots in which the magnitude of events for Discovery and Clipperton, and for Discovery and Quebrada transform faults were compared to each other. As the graphs show, seismic activity on Discovery is more related to that on Quebrada than to that on Clipperton. In a normal QQ plot, the straight line represents what our data would look like if they were perfectly normally distributed: the closer the squares are to the line, the more normally distributed our data look.

A semivariogram, covariance, or cross-covariance cloud depicts all possible pairs of points for a range of lag distances. It is therefore useful to find data points that may represent and error, as it is shown in figure 31 for the Clipperton transform fault. By underlining those values farthest from the average, the corresponding points on the map are highlighted; then by looking at the histogram, it is possible to see what magnitude they are and how they may have affected this dataset. It is now possible to proceed to manual elimination of the irrelevant data.

Datasets with hundreds or thousands of samples should be restricted to smaller domains, to avoid overcrowding the variogram/covariance cloud diagram (GIS default set at 300 points).

3.3.3 ANIMATION

Maps are the principal transmitter of knowledge for a GIS analysis. Maps let people effectively recognize spatial patterns, relationships and trends. By introducing a third dimension, time, to the map of the eastern equatorial Pacific with GIS extension Tracking analyst, it is possible to have an immediate impression of what the data look like, where most of the earthquakes happen, and if there are earthquake clusters. For example, in the animation, it appears clearly that the subduction zone is the most seismologically active area, while Clipperton transform fault has very few earthquakes. Descriptive information is given by changing the color of the earthquake as time passes, with earthquake points being first red, than pink after 10 days, orange after 20 days and disappearing after 30 days.

Although the animation does not have any statistical value in the analysis, it can be a powerful tool for educational purposes.

3.4. INFERENTIAL STATISTICS

Inferential statistics deal with making an educated guess about the characteristics of a population based on a sample from the population. In this research, to investigate possible correlations between the behavior of the oceanic crust in response to changes in SSH of the overlying water column, cross correlation analysis was carried out for the earthquake dataset with respect to the spreading zone, each transform fault and the subduction zone. Variance spectrum analysis was subsequently done to verify at what frequencies correlation was stronger.

3.4.1 CROSS CORRELATION

Cross correlation is a standard method of estimating the degree to which two series are correlated and it determines whether there is a positive, absent or negative linear relationship between two variables. In this case, it describes whether earthquakes are randomly distributed with respect with the periodic changes in SSH or not. An autocorrelation (earthquake data versus earthquake data for the same fault) was also carried in the lunar time scale, to investigate if there was a periodic cycle of events in the fault.

Different cross correlation analyses were carried out in the different time scales to investigate possible correlations between earthquakes and changes in SSH, and to explore possible correlations between seismicity in different zones.

Each seismic area was correlated with the changes in SSH of the water column corresponding to the area investigated. The null hypothesis states that with a value of r = 0 there is no correlation, and when r = +/- 1 there is a perfect positive/negative correlation respectively. For datasets in different time scales, the size of the cross correlation coefficient values necessary to accept or reject the null hypothesis was obtained from tables in a standard statistics text available on line (Bissonnette 2000). The p-value is the probability of getting a correlation as large as the observed value by random chance, when the true correlation is zero and it is a value used to test the hypothesis of no correlation. Small values for p (>0.05) indicate a significant r-value.

Correlation coefficient values were also plotted in a time series analysis for each subsequent time lag in the dataset. Time lagged cross correlation is used to correct for any temporal lag between the changes in SSH and the changes in stress change on the seafloor due to the depth of the water column. The time lag at which the maximum cross-correlation occurs determines the stress transfer of the system (Marechal et al. 2002). Cross correlation values were obtained by running a Matlab routine written by Joe Haxel, PMEL, Newport.

3.4.2. VARIANCE SPECTRUM ANALYSIS

Variance is a measure of the average distance between each of a set of data points and their mean value, equal to the sum of the squares of the deviation from the mean value. The variance spectrum is used to investigate at what frequency the variance deviates from the mean. By running the variance spectrum analysis on two different data sets (earthquakes and changes in SSH), it is possible to see if such data set have similar variation in variance and therefore are more correlated.

Variance spectra were analysed for each fault, using the SSH and the earthquake datasets to see at what frequencies the correlation is strongest. The spectra were used to express the variance as a function of frequency bands. Therefore, in this process, the datasets have been split up into contributions from different frequency bands.

For each seismic zone, three graphs were created, representing respectively the variance of the two datasets, the coherence between the two datasets and the phase. On the x-axis of the three graphs, the frequency "f" represents the number of events for a period of time, or wavelength. Therefore, to determine how many days the frequency represents, it is necessary to divide by 1/f which equals the number of days. For example, $f = 0.01$, is equal to a cycle of $1/0.01 = 100$ days. The graphs have frequencies running from $f = 0$ to $f = 0.035$ (28 days).

The graph on top shows the normalized power spectrum density (Normalized PSD). This is a logarithmic calculation of the variance at any given frequency. A continuous line represents data regarding SSH, meanwhile a dashed line shows earthquake data. The area over a certain frequency represents the level of variance at that particular frequency, therefore, the bigger the area, the greater the variance.

The variance spectra for SSH and number of events per lunar cycle were then compared in each frequency using a coherent square analysis on the second graph. This is a normalized cross-spectral density function and it measures the strength of association and relative linearity between the two processes. The square of coherency lies between 0 and 1. When $Coh^2 = 0$, the processes are independent and there is no linear time-invariant

relationship. Values that pass the confidence level of 0.8 are thought to have a correlation at that frequency. When $Coh^2 = 1$, for a given frequency $f = f_0$ then there is a linear relation between both signals (at the frequency $f = f_0$). When Coh = 1, then the SSH and earthquake events not only have the same frequencies, but are linearly related at these frequencies. The third graph represents the phase in which the correlation happened and has values varying from +180° to –180°. This indicates at what wavelength the correlation is present. The spectral analysis was performed using Matlab7, running a routine generously offered by Prof. Nick Pisias, Oregon State University.

METHODOLOGY: FIGURES

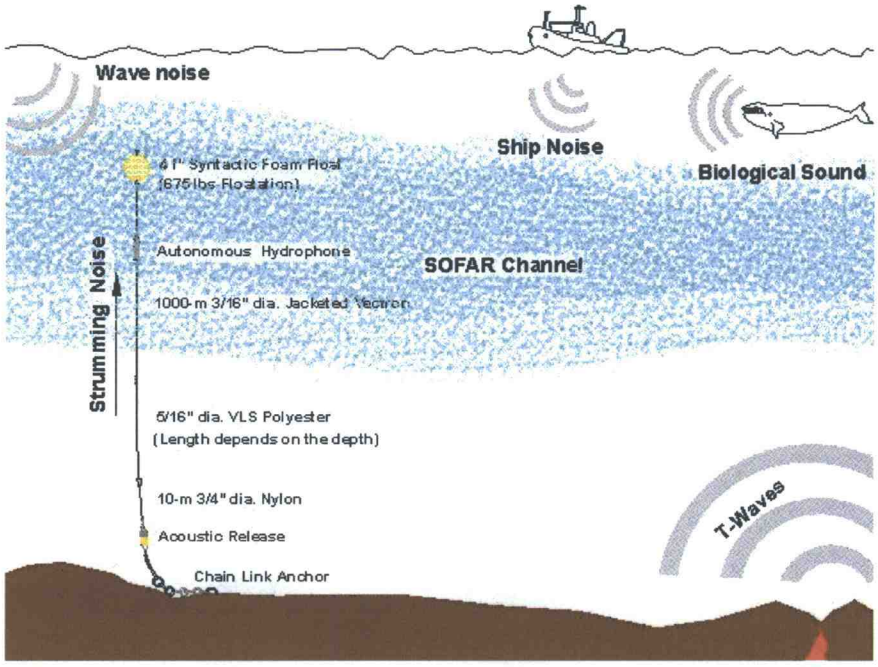

Figure 16: Elements for the data acquisition (Matsumoto 2004).

Table 1: Seismic events on seismic areas.

	# events	Max magnitude	Fault type	Fault length	Normalization (Event/length)
Clipperton	167	4.6	Strike-slip Left	85	1.96
Siqueros	1587	6.27	Strike-slip Right	145	10.9
Quebrada	1146	5.25	Strike-slip Left	130	8.8
Discovery	700	6.02	Strike-slip Left	92	7.6
Gofar	1136	5.38	Strike-slip Left	182	6.2
Yaquina	139	5.12	Strike-slip Left	190	0.7
Wilkes	304	5.12	Strike-slip Left	150	2
Galapagos SR	2990	5.76	Normal	522	5.7
MA	10170	7.55	Thrust	2700	3.7

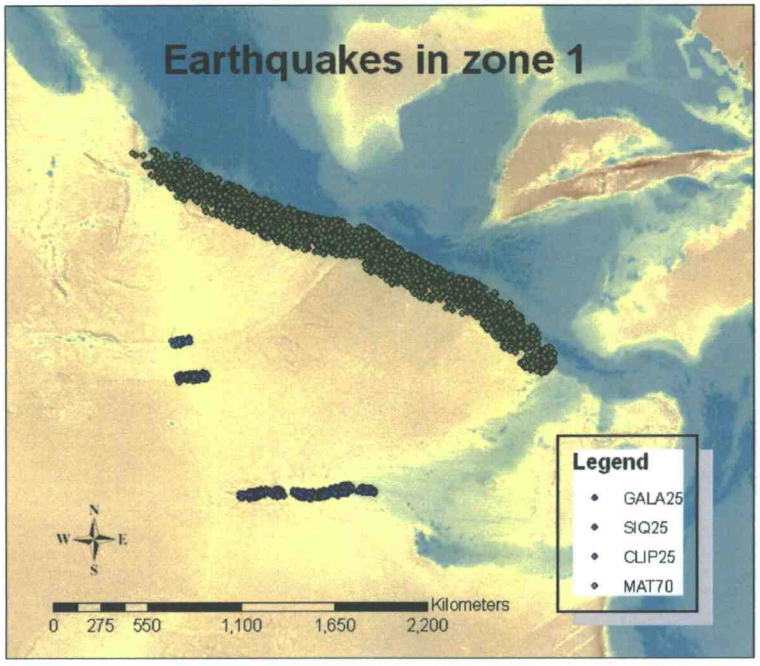

Figure 17: The Earthquake dataset in zone 1.

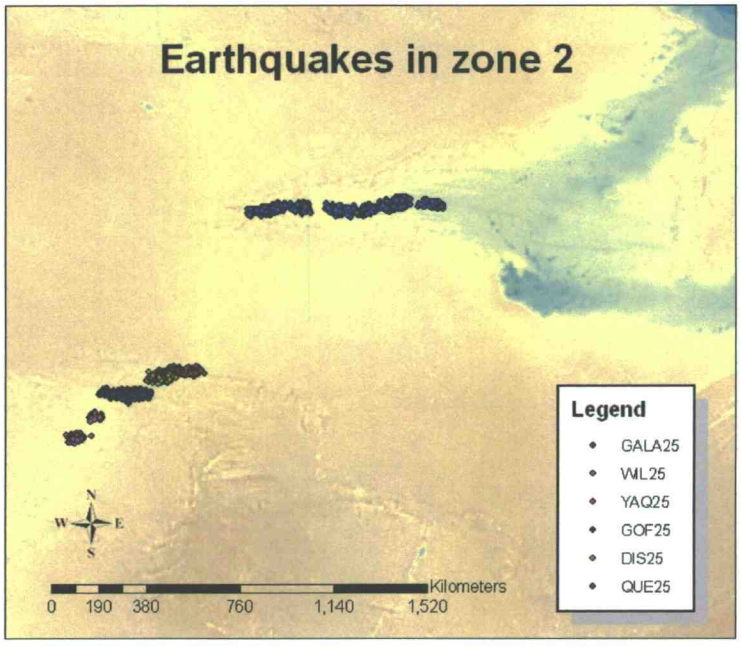

Figure 18: The Earthquake dataset in zone 2.

Table 2: Descriptive parameter of T/P Altimeter.

Resolution	Error	Size
Spatial	Some area +/-1km	0.5°*0.5° grid
Temporal		Every 10 days
Orbit height	2 cm rms	1336 km

Table 3: Extreme coordinated values for the areas of averages SSH/ fault.

	North	East	South	West
Clip-Siqueros	12	-100	7	-106
Que-Dis-Gofar	-2	-110	-7	-100
Yaquina	-6	-105	-12	-112
Wilkes	-10	-108	-16	-115
Subduction	+18	-85	7	-113

Table 4: Locations chosen to obtain the tidal data from the TMD.

	Latitude	Longitude
Siqueros -Clipperton	+8.677	-104
Middle American Trench	+15.14	-95
Galapagos Spreading Ridge	+1.995	-100
Quebrada-Gofar-Discovery	-3.94	-104
Wilkes-Yaquina	-9.7	-110

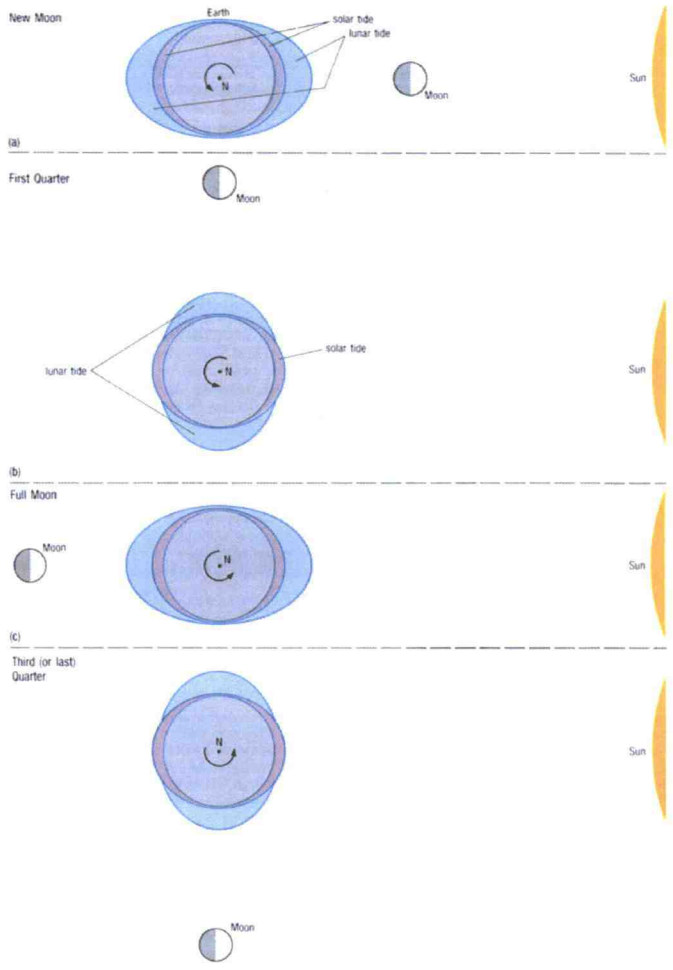

Figure 19: Moon cycles and tidal influence on the Earth.

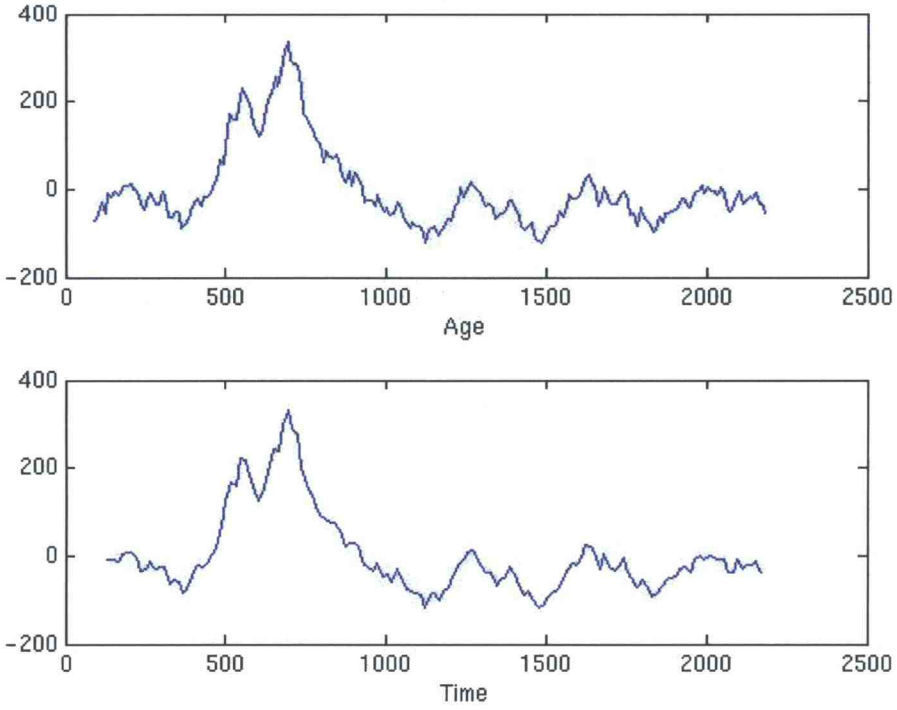

Figure 20: Time interpolation from 10 days data to 7.48 days. Time is in days in the x-axis, and SSH values are in cm in the y-axis.

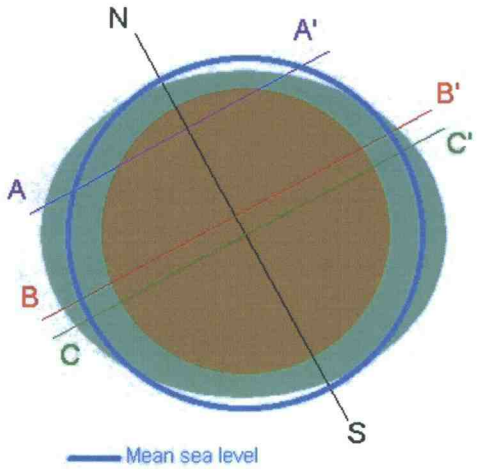

Figure 21: Tidal pool at different latitudes.

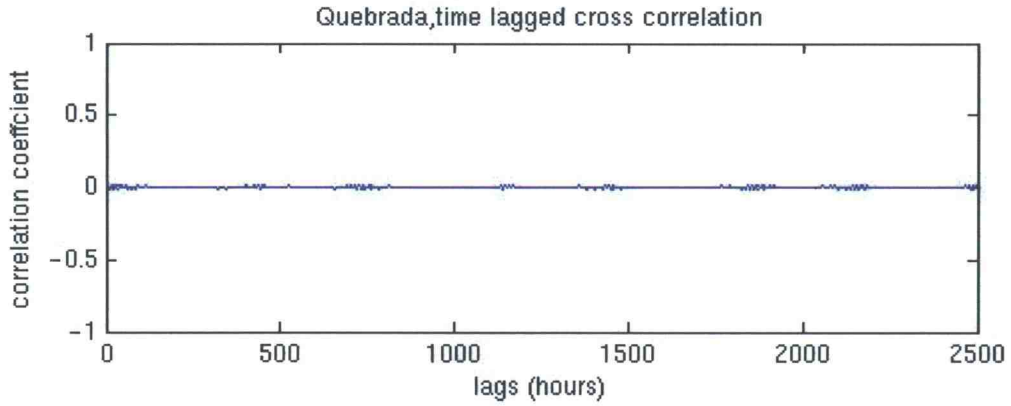

Figure 22: Cross correlation using the whole dataset.

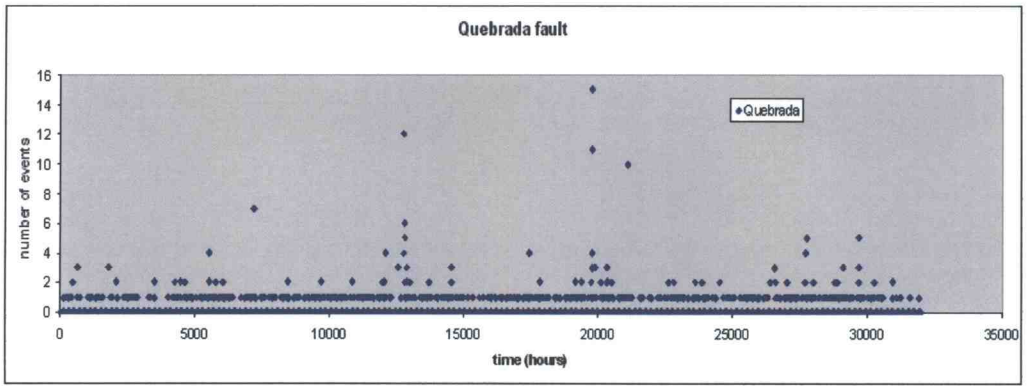

Figure 23: Number of earthquakes versus time per the Quebrada fault. The swarms were identified as variation from the usual seismicity.

Table 5: Clusters of earthquakes identified on the transform faults.

	Date	# Earth-quakes	Length (hours)	Latitude	Longitude
Siqueros	26-27 April 2001	113	24	8.424	-103.558
	10 May 1998	167	48	8.442	-102.952
Quebrada	2 November 1997	58	40	-3.781	-103.547
	21 August 1998	34	13	-3.76	-103.59
	16 October 1998	14	8	-3.826	-103.7
Discovery	16 October 1998	28	15	-4	-104
	26 June 2001	25	9	-3.9	-104.4
Gofar	15 August 1997	37	17	-4.5	-106
	18 September 1999	27	21	-4.5	-104.7
Wilkes	10 November 1999	45	13	-6.199	-107.284
Yaquina	27 May 1999	76	26	-5.4	-106.521

Table 6: Cluster of earthquakes identified on normal faults

	Date	# Earth-quakes	Length (hours)	Latitude	Longitude
Gala1	31 October 1996	16	16	2.116	-100.4
Gala2	7 April 1997	28	24	2.217	-100.37
Gala3	31 July 1997	26	10	2.22	-100.226
Gala4	27 December 1998	18	7	2.116	-100.4
Gala5	9 January 1999	13	7	2.208	-100.2
Gala6	10 August 1997	25	24	2.3	-95.4
Gala7	11 January 1998	18	24	2	-97.5
Gala8	22 May 1998	24	24	2.1	-97.7
Gala9	30 August 1998	315	120	2.1	-97.6
Gala10	22-23 September 1998	68	48	2.132	-97.48
Gala11	16 September 1999	35	24	2.151	-96.58
Gala12	22 December 1999	26	24	2.3	-95.6
Epr1	2 March 2001	27	12	8.695	-104.224
Epr2	28 July 1999	24	12	7.238	-102.697
Epr3	27 May 1996	50	48	3.435	-120.211

Table 7: Cluster of earthquakes identified on thrust faults

	Date	# Earth-quakes	Length (hours)	Latitude	Longitude
Mat1	16 July 1996	20	24	17.5	-101.2
Mat2	19-25 July 1997	120	48	15.891	-98.5
Mat3	3-4 February 1998	28	24	15.823	-96.5

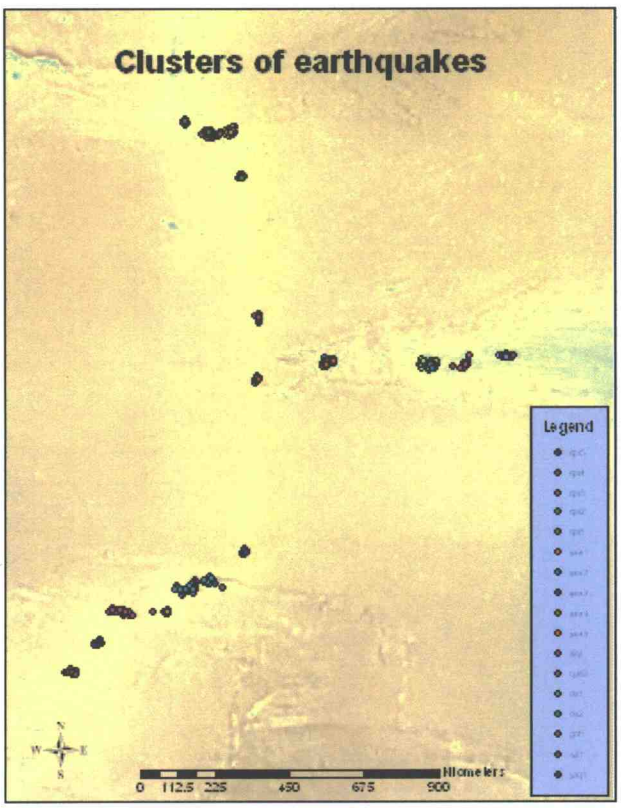

Figure 24: Location of clusters of earthquakes.

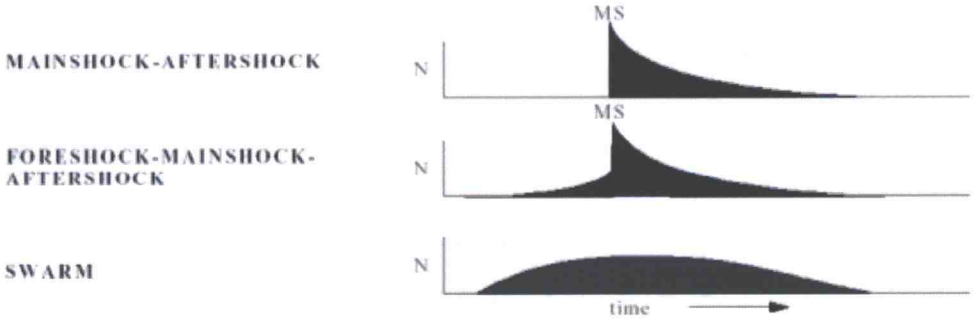

Figure 25: Different causes for earthquake's clusters (MS = Main Shock). (Benoit and McNutt 1996).

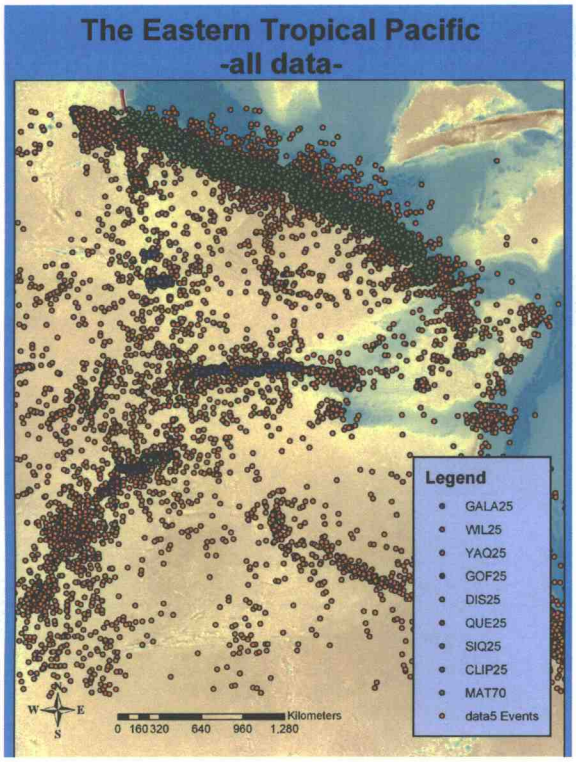

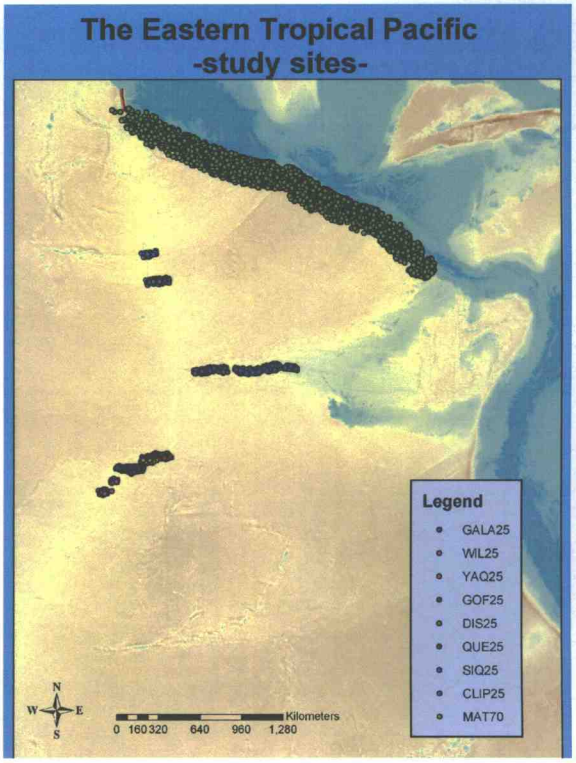

Figure 26 and 27: The dataset before and after the selection to separate the specific seismic zones. The area in green on the right side is the coast of South America. Central America occupies the top part of the map.

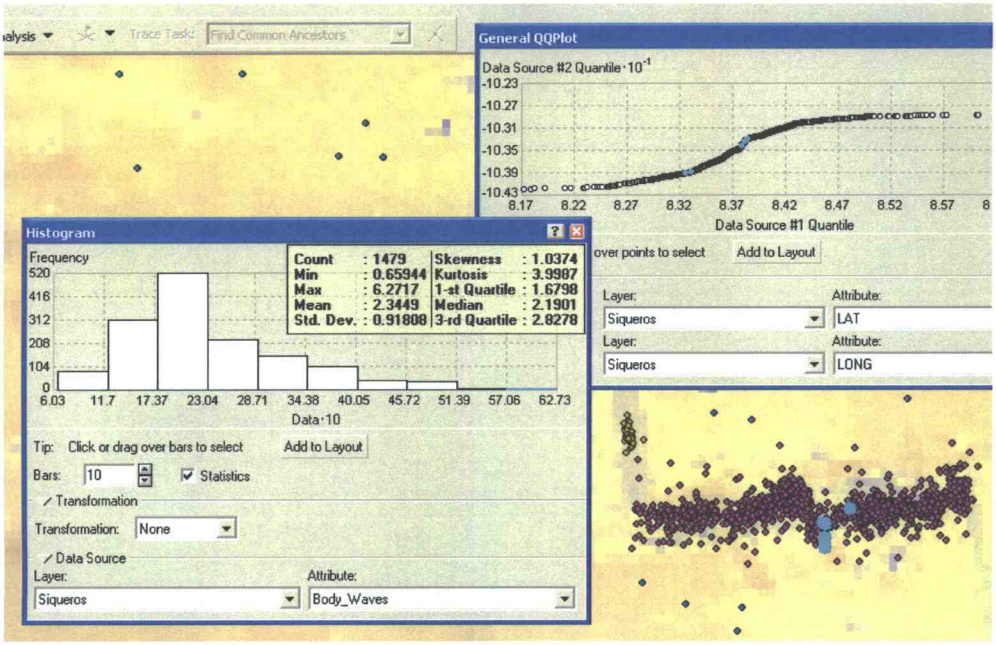

Figure 28: Histogram containing magnitude information for Siqueros fault. Earthquake with M>5.7 were selected. The selection is also visible on the map and on the QQPlot (blue points).

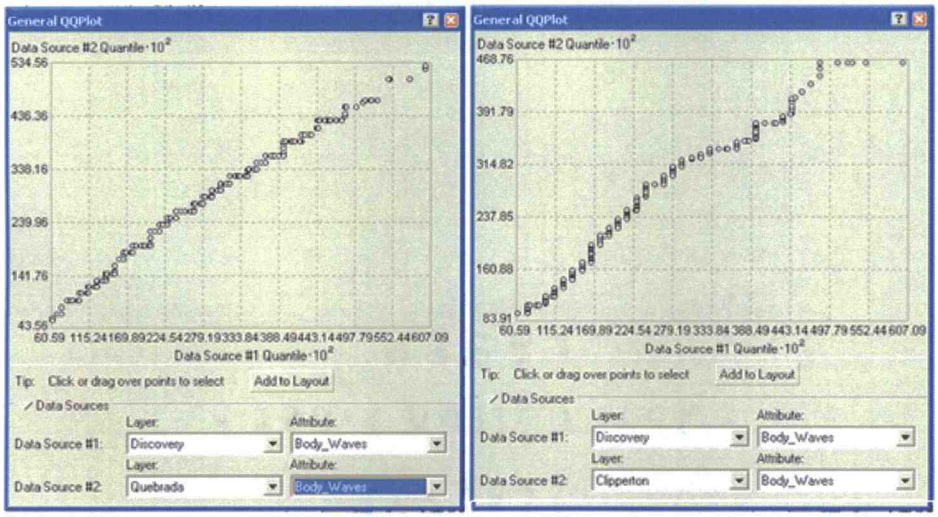

Figure 29 and 30: General QQ plot for Discovery and Quebrada and Discovery and Clipperton.

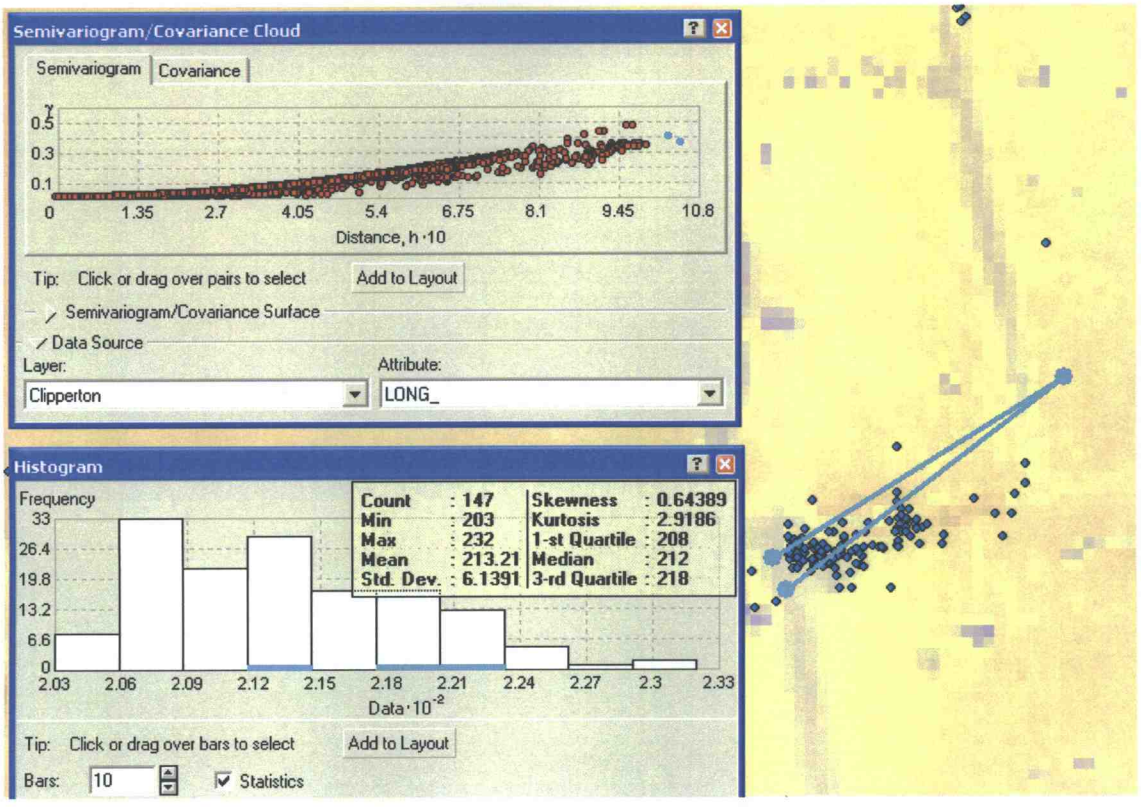

Figure 31: Semivariogram for the Clipperton fault. The further most points underlined in blue on the right side of the semivariogram probably represent an error in data selection, as also visible in the map. Magnitude of these points is shown in underlines in the histogram.

4. RESULTS & DISCUSSION

The following chapter describes the results obtained in the descriptive and in the inferential analysis (cross correlation analysis and variance spectrum analysis) for the two time scales used, and discusses the possible causes for such results. Graphs with results of the time-series cross correlation and the variance spectral analysis for each seismic area in the two time scales are available in the Appendix. Cross correlation coefficient values vary depending on the length of the dataset used. Critical values needed to reject the no correlation hypothesis are summarized in table 8 for convenience. An "a" value indicates correlation at a 99% confidence interval meanwhile a "b" value indicates a correlation at 95 % confidence interval.

4.1. DESCRIPTIVE STATISTICS

Data regarding each seismic zone were grouped to create tables summarizing information obtained from literature review, descriptive statistics made with GIS and results from inferential statistics (tables 9 and 10). The low seismicity in the Clipperton transform fault confirms the study of Gregg et al. (2004), which found that the fault is in a period of low seismicity. The two southernmost transform faults, Yaquina and Wilkes, have a larger average magnitude compared with the other faults in zone 2 (the average magnitude on the Nazca-Pacific plates increases going south), but when compared with the average magnitude of the two faults in zone 1, Clipperton and Siqueros, the difference in average magnitude is not significant.

4.2 MOON QUARTER TIME SCALE

Four different tests were made on the quarter moon time scale to look for correlation between SSH and earthquakes, autocorrelation, correlation between faults and correlation between each fault's seismicity and its average event magnitude.

4.2.1 CROSS CORRELATION: SSH AND EARTHQUAKES

Time-series cross correlation between the seismic zones and the changes in SSH obtained by T/P satellite show mostly no correlation. Even though some correlation is present, values are often at the threshold level, and therefore they do not represent definitive results (table 11). The strongest correlation between changes in sea surface height and number of earthquakes is in the Middle American Trench, with a total correlation coefficient value of 0.3079 and p-value of 0 (the value to reject the null hypothesis is 0.160 with 99% confidence interval in this case). The correlation increases in the subsequent 10 time lags (73 days), and then it decreases. It is important to consider correlation values at different time lags to be able to include the time necessary for the effects of changing sea surface height to reach the sea floor. It has to be noted that the Middle American Trench has the most reliable statistics since its dataset has the highest number of earthquakes recorded. The Middle American Trench is more likely to be affected by changes in SSH than transform faults since the fault motion is vertical and not horizontal (Yeats et al. 1997) and also it appears that at this time scale, the deformation of the lithosphere due to the earth tide may help the earthquake triggering process.

A correlation was also expected for the GSC, given that this kind of fault (normal) is most affected by vertical stresses. In this research, the results cannot confirm that earth tides are strong enough to work as a trigger mechanism for earthquakes in normal faults.

4.2.2 AUTOCORRELATION

Autocorrelation between faults was carried out to look for the presence of cycles in the fault's seismicity. Given the time scale used, the presence of a seismic cycle may indicate an influence from the moon's gravitational field. Results showed values on the threshold line in 5 of 9 cases, generally after 20 time lags. The correlation coefficient values obtained were not big enough to represent a significant result and therefore the hypothesis that there is a periodic pattern on a moon's quarter times scale, can be rejected.

4.2.3 CROSS CORRELATION BETWEEN FAULTS

Cross correlation analysis between faults was carried out to investigate the possibility of similar behavior between faults that may indicate a similar response to a regional change. The results are shown in table 12, with obtained r-values written in the upper right side of table and p-values written in the lower-left side of the table.

A very weak correlation between seismic areas was present for some faults (table 12). However, most of these correlations were close to the threshold level and never showed significant peaks. The only exception is given by the time-series cross correlation analysis between Discovery and Quebrada transform faults. These two faults show the strongest correlation, with positive peaks approximately every 50 time lags (10 months) and a correlation coefficient reaching 0.618 with p-value of 0 (figure 35).

Discovery and Quebrada are two transform faults in zone 2 that are located very close to each other. Correlations in earthquake event peaks may indicate that these faults slip at the same time, and therefore in this area the plate is moving rigidly. Their common seismicity may indicate that on a small spatial scale (the two faults are ~35 km apart), the plate moves rigidly, meanwhile the lack of correlation between the other faults indicates that on a bigger spatial scale, the plate is moving more elastically. The Quebrada and the

Discovery transform faults also had a similar cluster on the 16th of October 1998, as later shown in the hourly-based analysis.

The variance spectrum analysis of these two faults shows that correlations are present on different frequencies, and that earthquakes on the faults happen randomly through time not being correlated to any specific lunar phase.

4.2.4. CROSS CORRELATION: NUMBER OF EVENTS VERSUS AVERAGE MAGNITUDE

The following test was carried to seek a relationship between the number of events recorded per cycle and the average magnitude. Gutenberg and Richter have in fact found that the number of earthquakes of magnitude M is proportional to 10^{-bM} (Gutenberg-Richter law). The line gives the Gutenberg-Richter prediction (b) is given by the slope of the line drawn after plotting the log of number of earthquakes against magnitude. The value of b seems to vary from area to area, but worldwide it seems to be around b=1. (SimScience 2005). If the result is positive, then I may assume that the time scale used is not totally random and does have an effect on the occurrence of the earthquakes themselves. Correlation coefficient values are shown in table 13.

Correlation between the number of earthquakes and the average magnitude was present in all the transform faults but Discovery, while both the subduction zone and spreading center showed no correlation. These results suggested that the time scale used was appropriate for the events in the transform faults, meanwhile possible cycles in normal and thrust faults may not follow the lunar cycle.

4.3. HOURLY TIME SCALE

Time-series cross correlation analyses were carried out for clusters of earthquakes happening within the study area. The clusters are due to either after-shocks or fore-

shocks, and to swarms of earthquakes correlated to volcanic activities. The number of earthquakes was counted and grouped by hour, beginning one hour before the start of the cluster and finishing when the earthquake activity diminished to the normal levels. The following section describes individually the results obtained for normal faults, strike-slip transform faults and thrust faults.

4.3.1. NORMAL FAULTS (Galapagos Spreading Center)

Normal faults should be the most sensitive to changes in sea surface height since the main stress acting on them is the vertical stress. Fifteen clusters happening within a 15 km radius were identified and analysed. Correlations with sea surface height were found in 8 of 15 cases, of which 5 of 8 were positively correlated and 3 of 8 were negatively correlated. This indicates that earthquakes have more or less the same chance to happen in either low or high tide. Results are summarized in table 14. "+" sign indicates positive correlation or higher sea surface height, while "-" sign indicates negative correlation or lower sea surface height. The sign "->" means "going to" and it is used for those earthquakes happening in transitional periods from one moon phase to another.

The strongest correlations were usually found within one or two time lags. The two strongest correlations happened in the Galapagos Spreading Center in the same location (-100.4°W, 2.116°N), the swarm on the 31st of October 1996 (r = -0.9294), and the swarm on the 27th of December 1998 (r = 0.8467). In both cases, the first events happened in periods of low sea surface height, with subsequent peaks in earthquake activity during higher sea surface height (figures 36-37). Strong correlations were also found for the clusters on the 9th of January 1999 (r= 0.6603) and on the 22nd of May 1998 (r=0.7009) (figures 38-39). The magnitude of the earthquakes was usually low, varying from 0.6 to 4 in most cases. Clusters happening the 22nd of May 1998, 30th of August

1998 and the 22nd of December 1999 had single events with magnitude from 4.8 to 5.1, followed by earthquakes with lower magnitude.

Comparing the dates in which the clusters happened with the phase of the moon, no correlation with changing moon phase were found: 4 of 15 clusters were found either during full moon (3 clusters) or during new moon (1); 5 of 15 clusters happened during moon's quarters (4 first quarters, 1 last quarter); 3 of 15 clusters happened during increasing periods of moon's attraction (2 from last quarter to new moon, 1 from first quarter to full moon); 3 of 15 clusters were found during decreasing moon phase (2 from new moon to first quarter, 1 from full moon to last quarter). This indicates that earth tides created by the change of the gravitational pull of the moon do not have a significant contribution in the triggering of earthquake clusters when grouped on an hourly basis.

Tidal changes in sea surface height showed instead some correlations with earthquake clusters. In 13 of 15, the first earthquake happened during a period of lower sea surface height, when the constraining vertical stress is at its minimum. Subsequent peaks in earthquake activities happened in periods of lower sea surface height in 8 of 15 cases and in periods of height sea surface 9 of 15 cases (some clusters had more than one peak). Results showed therefore that peaks in earthquake activity during a cluster do not have any preference for lower or higher sea surface height, but that the first earthquake of the cluster may be influenced by these changes.

Clusters which occurred on the 22nd of May 1998 (figure 38) and the 9th of January 1999 (figure 39), also showed positive correlations. In the case of the 22nd of May 1998, most earthquakes happened when the sea surface height was at the lower level. For the 9th of January 1999, the first earthquakes happened when the sea surface height was lower, but most of the earthquakes happened at higher sea surface height.

Along the East Pacific Rise no correlation was found, although, in three cases, the first earthquake happened towards periods of low sea surface height. In general, in normal faults, changes in sea surface height seems to play a role in earthquake triggering

when the sea surface height is lower and therefore the constraining vertical force is also at minimum.

4.3.2 TRANSFORM FAULTS (Fracture Zones)

Eleven clusters were identified along the transform faults in the study areas. In 9 of 11 cases, the magnitude of the events is not constant, and earthquakes of smaller magnitude usually follow one to three earthquakes with larger magnitude. Therefore, these clusters identified are due to shocks and aftershocks, or foreshock- shock-aftershocks. In these cases, the horizontal stress should be more important than the vertical stress and changes of sea surface height are less influential for the accumulation and release of energy during a previous earthquake. The role of the confining pressure given by the sea surface height may be more important only for the main shock. The majority of the events did happen during period of high tide (5 of 11 cases) and low tide (6 of 11 cases), rather than during transitional times. Correlation with sea surface height was present in 8 of 11 cases, all with a time lag of about 5 hours. Negative correlation during this time happened in 3 of 8 cases, meanwhile 5 of 8 cases showed a positive correlation. Table 15 summarizes the results obtained for the transform faults.

In transform faults, moon phases did not seem to play an important role as a triggering mechanism for earthquakes. In 2 of 11 cases the clusters happened when the gravitational pool was at maximum (full and new moon). In 2 of 11 cases the clusters happened during the first quarter. In 5 of 11 cases the clusters happened in increasing gravitational pull (3 from new moon to first quarters, 2 from third quarter to full moon), while in 3 of 11 cases the clusters happening in periods of decreasing pull (3 from new to first quarter). Therefore, in transform faults as for normal faults, earth tides do not have a significant contribution in the triggering of earthquake clusters.

Earthquakes in transform faults seem to be uncorrelated with changes in sea surface height. In 4 of 11 cases the first earthquake happened during high sea surface height,

while 4 of 11 happened in low sea surface height. 3 of 11 earthquakes happened during periods of increasing sea surface height. Following peaks in events happened 5 of 11 times in high sea surface conditions, while 6 of 11 in low sea surface height. Changes in sea surface height did not appear to play a particular role in the earthquake triggering process.

In two cases, it was possible to observe a migration in events from one side of the fault to the other. In Siqueros on the 10th of May 1998, 166 events occurred within 48 hours, following a major event. The cluster occupies the easternmost 55 km of the fault, with the main shock (magnitude = 5.2) followed by low magnitude earthquakes around the area and other bigger earthquakes migrating westward. This was an example of lateral stress transfer along the first half the fault, starting from east, going west and it was probably correlated with an episode of slip along the eastern side of the fault (figure 40). The western side of the fault did not show any cluster during the time scale included in this study. There was not any significant correlation between earthquake events and changes in sea surface height. Figure 40 shows the location of the cluster, the black arrows indicate the direction of movement of the Cocos and Nazca plates and the blue arrow shows the direction of migration of the earthquakes during the 48 hours. The blue dot shows the location of the main earthquake. The red line underlines the location of Siqueros fault. In the case of the Quebrada fault, 21st August 1998 cluster, the migration of the earthquakes seemed to be to the east (the opposite of Siqueros) (figure 41): Quebrada is in fact a right-lateral fault, while Siqueros is a left-lateral and therefore their stress transfer acts in opposite directions. In Quebrada's cluster, 34 earthquakes happened in a 24 km radius within 13 hours. The first main shock with magnitude 5 (earthquake #5) and the two subsequent stronger earthquakes (earthquake #10, magnitude 4.6; and earthquake #22, magnitude 4.2) happened during high sea surface height, the first happening on the western side of the fault and the subsequent two happening to the east. All the remaining earthquakes have a magnitude of 1 to 2.

The two cases described above are examples of shock and aftershocks in which there is a stress transfer in the x direction. There was not any significant correlation with changes in sea surface height. Another example of mainshock-aftershock earthquakes with event migration to the east is represented by the left-lateral Discovery fault on 26th June 2001, where 25 earthquakes happened in a 35 km radius within 9 hours. This main shock (earthquake #3, $M_w = 6$) happened during decreasing sea surface height.

In the Yaquina fault, on the 27th of May 1999, 76 earthquakes happened in 26 hours. These earthquakes have low magnitude ($M_{max} = 3.9$) and they happened randomly with no apparent migration. The earthquake activity started with a peak in low sea surface height and continued through the next two tidal cycles. Correlation with changes in sea surface height is stronger than in other clusters, but still not significant (figure 42).

Generally, although some cluster of earthquakes showed a correlation with sea surface height in the first hours (especially after 5 time lags), the correlations between number of events and changes in sea surface height were not significant.

4.3.3 THRUST FAULTS (Subduction Zone)

Three different clusters were identified and analyzed in the Middle American Trench. No significant correlation was found between the numbers of earthquakes and the changes in sea surface height. Figure 43 shows the location of Mat1 and Mat2, with the first earthquakes underlined in blue.

In the three clusters selected, the first earthquake happened deeper in the subduction zone where the subducting crust is dehydrated as a result of increasing pressure and heat. This is the location where other, stronger earthquakes happened. Subsequent earthquakes with lower magnitude happened up-dip along the downgoing slab toward the sea, with most of the earthquakes being just underneath the trench. Therefore, there was a general tendency of earthquakes to migrate from the deeper subducting crust toward the trench. This may indicate that the first movement of the place occurred deeper in the subducting

slab, followed by shallower earthquakes. Another explanation of this observed phenomena it is that earthquake-generated waves produced deeper in the subducting oceanic slab have to travel thought the crust before being radiated into the ocean and being trapped into the SOFAR channel. This may produce errors in timing and location.

The sample set of earthquakes used for the subduction zone plate boundary is very small and therefore results obtained cannot be considered definitive. The results show no significant correlation. In 2 of 3 cases, the first earthquake happened in a period of low SSH: in one case the gravitational pull from moon and sun were at maximum, while in the other case the pull was decreasing. In the third case, the first earthquake happened in increasing SSH, in a period of increasing moon attraction. However, correlation with sea surface height is not probable, since the first stronger earthquake happened deeper in the crust, in regions that are not directly affected by the height of the water column. It is more probable that earth tides will exercise a major influence as triggering mechanism: 2 of 3 clusters happened when the moon pull was at maximum (1 full moon and 1 new moon) while 1 of 3 happened during a period of increasing pull (from first quarter to full moon). Figures 44-47 show examples of the results obtained from the cross correlations. The findings confirm the results obtained in cross correlation analysis ran every lunar cycle, in which the subduction zone appeared to have the stronger correlation with earth tides.

RESULTS & DISCUSSION: FIGURES

Table 8: Correlation coefficients values necessary to reject the null hypothesis for the two timescales used.

	Length dataset	r-value (0.5 error)	r-value (0.01 error)
Earth tides	276 cycles	~0.120	~0.160
Ocean tides	120 hours	0.179	0.234
	48 hours	~0.300	~0.390
	24 hours	0.404	0.515

Tables 9: Summary of all information gathered for the different seismic zones in zone 1.

	Clipperton	Siqueros	Subduction	GSC
Length (km)	85	145	2500	1075
Fault type	Transform Lx	Transform Rx	Thrust N-W	Normal N-S
Spreading rate upper*	10.5	10-11	8	4.4-5.2
Spreading rate lower*	10-11	12.3		
# of events	167	1587	10170	2990
M_{max}	4.6	6.3	7.3	5.8
M_{ave}	2.22	2.35	2.7	2.01
Segments	single			
Plates	Cocos-Pac	Cocos-Pac	Coc-MidA	Cocos-Naz
Topography & other	Low seismicity period		Max depth = 6.67 km Ring of Fire	

*Spreading rates are in cm/year, from http://www.ldeo.columbia.edu/users/menke/plates.html

Tables 10: Summary of all information gathered for the different seismic zones in zone 2.

	Quebrada	Discovery	Gofar	Yaquina	Wilkes
Length	130	92	182	190	150
Fault type	Transform Lx	Transform Lx	Transform Lx	Transform Lx	Transform Lx
Spreading rate upper *	13.5	13.5	13.5	14.2	14.5
Spreading rate lower*	13.9	13.9	14.1	14.5	14.7
# of events	1146	700	1136	139	304
M_{max}	5.2	6	5.4	5.9	5.3
M_{ave}	2.09	2.13	2.14	2.27	2.39
Segment	Multiple segments. Intra-transform spreading centers				
Plates	Naz-Pac	Naz-Pac	Naz-Pac	Naz-Pac	Naz-Pac
Topography & Others					Only 100 km are seismisically active

*Spreading rates are in cm/year, from http://www.ldeo.columbia.edu/users/menke/plates.html

Table 11: r-values and p-values for cross correlation between SSH and earthquakes on a moon's quarter timescale. r-value used to reject the null hypothesis of no correlation r = 0.160 (0.01 confidence level); r = 0.120 (0.05 confidence level).

	r-value	p-value
Clipperton	0.0034	0.9553
Siqueros	0.1095	0.0699
GSC	0.1325a	0.0280
MAT	0.3079a	0
Quebrada	0.1146	0.0576
Discovery	0.0120	0.8430
Gofar	0.1604a	0.0077
Yaquina	0.0263	0.6639
Wilkes	0.0262	0.6649

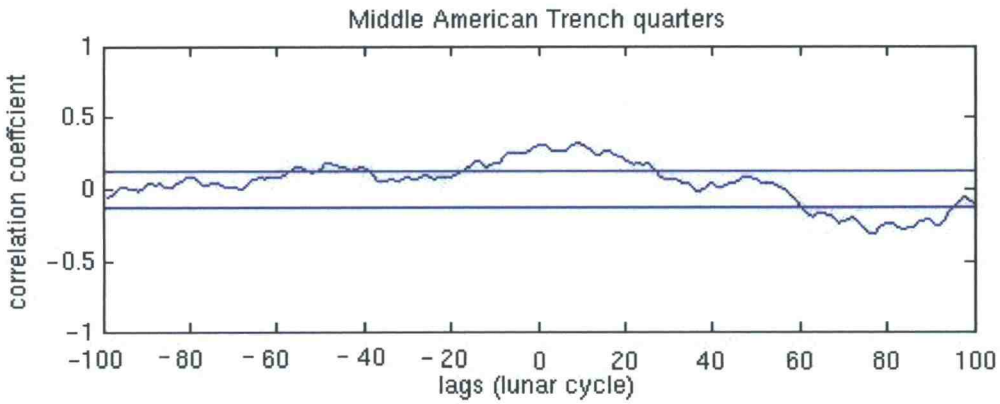

Figure 32: Time series cross correlation analysis for the middle American trench. The value 100 on the x-axis actually represents 0 lags, with increasing lags to the right and decreasing lags to the left.

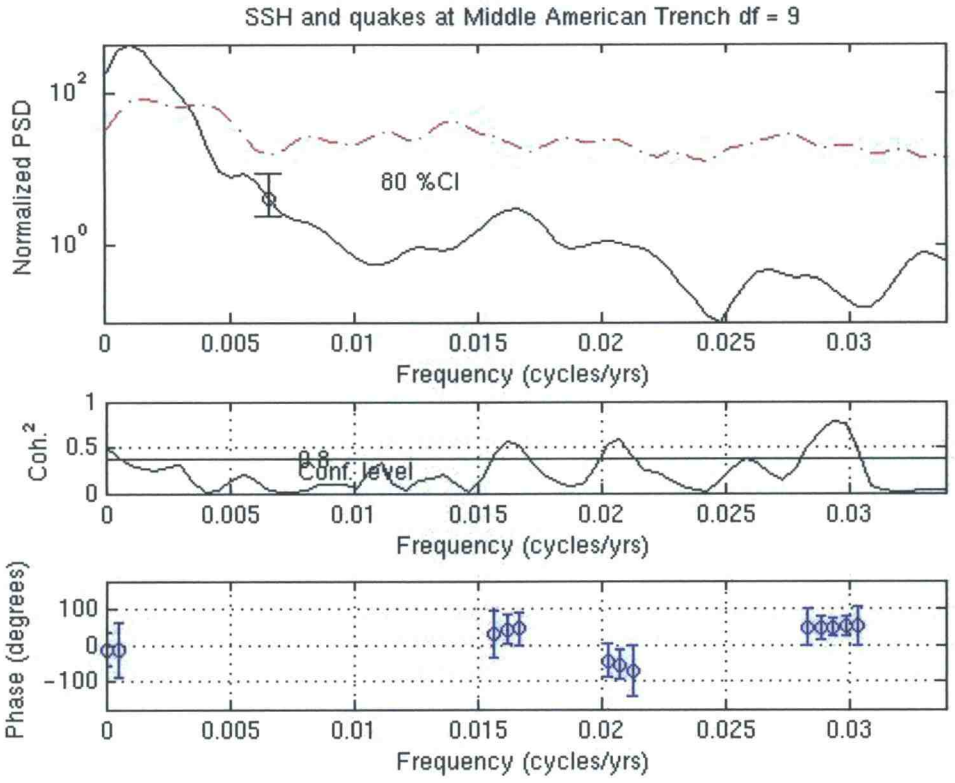

Figure 33: Variance spectrum for MAT, lunar timescale at 0 lags.

Table 12: Time series cross correlation coefficient between faults. r-value to reject the null hypothesis of no correlation r = 0.160 (0.01 confidence level); r = 0.120 (0.05 confidence level). Values on the upper right side represent r-values; values on the lower left side represent p-values.

	Oro	Clip	Siq	Que	Dis	Gof	Yaq	Wil	Sub	GSC
Oro	1	.081	.059	-.009	.013	.059	.007	-.029	.05	.102
Clip	.18	1	.045	-.043	-.025	-.039	-.019	.018	.051	.146b
Siq	.329	.462	1	.021	.004	.0315	-.021	-.047	.121b	.036
Que	.883	.474	.727	1	.618a	.155b	.02	.1107	.188a	.0117
Dis	.831	.675	.949	0	1	-.012	-.045	.064	.971	-.008
Gof	.328	.675	.949	.01	.845	1	.0289	.084	.169a	-.002
Yaq	.905	.075	.725	737	.454	.633	1	.204a	.076	.0042
Wil	.634	.768	.432	.096	.29	.165	.0006	1	.191a	-.004
Sub	.402	.399	.045	.002	.108	.005	.209	.001	1	.109
GSC	.093	.016	.549	.847	.89	.976	.945	.807	.07	1

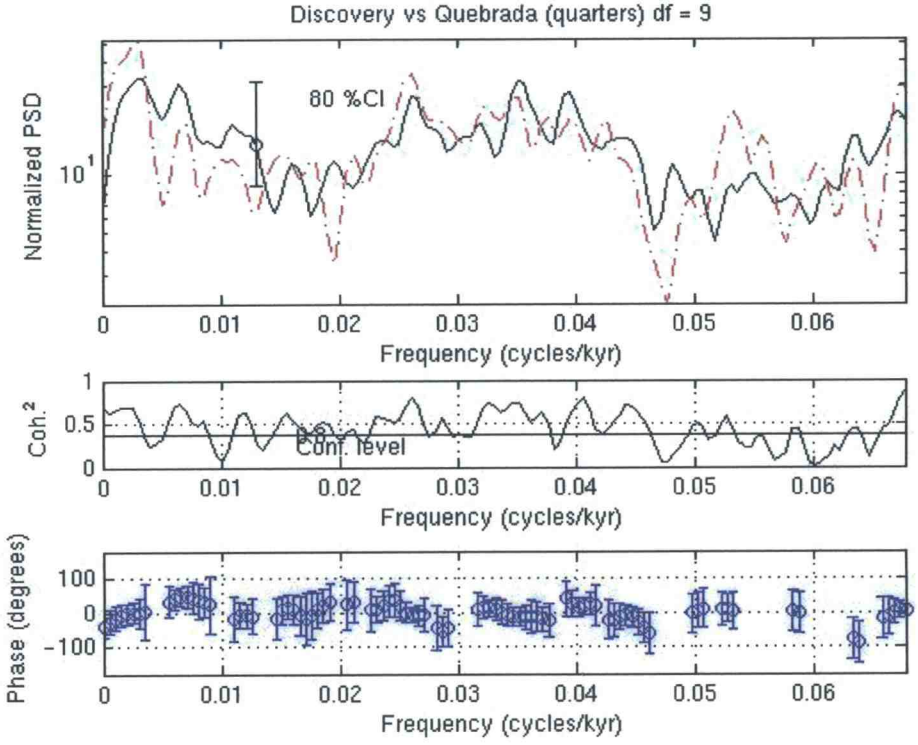

Figure 34: Variance spectrum for Discovery and Quebrada faults at 0 lags.

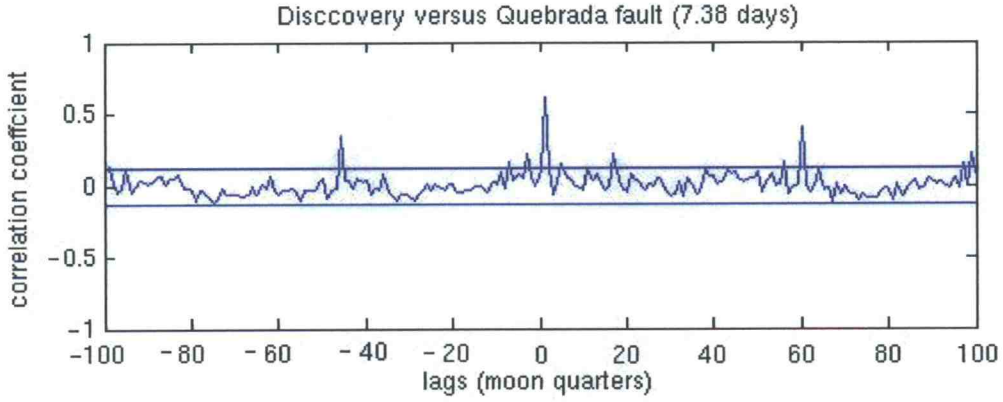

Figure 35: Time series cross correlation between Discovery and Quebrada transform faults. The value 100 on the x-axis actually represents 0 lags, with increasing lags to the right and decreasing lags to the left. Peaks are present at 50 (-50) and 160 (+60) lags.

Table 13: Correlation coefficient values for earthquakes versus average magnitude. r-value to reject the null hypothesis of no correlation r = 0.160 (0.01 confidence level); r = 0.120 (0.05 confidence level).

	r-value	p-values
Orozco	.4935a	0
Clipperton	.6911a	0
Siqueros	.1773a	.0033
Quebrada	.2504a	0
Discovery	-.0137	.8224
Gofar	.3025a	0
Yaquina	.1246b	.04
Wilkes	.4081a	0
Subduction	.0703	.2481
Galapagos	.1	.0998

Table 14: Clusters in normal faults.

	Date	Correlation (5 time lags)	Tidal phase when the 1st earthquake occurred	Moon phase
Gala1	31 October 1996	+	-	○ to ◑
Gala2	7 April 1997	-	-> -	●
Gala3	31 July 1997	No	-	◐ to ●
Gala4	27 Dec. 1998	+	-	◐
Gala5	9 January 1999	+	-	◑
Gala6	10 August 1997	No	-	◐
Gala7	11 January 1998	No	-> +	○
Gala8	22 May 1998	+	-	◐ to ●
Gala9	30 August 1998	+	-	● to ◐
Gala10	22-23 Sept. 1998	-	+	● to ◐
Gala11	16 Sept. 1999	No	-	-> ◐
Gala12	22 Dec. 1999	-	-	○
Epr1	2 March 2001	No	-	◐
Epr2	28 July 1999	No	-	○
Epr3	27 May 1996	No	->-	○ to ◑

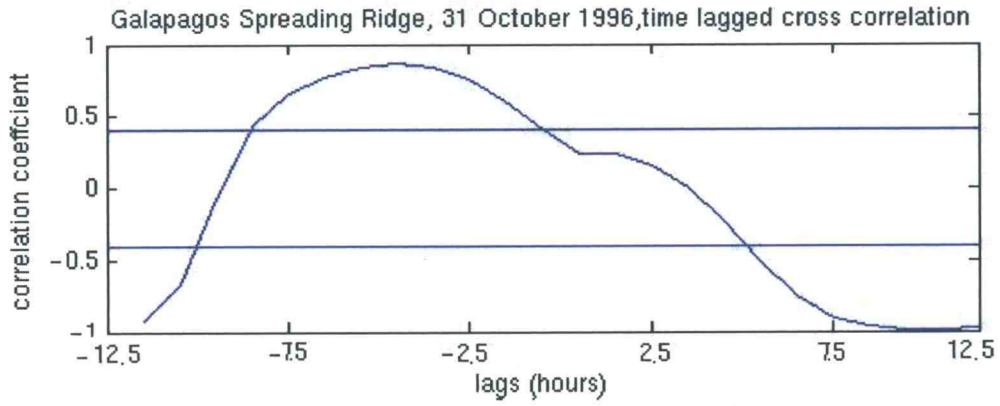

Figure 36: Cross correlation in GSR, earthquakes on 31 October 1996 versus SSH.

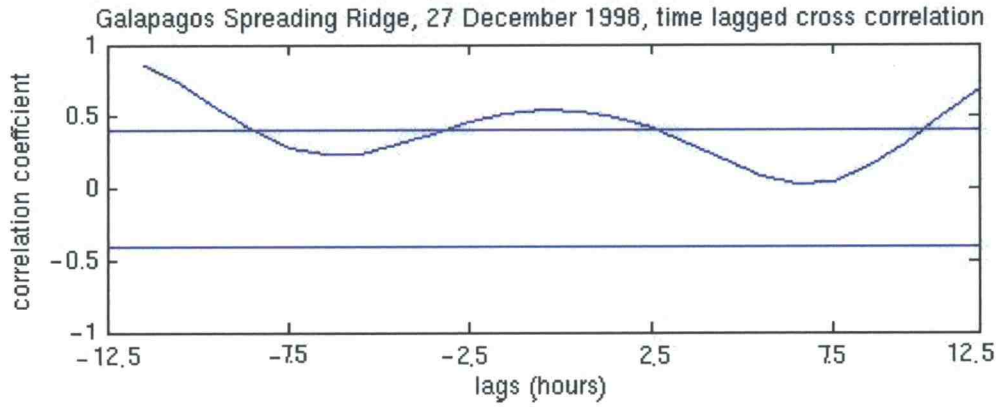

Figure 37: Cross correlation in GSR, earthquakes on 27 December 1998 versus SSH

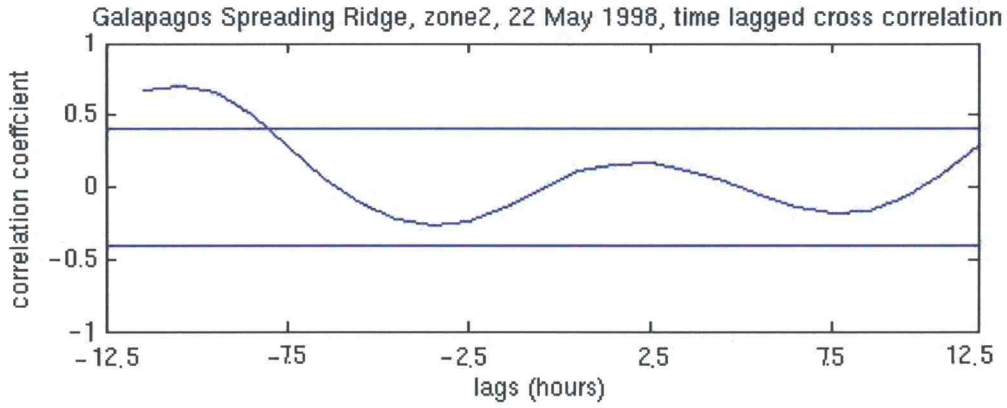

Figure 38: Cross correlation in GSR, earthquakes on 22 May 1998 versus SSH.

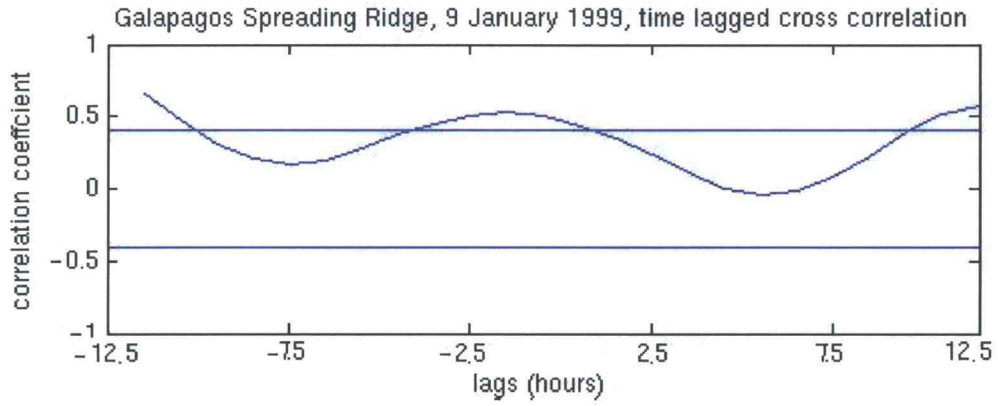

Figure 39: Cross correlation in GSR, earthquakes on 9 January 1999 versus SSH.

Table 15: Clusters in transform faults.

	Date	Correlation (5 time lags)	Tidal phase when the 1st earthquake occurred	Moon phases
Siqueros	26-27 April 2001	-	->+	● to ◐
	10 May 1998	+	->+	-> ○
Quebrada	2 Nov.1997	-	->+	● to ◐
	21 August 1998	No	-	●
	16 October 1998	-	+	◐ to ●
Discovery	16 October 1998	No	+	◐ to ●
	26 June 2001	No	+	-> ◐
Gofar	15 August 1997	+	-	○ to ◑
	18 Sept. 1999	+	+	◐ ->
Wilkes	10 Nov. 1999	+	-	● to ◐
Yaquina	27 May 1999	+	-	◐ to ○

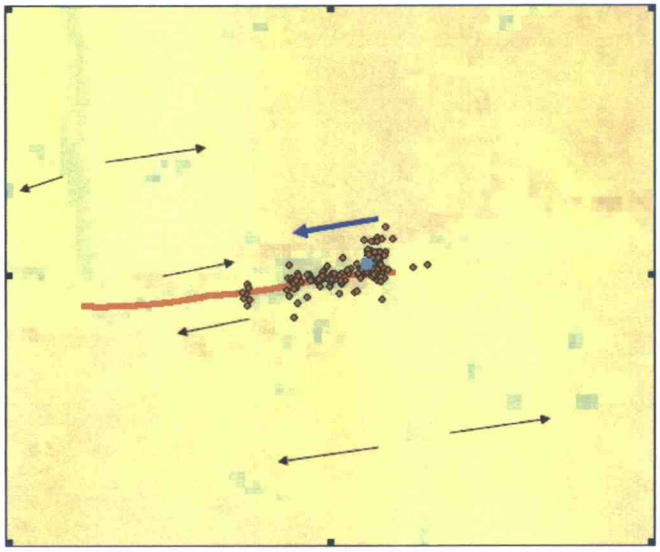

Figure 40: Location of cluster in Siqueros. The blue dots represent the location of the first strong earthquake.

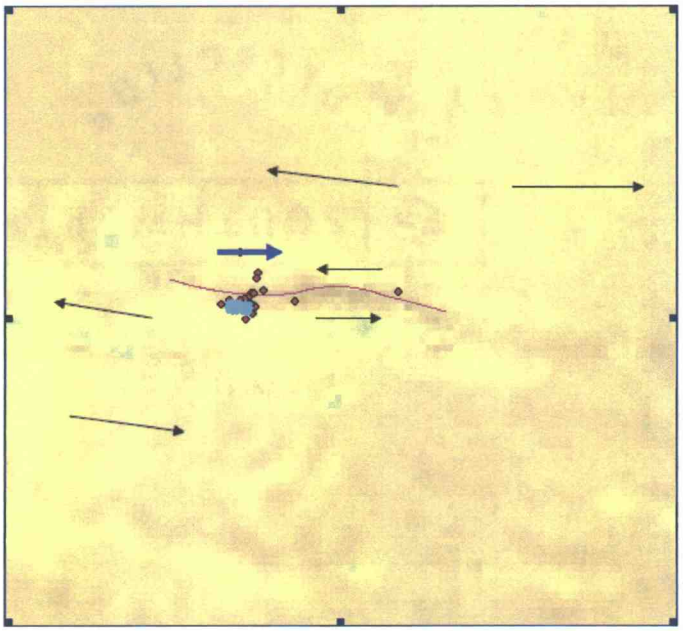

Figure 41: Location of cluster in Quebrada. The blue dots represent the location of the first strong earthquake.

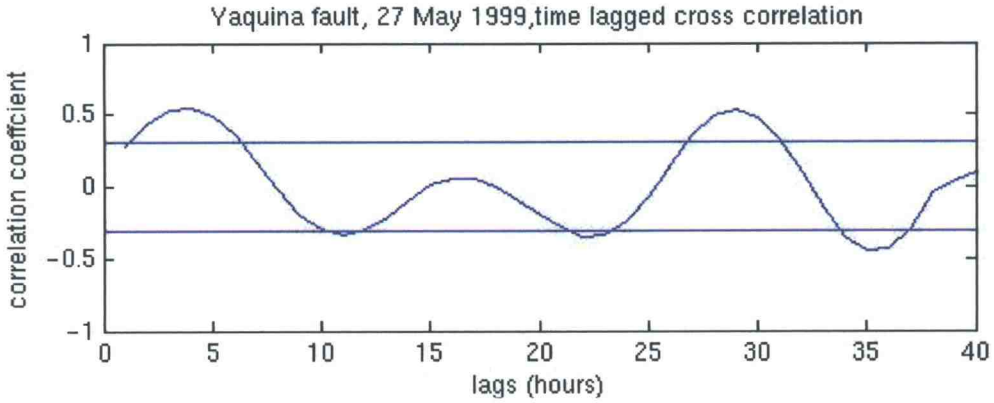

Figure 42: Cross correlation in the Yaquina Fault, earthquakes on 27 May 1999 versus SSH.

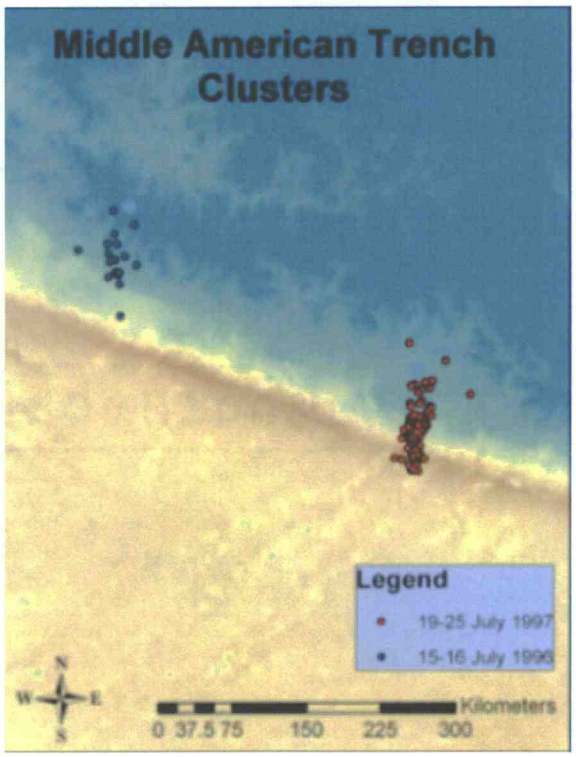

Figure 43: Location of cluster for MAT1-2. First earthquakes are underlined in blue.

Table 16: Clusters in the Middle American Trench.

	Date	Correlation (5 time lags)	Tidal phase when the 1st earthquake occurred	Moon phases
Mat1	15-16 July 1996	No	->-	●
Mat2	19-25 July 1997	No	->-	○ to ◑
Mat3	3-7 February 1998	No	->+	◐ to ○

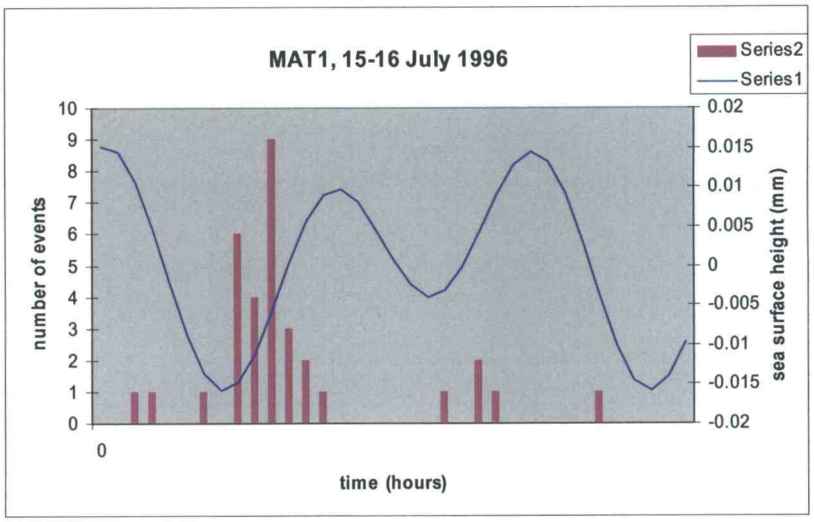

Figure 44: Number of earthquakes (series2) versus changes in SSH (series1) for cluster of 15-16 July 1996.

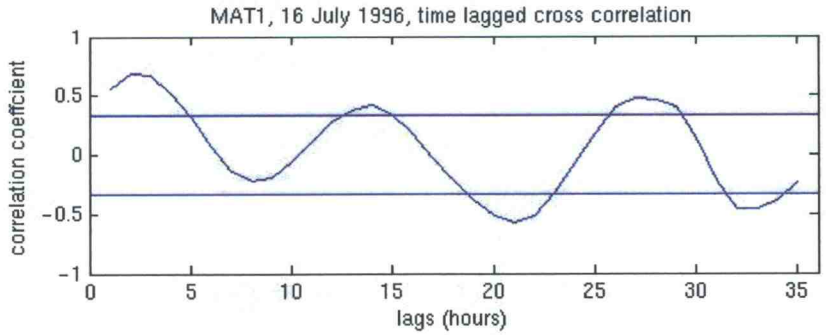

Figure 45: Correlation coefficient for cluster of 16th July 1996.

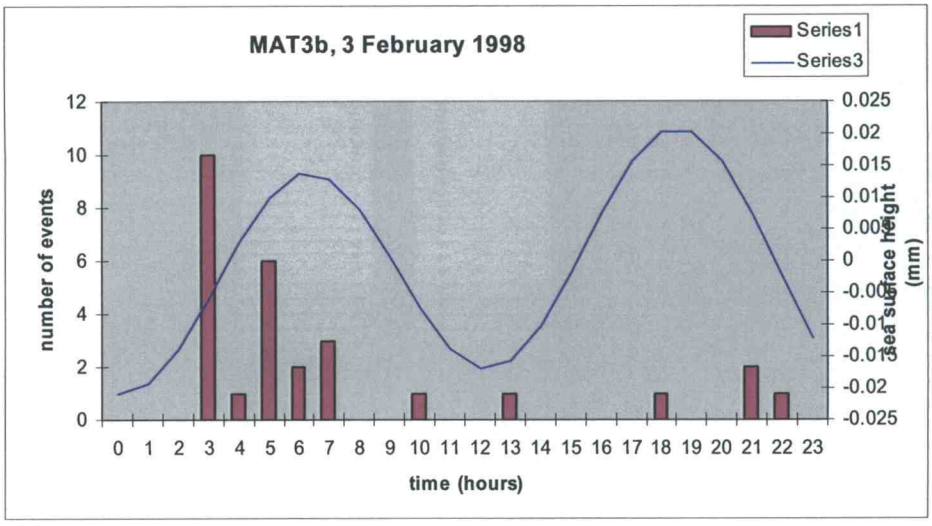

Figure 46: Number of earthquakes (series2) versus changes in SSH (series1) for cluster of 3rd February 1998.

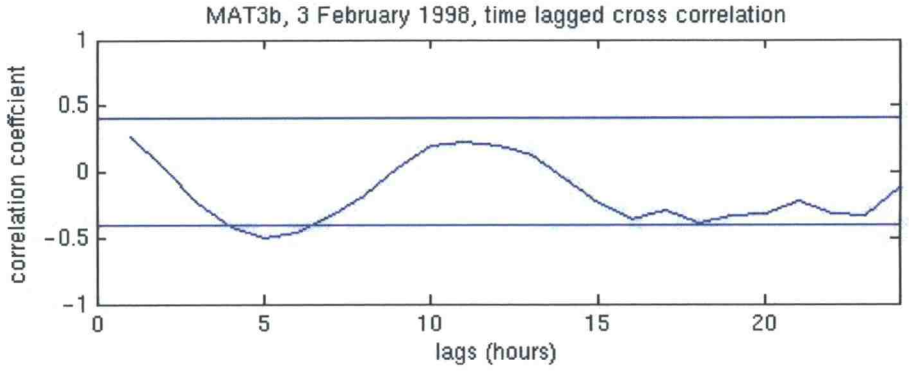

Figure 47: Correlation coefficient for cluster of 3rd February 1998.

5. CONCLUSIONS

This study investigated possible linkages between the seismicity rate on three different kinds of plate boundaries in the eastern equatorial Pacific and changes in SSH due to ocean tides, solid earth tides and oceanographic conditions. Cross correlation analyses were carried out between numbers of earthquakes on two different time scales, the first one would take into account the influence of the solid earth, and the second one would consider the influence of changing SSH due to ocean tides and oceanic conditions. Correlations with solid earth tides were expected for thrust and normal faults, which are the Middle American Trench and the Galapagos Spreading Center. Correlations were also expected for swarms occurring on these kinds of faults on an hourly time scale.

Four significant results were obtained. First, on a lunar time scale a correlation between the Middle American Trench and changes in SSH due to changing oceanic conditions was found. Since deep earthquakes are not influenced by the ocean weight, it is most probably that earth tide may play a role on the triggering of earthquakes in this kind of fault, as also suggested by Cochran et al. (2004). Second, still on the lunar time scale, the seimicity in the Quebrada transform fault showed a high correlation with the close-by Discovery transform fault, suggesting that at this spatial-temporal scale, the plate moves in a rigid way. Third, autocorrelation carried out for each fault on the lunar time scale showed that the seismicity on the faults does not follow a cyclic pattern, with earthquake peaks occur randomly. Fourth, on an hourly time scale, four swarms occurring along the Galapagos Spreading Ridge showed a strong correlation with the tidal fluctuation in SSH, with the first earthquakes occurring during low SSH, as suggested in the hypothesis. Generally, no significant correlations with changing SSH on the two time scales were found in the transform faults. In summary, this study confirms findings from past research (Cochran et al. 2004; Tolstoy et al. 2001; Wilcok 2001), that changes in SSH and solid earth tides could work as a possible trigger mechanisms on some earthquakes located in normal and thrust faults.

GIS resulted to be a powerful tool for summarizing and conveying vast amount of information. GIS was used successfully to extract data regarding selected faults from the whole data set, to delete possible location error, to carry descriptive statistics and to isolate cluster of earthquakes. Thanks to the GIS, the quality and the precision of the data used improved. A beginner GIS lab-book was created (appendix 2) and it was made available on the web for researched and university students.

6. REFERENCES

- Aki, K., (1992). Higher-Order Interrelations Between Seismogenic Structures and Earthquake Processes, Tectonophysics 211: (1-4) 1-12.
- Astronomical Application Department, (2005). http://aa.usno.navy.mil/data/docs/RS_OneDay.html
- Bissonnette, V. L., (2000). http://fsweb.berry.edu/academic/education/vbissonnette/tables/r.pdf
- Boettcher, M.S., Jordan, T.H., (2005). Foreshock sequences and short-term earthquake predictability on East Pacific Rise transform faults, Nature 434: 457-461.
- DeMets C., (2001). A new estimate for present-day Cocos-Caribbean plate motion: implications for slip along the central American volcanic arc, Geophysical Research Letters.
- Canales, P., Danobeitia, J.J., Detrick, R., Hooft, E., Bartolome,' R., Narr D., (1997). Variation in axial morphology along the Galapagos spreading center and the influence of the Galapagos hotspot, Journal of Geophysical Research, 102, 27: 341-354.
- Canales, J. P., Detrick, R. S., Sinton, J., (2002). Crustal thickness along the western Gala.pagos Spreading Center and the compensation of the Galapagos hotspot swell, Earth Planet. Science Letters 203: 311-327.
- Carbotte, S. M., Macdonald, K. C., (1992). East Pacific Rise 8 degrees -10 degrees 30'N; evolution of ridge segments and discontinuities from SeaMarc II and threedimensional magnetic studies, Journal of Geophysical Research 97: 6959-6982.
- Case, K., (1995). http://podaac.jpl.nasa.gov:2031/SENSOR_DOCS/topex_alt.html
- CSR/TSGC, (1999). http://www.tsgc.utexas.edu/topex/topexfaq.html

- Cheney, R., Tai,C., K., Lillibridge, J., Kuhm, J., J. ,M., Behringer, D., (1998). operational altimeter data processing and assimilation for El Nino forecasts, Aviso Altimetry, newletter 6
- COMET, (2006). http://meted.ucar.edu/hurrican/strike/text/htc_t2.htm
- Cornier, M., (1997).The ultrafast East Pacific Rise: instability of the plate boundary and implications for accretionary processes, Philosophical Transactions of The Royal Society: 355: 341-367
- Cochran E., Vidale J.E., Tanaka S., (2004). Earth tides can trigger shallow thrust fault earthquakes, Sciencexpress, 10.1126, 1
- Curewitz D., Karson A., (1998). Geological consequences of dike intrusion at mid-ocean ridge spreading centers: Faulting and magmatism at Mid ocean ridges, Geophysical monograph, 117-136.
- Dziak, R., (2001). Empirical relationship of T-wave energy and fault parameters of northeast Pacific Ocean earthquakes: Geophysical Research Letters, 28 (13): 2537-2540.
- Dziak, R., Bohnenstiehl, D.R., Matsumoto H., Fox C.G., Smith D.K., Tolstoy M., Lau T.K., Haxel H.J., Fowler M.J., (2004). P- and T- wave detection thresholds, Pn velocity estimate and detection of lower mantle and core P-wave on ocean sound-Channel hydrophones at the Mid-Atlantic Ridge, Bulletin of the Seismological Society of America, 94 (2): 665-677.
- Floyd, J. S., Tolstoy, M., Mutter, J. C., Scholz, C. H., (2002). Seismotectonics of mid-ocean ridge propagation in Hess Deep, Science 298: 1765-1768.
- Fortes A. D., (1999). Origin of the Martial hemispheric dichotomy, http://www.es.ucl.ac.uk/research/planetaryweb/undergraduate/dom/mars_discrimi nating.
- Fox, C.G.; Matsumoto, H.; Lau, T.A., (2001). Monitoring Pacific Ocean seismicity from an autonomous hydrophone array, Journal of Geophysical Research 106 (B3): 4183-4206

- Fu L.L., Cazenave A., (2001). Satellite altimetry and earth sciences, International Geophysics Series. 69: 463.
- Fu L.L., Chao Y., Fukumori I., Perigaud C., Boulanger J.P., (1998). Seasonal-to-interannual variability from altimetry and modelling, Aviso Altimetry, newletter 6
- Glasby, G. P., Kasahara J., (2001). Influence of tidal effects on the periodicity of earthquakes in diverse geological setting with particular emphasis in submarine hydrothermal system, Earth-Science Reviews 52: 261-297.
- Gregg, P. M., Lin, J., Smith, D. K., (2004). Characteristics and Possible Triggering Relationship of Earthquakes at the Pacific Transform Faults, 8123 Dynamics, seismotectonics, 3025 Marine seismics (0935), 3040 Plate tectonics (8150, 8155, 8157, 8158)
- Gross. R.S., Chao Y. Marcus S.L., Dickey J.O., (1998). T/P, gravity and the earth's rotation: investigating mechanisms and effects of sea level change, Aviso Altimetry, newletter 6
- Haines B., Born G., Christensen E., Gill S., Kubitschek D., (1998). The harvest experiment: T/P absolute calibration results from five years of continuous data, Aviso Altimetry, newletter 6.
- Haymon, R., Cormier M., Ridge 2000 proposal for an integrated study site at a fast spreading ridge: the east pacific rise, 8-11 N.
- Haxel, J., (2005). NOAA Vents Program. Personal communication.
- Kasahara J., Nakao S., Koketsu K., (2001). Tidal influence on the 200 Mikaye-jima eruption and its implications for hydrothermal activity and volcanism: Proceedings of the Japan Academy 77 (SerB): 98-103.
- Kasahara, J., Sato, T., (2000). Tidal effects on volcanic earthquakes and deep-sea hydrothermal activity revealed by ocean bottom seismometer measurements. Journal of Geodetic Society, Japan.
- Kasahara, J., (2002). Tides, earthquakes and volcanoes, Geophysics, Science 297 (5580): 348-349.

- Kelley C., (1995). TOPEX Altimeter Sensor/Instrument Document, Document # PODAAC 028.D003, Podaac.jpl.nasa.gov.
- Kellogg N. & Hunter K., (2000). http://www.jclahr.com/science/earth_science/tabletop/earthshaking/index.html
- Kureth C.L., Rea K., (1981). Large-scale oblique features in an active transform fault, the Wilkes fracture zone near 9°S on the East Pacific Rise, Marine Geophysical Researches (Historical Archive) 5 (2): 119 – 137.
- La Femina, P. C., Dixon T. H., Strauch, W., (2002). Bookshelf faulting in Nicaragua, Geology 30 (8): 751-754.
- Liggett, P., (2003). http://podaac.jpl.nasa.gov/products/ product172.html
- Macdonald, K, Sempere, J., Fox, P. J., (2004). East Pacific Rise from Siqueiros to Orozco fracture zones: Along-strike continuity of axial Neovolcanic zone and structure and evolution of overlapping spreading centers, Journal of Geophysical Research 89 (B7): 6049-6069.
- Manea M., Manea C. V., Kostoglodov V., (2003). Sediment fill in the Middle America Trench inferred from gravity Anomalies, Geofísica Internacional 42 (4): 603-612
- Marechal J.C., Sarma M.P., Ahmed S., Lachassagne P., (2002). Establishment of earth itde effect on water level fluctuations in an unconfined hard rock aquifer using spectral analysis, Current Science, 83 (1): 61-64.
- Matsumoto, H., (2004). http://www.pmel.noaa.gov/vents/acoustics/images/haru-mooring-big.gif
- Macdonald, K.C., Fox, P.J., Carbotte, S., Eisen, M., Miller, S., Perram, L. , Scheirer, D., Tighe, S., Weiland, C., (1992). The East Pacific Rise and its flanks, 8°-17°N: History of segmentation, propagation and spreading direction based on SeaMARC II and Sea Beam studies, Marine Geophysic Research 14, 299-334.
- McGuide J., (2005). http://web.mit.edu/mitwhoi/www/research/mgg/oceanic_transform_faults.html

- McGuire, J., Boettcher, M.S., Jordan T.H., (2005). Foreshock sequences and short-term earthquake predictability on East Pacific Rise transform faults, Nature 434: 457-461
- Morgan, W.J., Rodrigues, D., Amsterdam, T, (1978). A second type of hotspot island, J. Geophys. Res. 83: 5355-5360.
- Mussett, A., Aftab K., (2000). Looking into the earth, an introduction to geological oceanography, Cambridge university press, pp 316-.
- Niwa Science, (2006). http://www.niwascience.co.nz/shared/elnino4.gif
- NOAA (2005). http://www.pmel.noaa.gov/vents/data/index.html
- NOAA/PMEL, (2005). http://www.pmel.noaa.gov/
- Odias A., (1998). Introducción: sismicidad y sismotectónica de América Central y del Sur, Física de la Tierra Y lO: 11-17
- Padman, L., Erofeeva, L., (2003). http://www.esr.org/polar_tide_models/Model_AOTIM5.html
- Perfit, M.R., Chadwick, W. W., (1998). Magmatism at Mid-Ocean Ridge: constrains from Volcanological and Geochemical investigations: Faulting and magmatism at Mid ocean ridges, Geophysical monograph 106: 59-116.
- Phillips, T. (2006). http://www.math.nus.edu.sg/aslaksen/teaching/tides.html
- Pisias, N. (2005). Oregon State University. Personal communication.
- Pockalny, R. A., Fox, P. J., Fornari, D. J., Macdonald, K. C., Perfit, M. R., (1997). Tectonic reconstruction of the Clipperton and Siqueiros Fracture zones: Evidence and consequences of plate motion change for the last 3 Myr, Journal of Geophysical Research 102: 3167- 3182.
- Ray, D.R., Egbert, G.D., Cartwright, D.E., (2004). Altimetric studies of ocean tidal dynamics, AVISO Altimetry 6.
- Segar, D., (1998). Introduction to ocean sciences, Wadsworth publishing company, 188-192.

- SimScience, (2005). http://simscience.org/crackling/Advanced/Earthquakes /GutenbergRichter.html
- Stein, R. S. (1999). The role of stress transfer in earthquake occurrence, Nature 402: 605 – 609.
- Stein, R., (2004). Earth science: earthquakes and lunar tides, Science 3005: 1248.
- Tanaka, S., Ohtake, M., Sato, H., (2002). Evidence for tidal triggering of earthquakes as revealed from statistical analysis of global data, Journal of Geophysical Research 107 (B10): 1-11.
- Tolstoy, M., Vernon F.L., Orcutt J.A., Wyatt, F. K., (2002). Breathing of the seafloor: Tidal correlations of seismicity at Axial volcano, Geology 30 (6): 503-506.
- Tsuruola, H., Ohtake, M., Sato, H., (1995). Statistical test of the tidal triggering of earthquakes: contribution of the ocean tide loading effect, Gephysical Journal International 122: 183-194.
- USGS, (1998). http://hvo.wr.usgs.gov/volcanowatch/1998/98_05_28.html
- USGS, (1999). http://pubs.usgs.gov/publications/text/fire.html
- USGS, (2004). http://pubs.usgs.gov/gip/earthq1/plate.html
- Van der Pluijm B.A, Marshak S., (2004).
- Vidale, J. E., Agnew, D. C., Johnson, M. J. S., Oppenheimer D. H., (1998). Absence of earthquake correlation with Earth tides: An indication of high preseismic fault stress rate, Journal of Geophysical Research 1-3: 567–24.
- Wilcock, W. S. D., (2001), Tidal triggering of microearthquakes on the Juan de Fuca Ridge, Geophysical Research Letters 28: 3999-4002.
- Wolter, K., Timlin, M.S., (1993). Monitoring ENSO in COADS with a seasonally adjusted principal component index. Proc. of the 17th Climate Diagnosti
- Yeats, R. S., Sieh, K., Allen, C. R., (1997). The geology of earthquakes, Oxford university press, 568.

7. APPENDIX 1

1. Cross correlation analysis SSH versus Earthquakes event for moon quarters
(time lag = 7.38 days)
Solid lines represent r-values that can reject the null hypothesis (r = 0.125, error of 0.5)

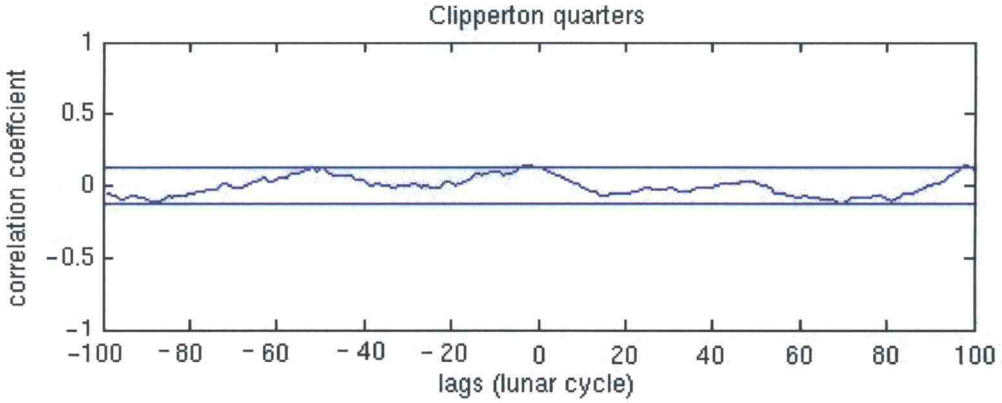

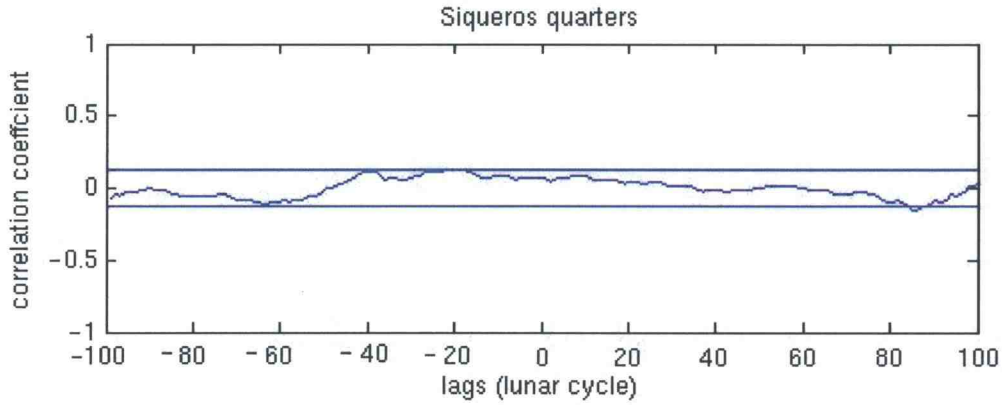

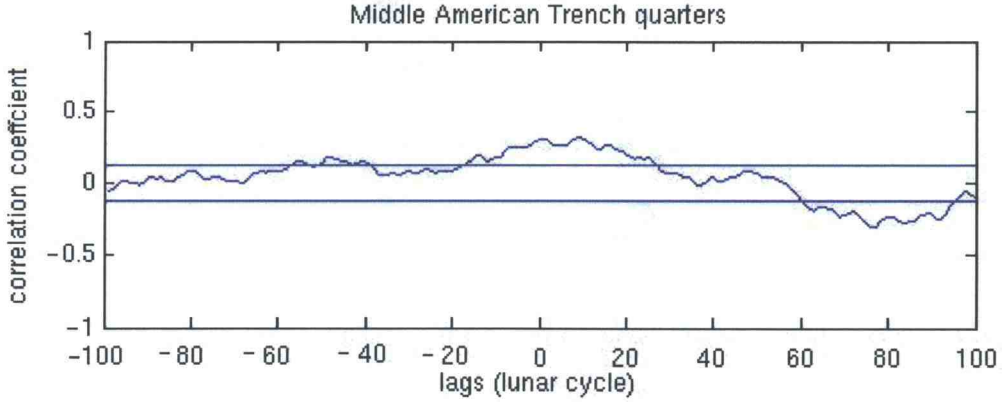

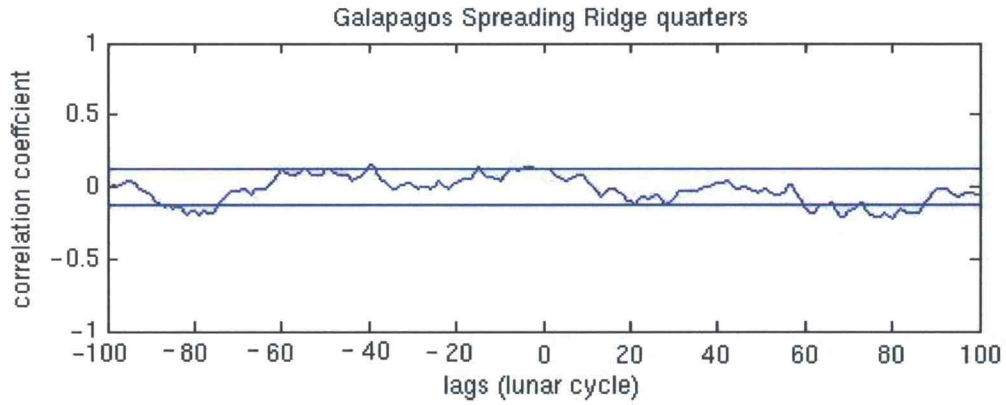
Galapagos Spreading Ridge quarters
correlation coeffcient
1
0.5
0
-0.5
-1
-100 -80 -60 -40 -20 0 20 40 60 80 100
lags (lunar cycle)

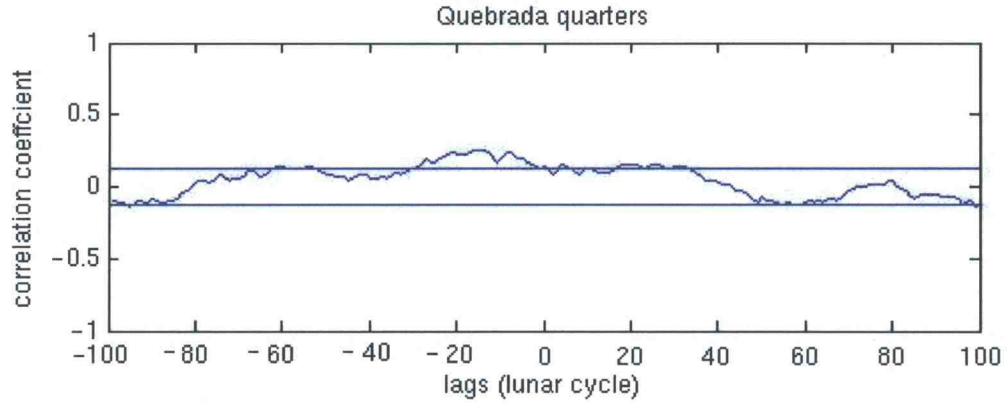
Quebrada quarters
correlation coeffcient
1
0.5
0
-0.5
-1
-100 -80 -60 -40 -20 0 20 40 60 80 100
lags (lunar cycle)

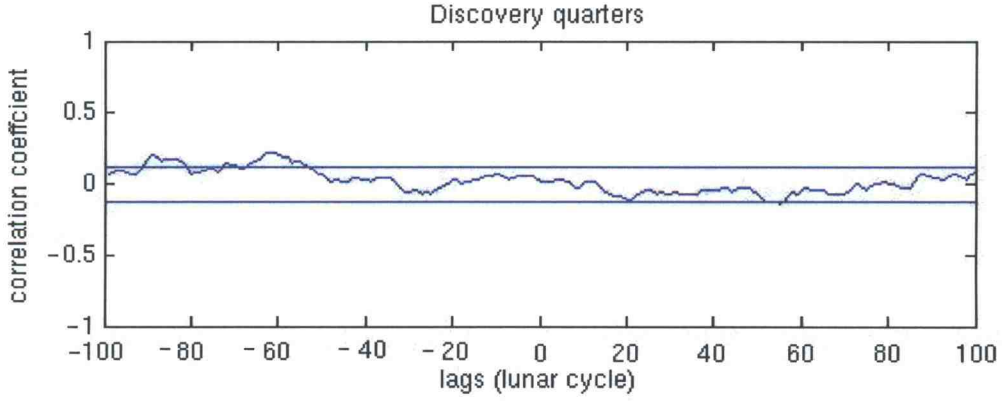
Discovery quarters
correlation coeffcient
1
0.5
0
-0.5
-1
-100 -80 -60 -40 -20 0 20 40 60 80 100
lags (lunar cycle)

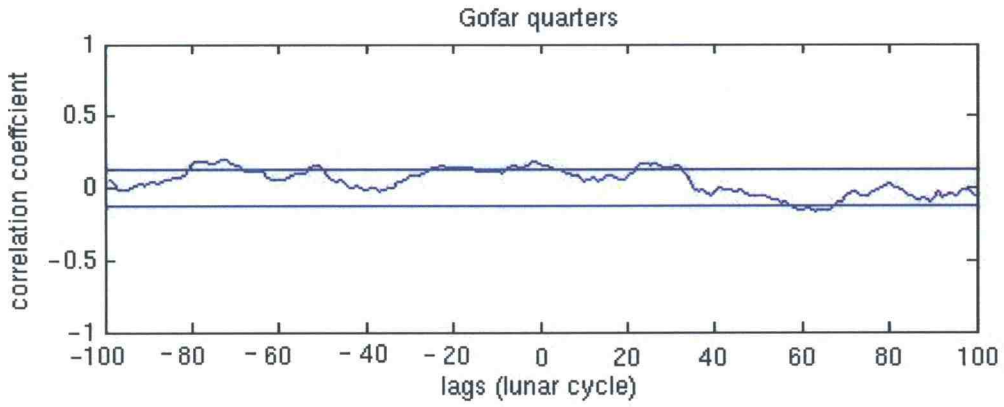
Gofar quarters
correlation coeffcient
1
0.5
0
-0.5
-1
-100
-80
-60
-40
-20
0
20
40
60
80
100
lags (lunar cycle)

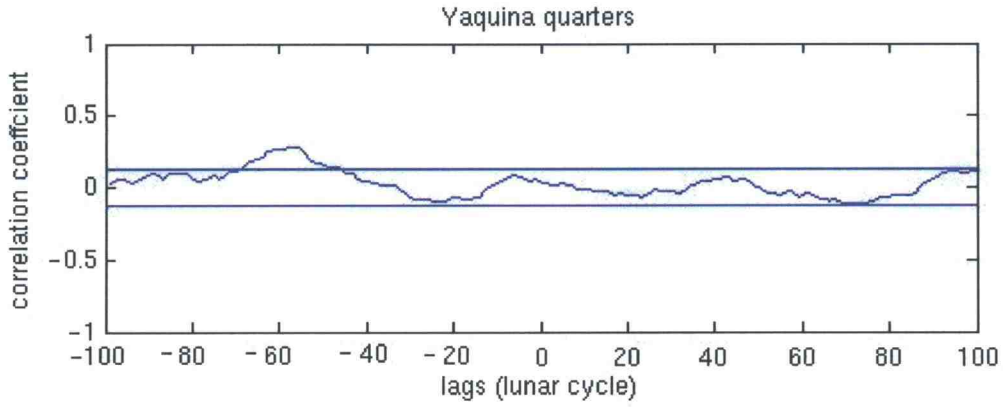
Yaquina quarters
correlation coeffcient
1
0.5
0
-0.5
-1
-100
-80
-60
-40
-20
0
20
40
60
80
100
lags (lunar cycle)

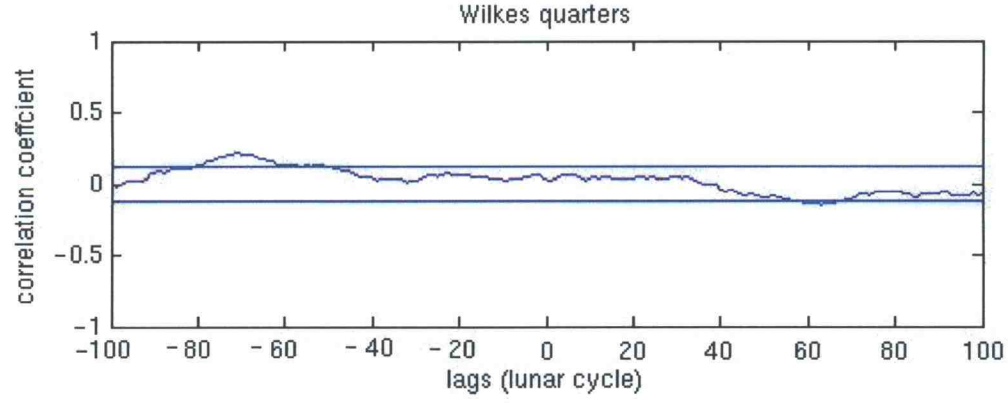
Wilkes quarters
correlation coeffcient
1
0.5
0
-0.5
-1
-100
-80
-60
-40
-20
0
20
40
60
80
100
lags (lunar cycle)

1.2 Variance Spectrum analysis between SSH and earthquakes
(Time lag = 7.38 days)

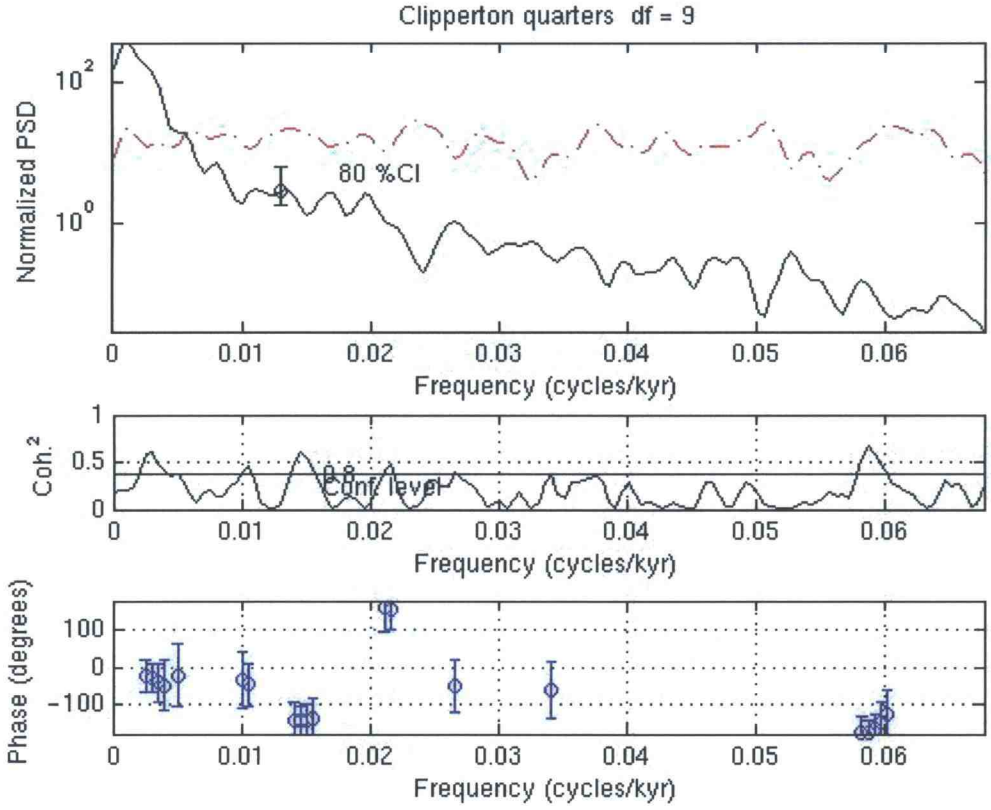

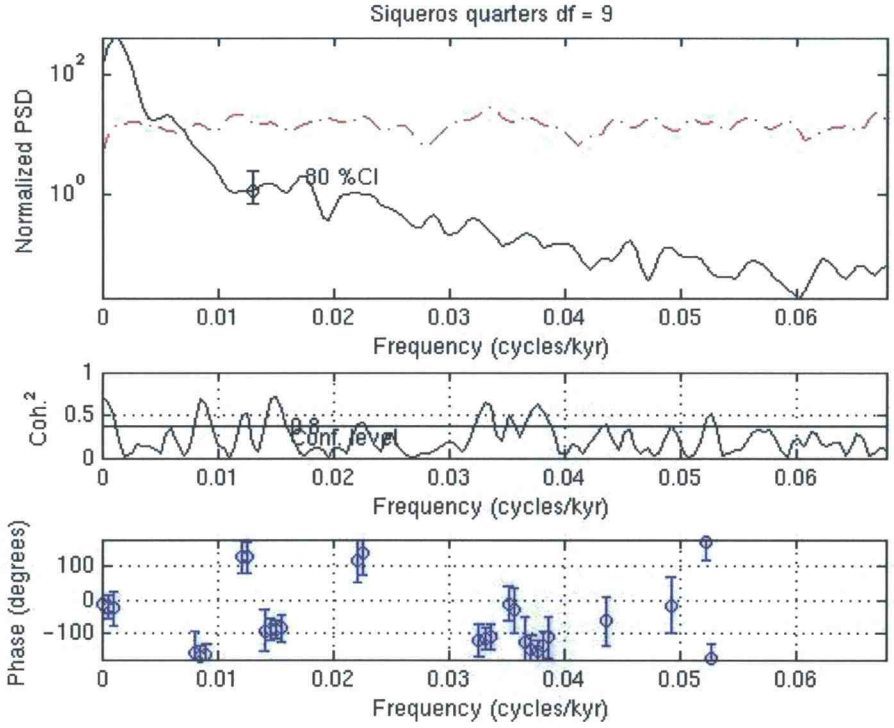
Siqueros quarters df = 9
Normalized PSD
10^2
10^0
80 %CI
0 0.01 0.02 0.03 0.04 0.05 0.06
Frequency (cycles/kyr)
Coh.^{2}
1
0.5
0
95% Conf. level
0 0.01 0.02 0.03 0.04 0.05 0.06
Frequency (cycles/kyr)
Phase (degrees)
100
0
-100
0 0.01 0.02 0.03 0.04 0.05 0.06
Frequency (cycles/kyr)

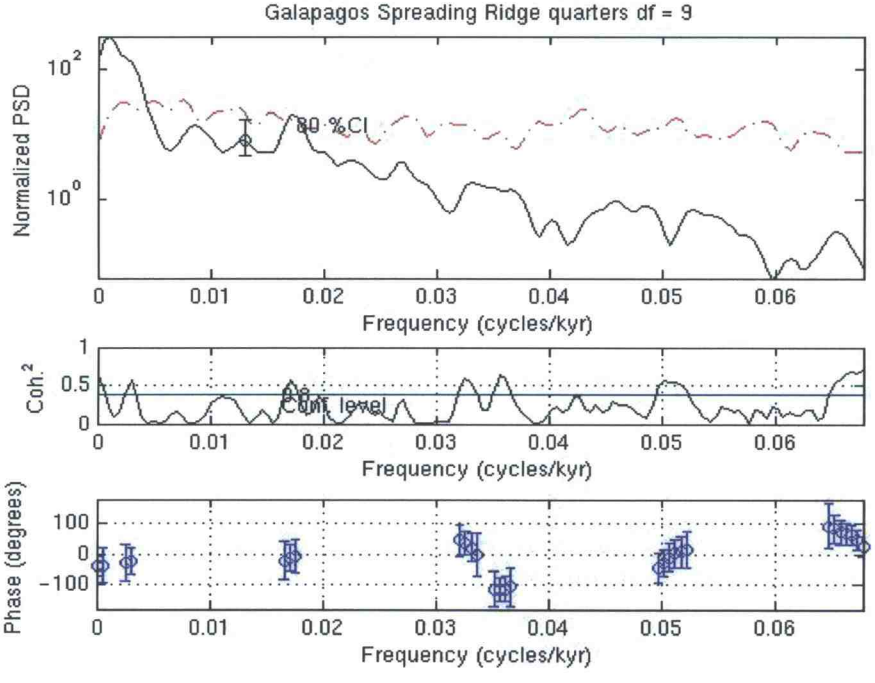
Galapagos Spreading Ridge quarters df = 9
Normalized PSD
10^2
10^0
80 %CI
0 0.01 0.02 0.03 0.04 0.05 0.06
Frequency (cycles/kyr)
Coh.^{2}
1
0.5
0
95% Conf. level
0 0.01 0.02 0.03 0.04 0.05 0.06
Frequency (cycles/kyr)
Phase (degrees)
100
0
-100
0 0.01 0.02 0.03 0.04 0.05 0.06
Frequency (cycles/kyr)

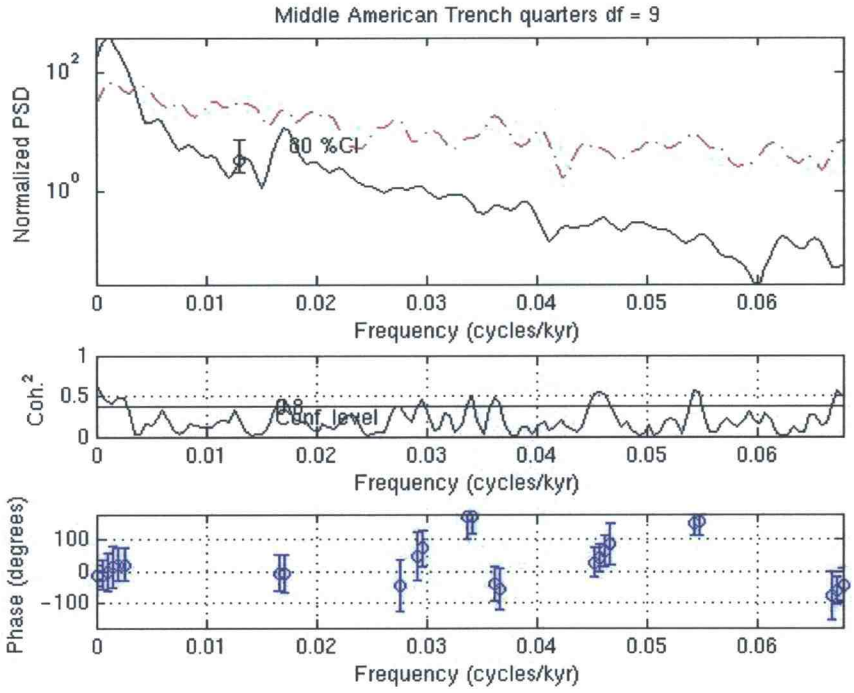
Middle American Trench quarters df = 9
Normalized PSD
80 %CI
Frequency (cycles/kyr)
Coh.²
90 % Conf. level
Frequency (cycles/kyr)
Phase (degrees)
Frequency (cycles/kyr)

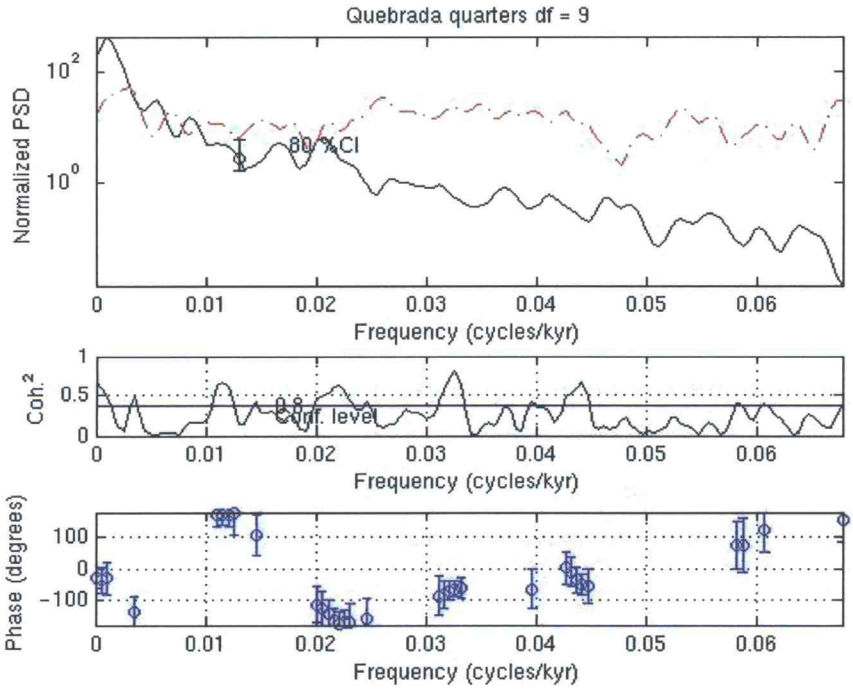
Quebrada quarters df = 9
Normalized PSD
80 %CI
Frequency (cycles/kyr)
Coh.²
90 % Conf. level
Frequency (cycles/kyr)
Phase (degrees)
Frequency (cycles/kyr)

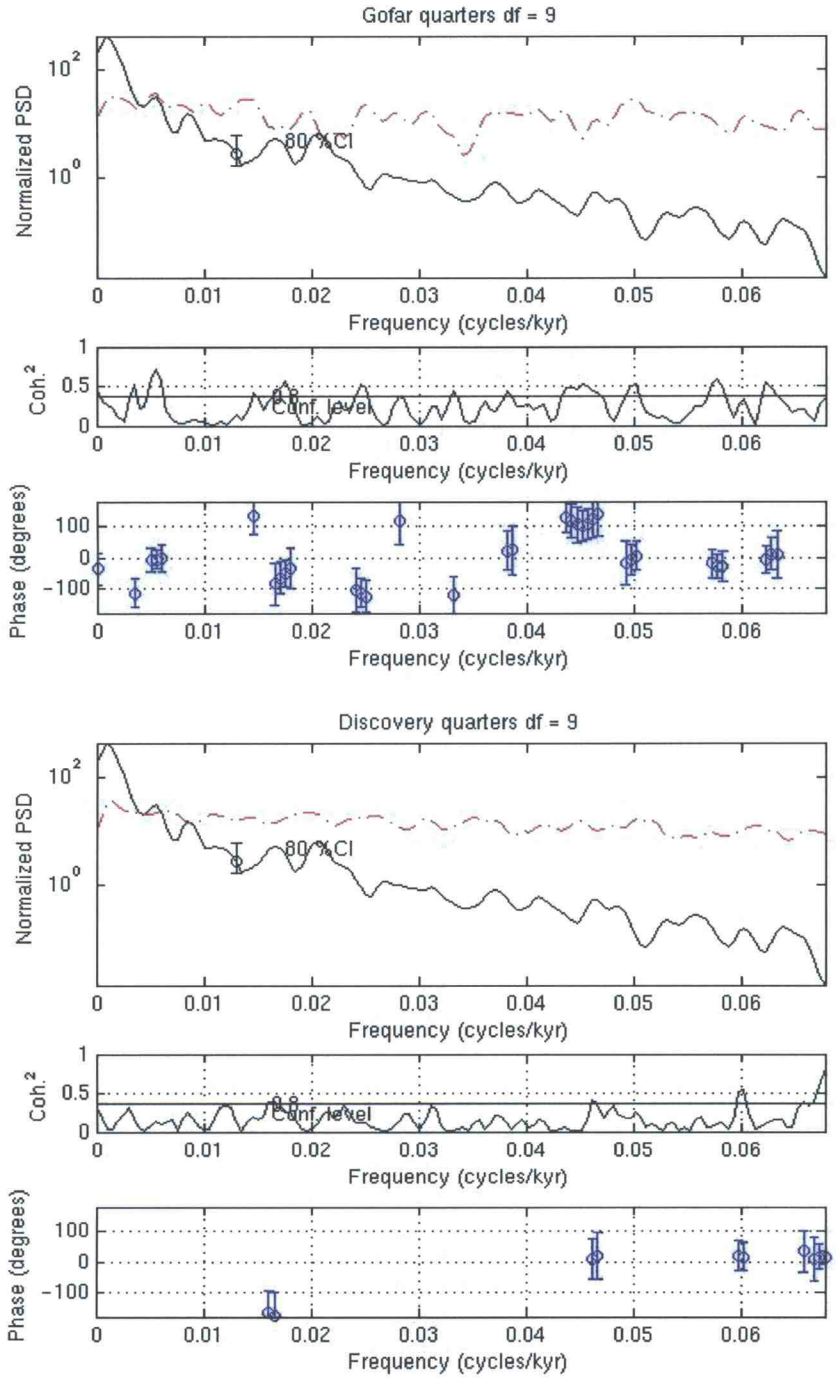
Gofar quarters df = 9
Normalized PSD
80 %CI
Frequency (cycles/kyr)
Coh.²
0.8
Conf. level
Frequency (cycles/kyr)
Phase (degrees)
Frequency (cycles/kyr)
Discovery quarters df = 9
Normalized PSD
80 %CI
Frequency (cycles/kyr)
Coh.²
0.8
Conf. level
Frequency (cycles/kyr)
Phase (degrees)
Frequency (cycles/kyr)

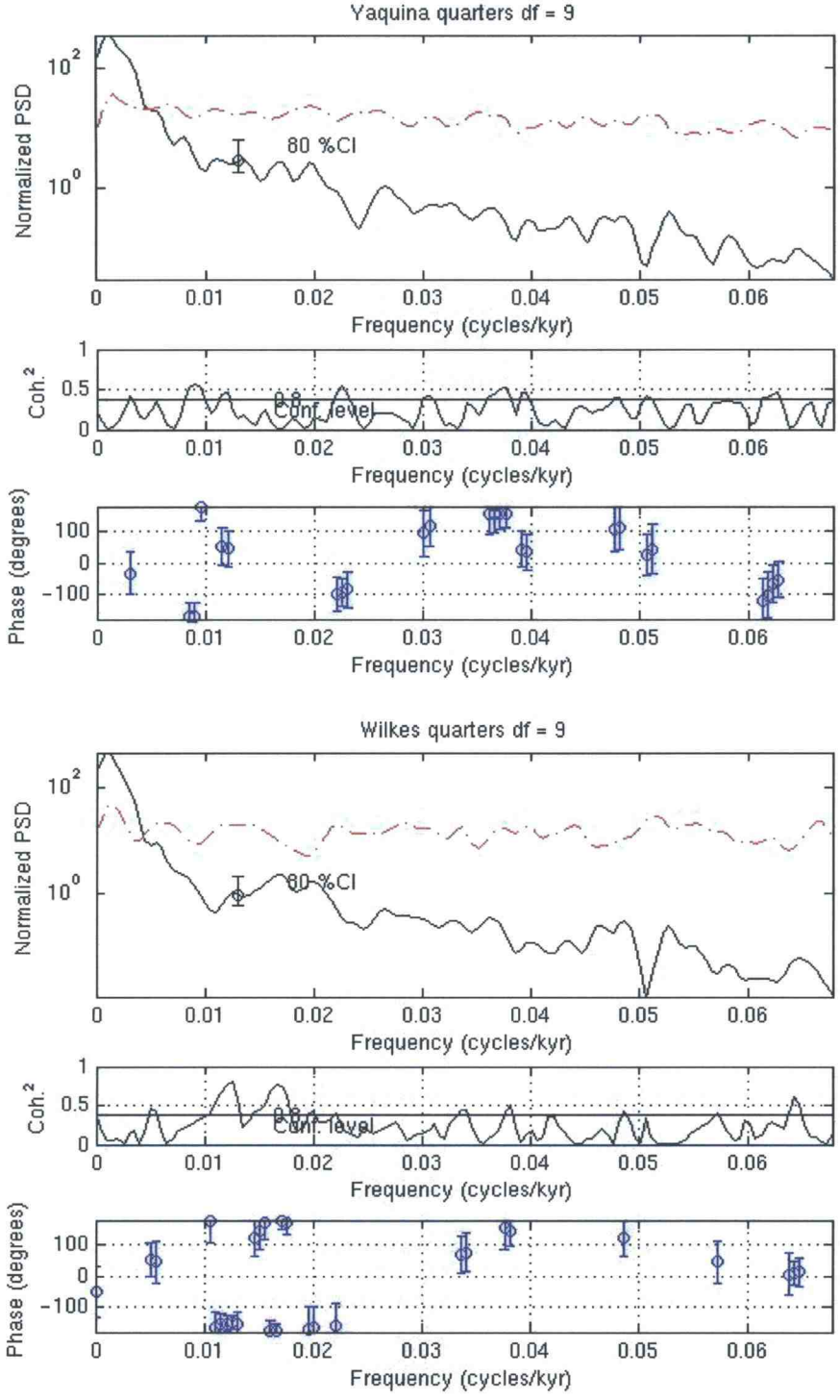
Yaquina quarters df = 9
Normalized PSD
80 %CI
Frequency (cycles/kyr)
Coh.²
0.8 Conf. level
Phase (degrees)
Wilkes quarters df = 9
Normalized PSD
80 %CI
Frequency (cycles/kyr)
Coh.²
0.8 Conf. level
Phase (degrees)
Frequency (cycles/kyr)

2. Autocorrelation between fault seismicity
(Time lag = 7.38 days)
Solid line represents r-value to reject null hypothesis with 99% confidence level.

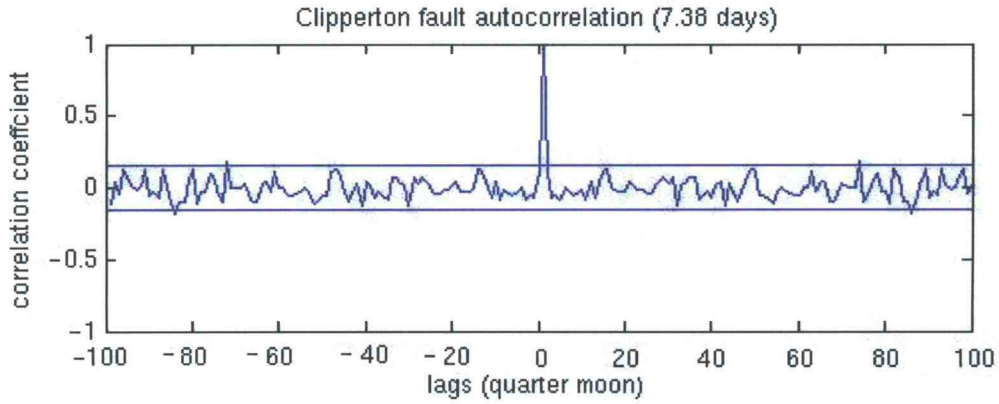

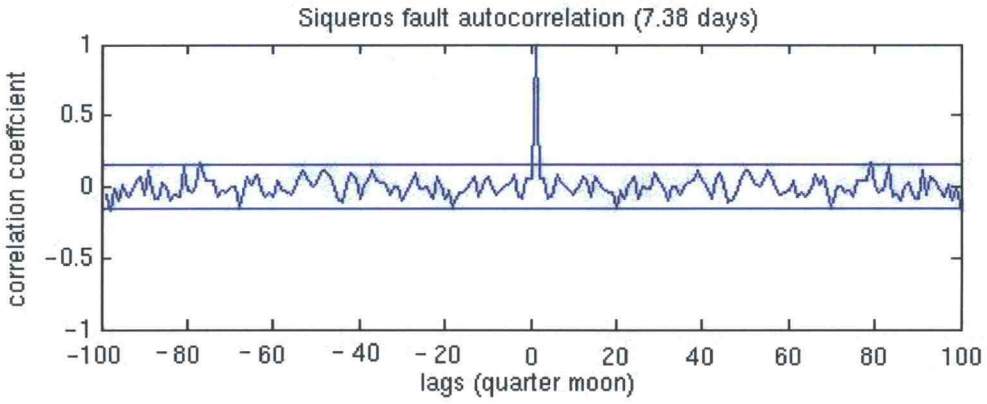

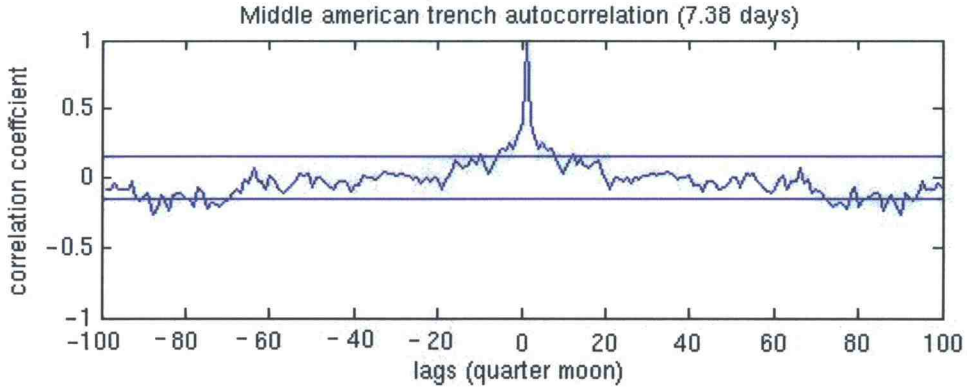

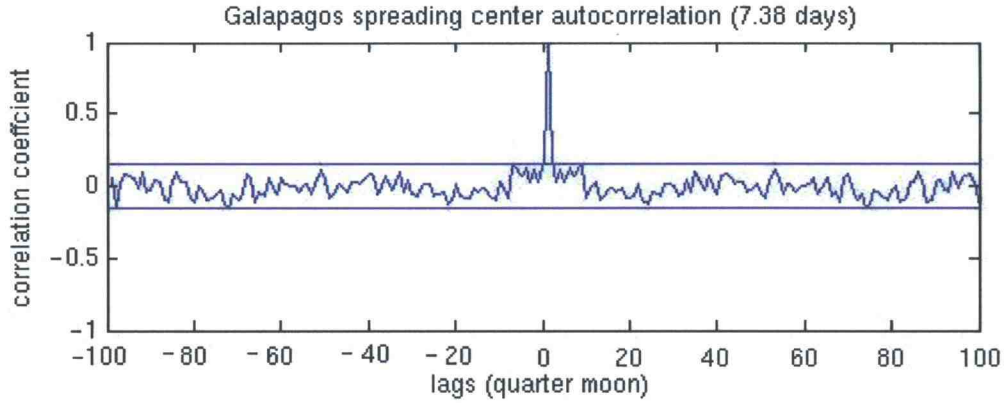
Galapagos spreading center autocorrelation (7.38 days)
correlation coeffcient
1
0.5
0
-0.5
-1
-100 -80 -60 -40 -20 0 20 40 60 80 100
lags (quarter moon)

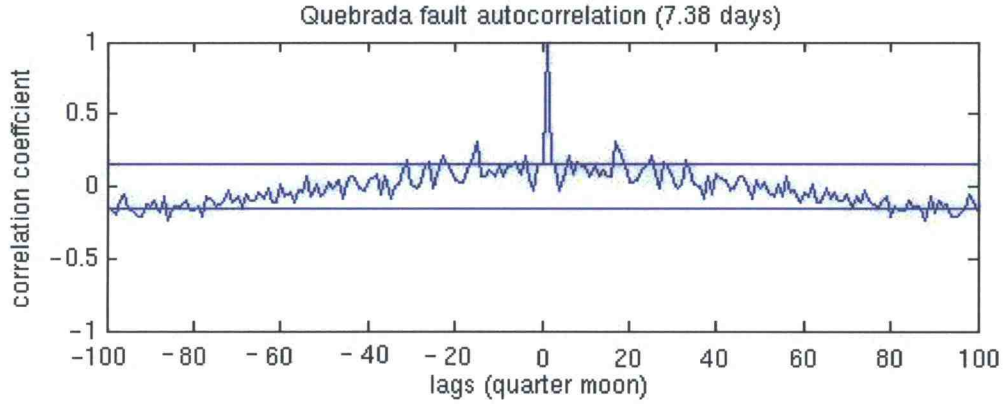
Quebrada fault autocorrelation (7.38 days)
correlation coefficient
1
0.5
0
-0.5
-1
-100 -80 -60 -40 -20 0 20 40 60 80 100
lags (quarter moon)

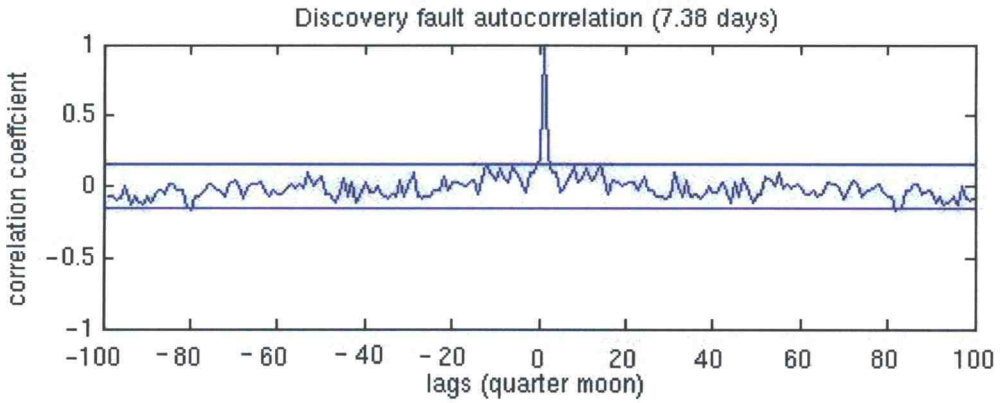
Discovery fault autocorrelation (7.38 days)
correlation coefficient
1
0.5
0
-0.5
-1
-100 -80 -60 -40 -20 0 20 40 60 80 100
lags (quarter moon)

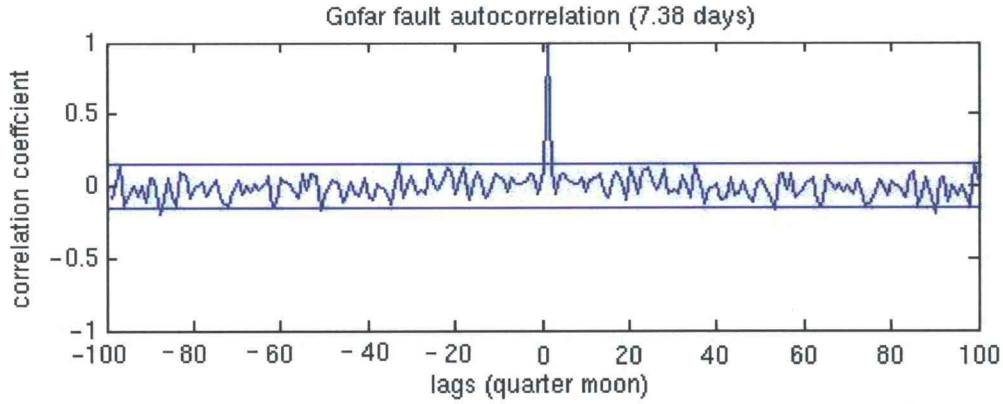
Gofar fault autocorrelation (7.38 days)
correlation coefficient
1
0.5
0
-0.5
-1
-100 -80 -60 -40 -20 0 20 40 60 80 100
lags (quarter moon)

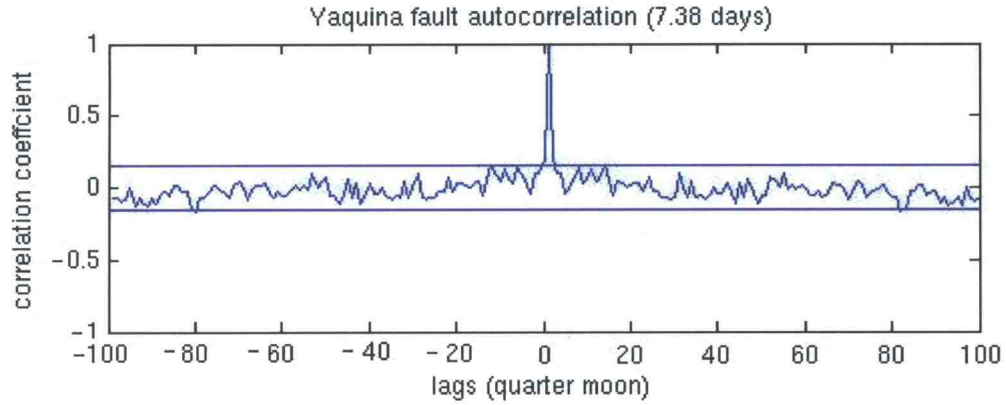
Yaquina fault autocorrelation (7.38 days)
correlation coeffcient
1
0.5
0
-0.5
-1
-100 -80 -60 -40 -20 0 20 40 60 80 100
lags (quarter moon)

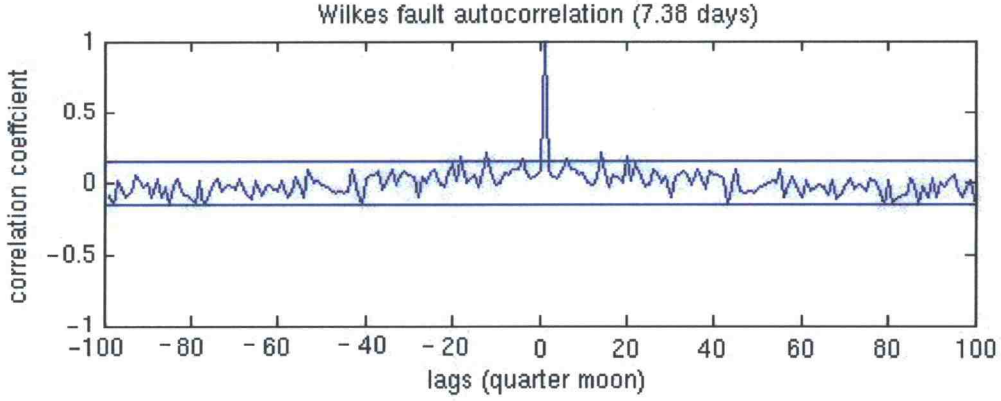
Wilkes fault autocorrelation (7.38 days)
correlation coefficient
1
0.5
0
-0.5
-1
-100 -80 -60 -40 -20 0 20 40 60 80 100
lags (quarter moon)

3. Cross Correlation analysis between seismic areas for quarters
(time lag = 7.38 days)
Solid lines represent r-values that can reject the null hypothesis (r = 0.125, error 0.5)

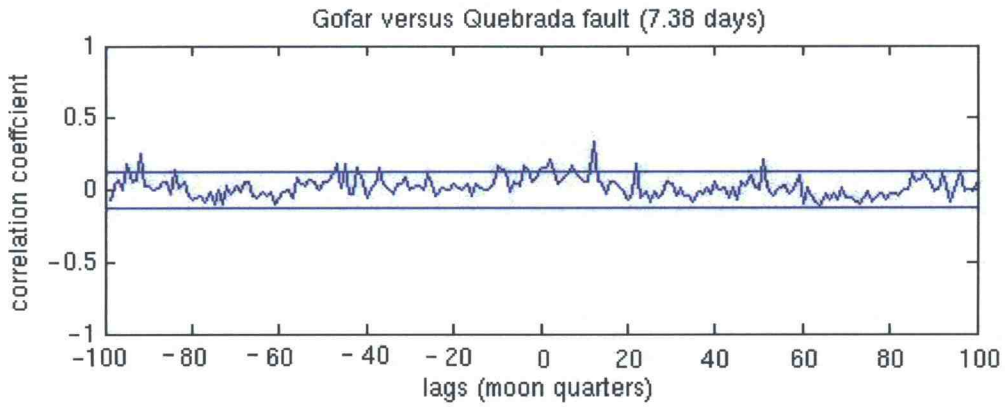

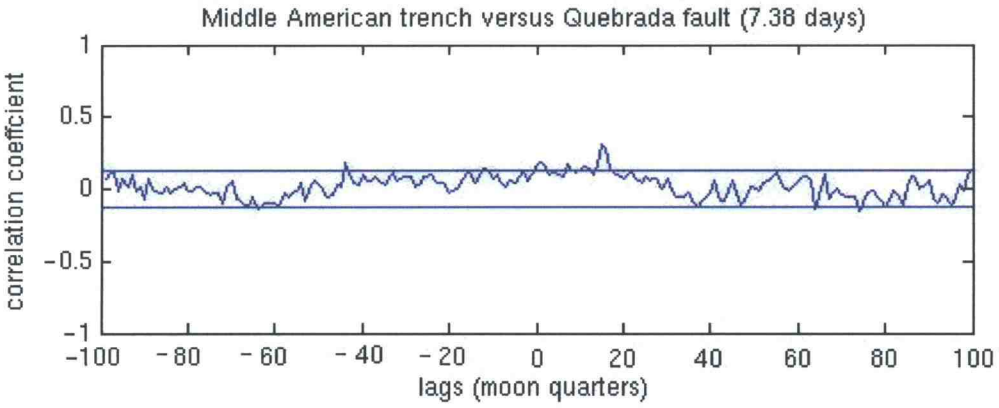

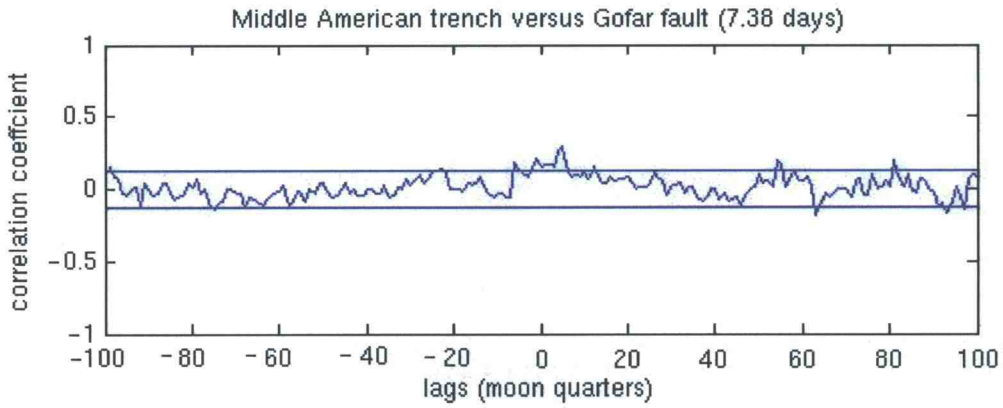
Middle American trench versus Gofar fault (7.38 days)
correlation coefficient
1
0.5
0
-0.5
-1
-100 -80 -60 -40 -20 0 20 40 60 80 100
lags (moon quarters)

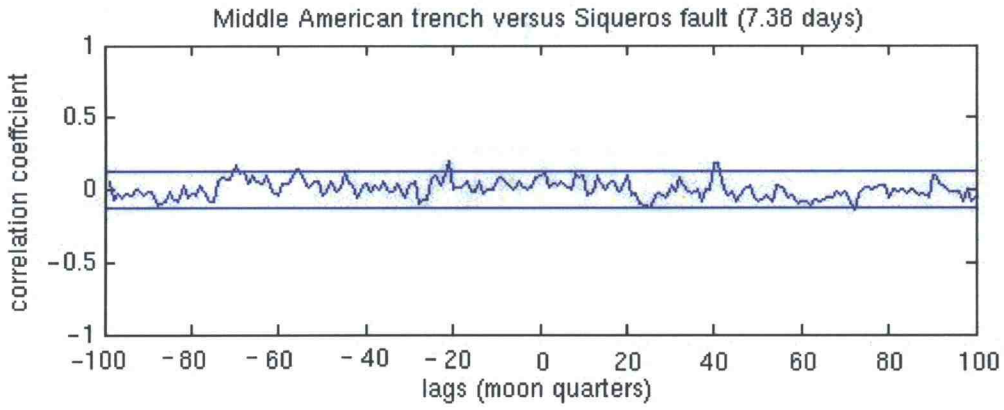
Middle American trench versus Siqueros fault (7.38 days)
correlation coefficient
1
0.5
0
-0.5
-1
-100 -80 -60 -40 -20 0 20 40 60 80 100
lags (moon quarters)

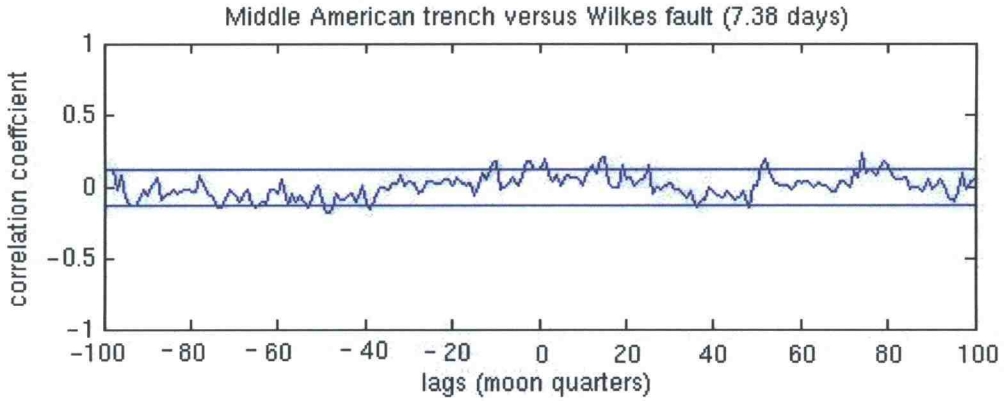
Middle American trench versus Wilkes fault (7.38 days)
correlation coefficient
1
0.5
0
-0.5
-1
-100 -80 -60 -40 -20 0 20 40 60 80 100
lags (moon quarters)

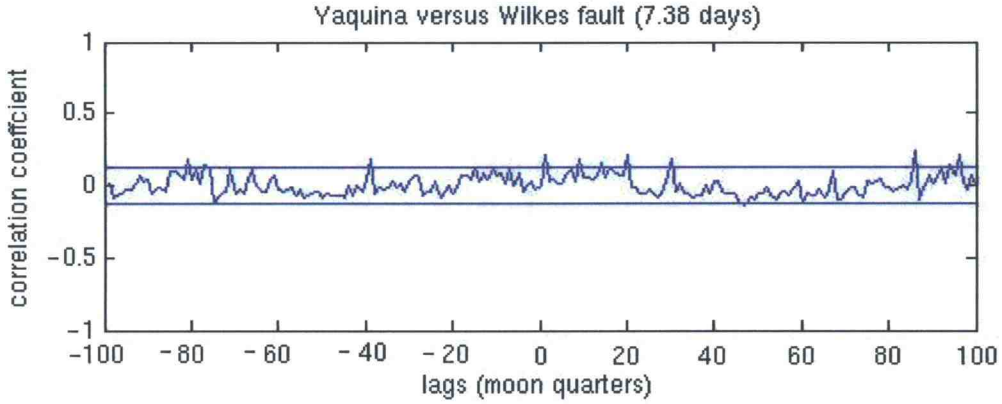
Yaquina versus Wilkes fault (7.38 days)
correlation coeffcient
1
0.5
0
-0.5
-1
-100 -80 -60 -40 -20 0 20 40 60 80 100
lags (moon quarters)

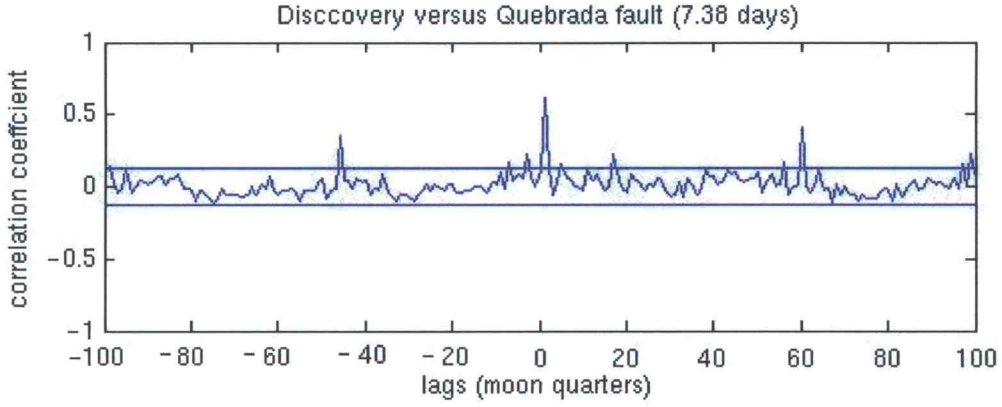
Disccovery versus Quebrada fault (7.38 days)
correlation coeffcient
1
0.5
0
-0.5
-1
-100 -80 -60 -40 -20 0 20 40 60 80 100
lags (moon quarters)

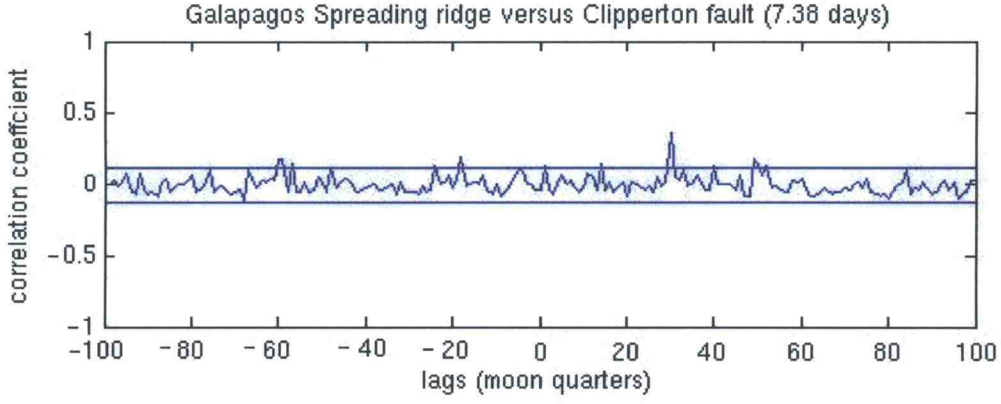
Galapagos Spreading ridge versus Clipperton fault (7.38 days)
correlation coeffcient
1
0.5
0
-0.5
-1
-100 -80 -60 -40 -20 0 20 40 60 80 100
lags (moon quarters)

3.1 Variance Spectrum analysis between seismic zones
(Time lag = 7.38 days)

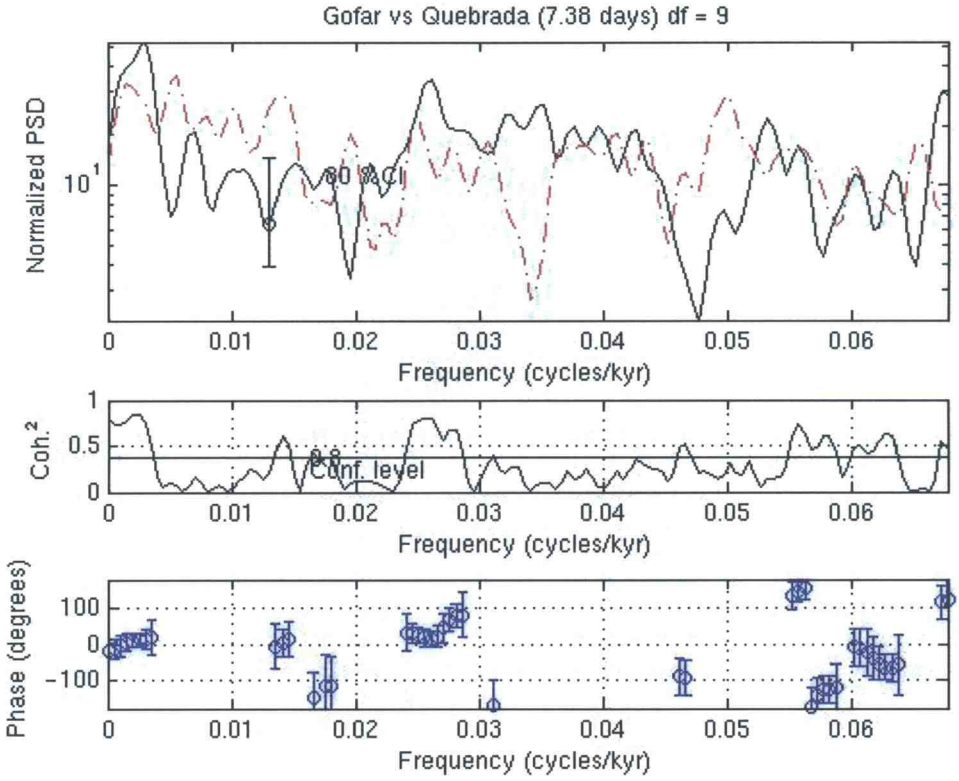

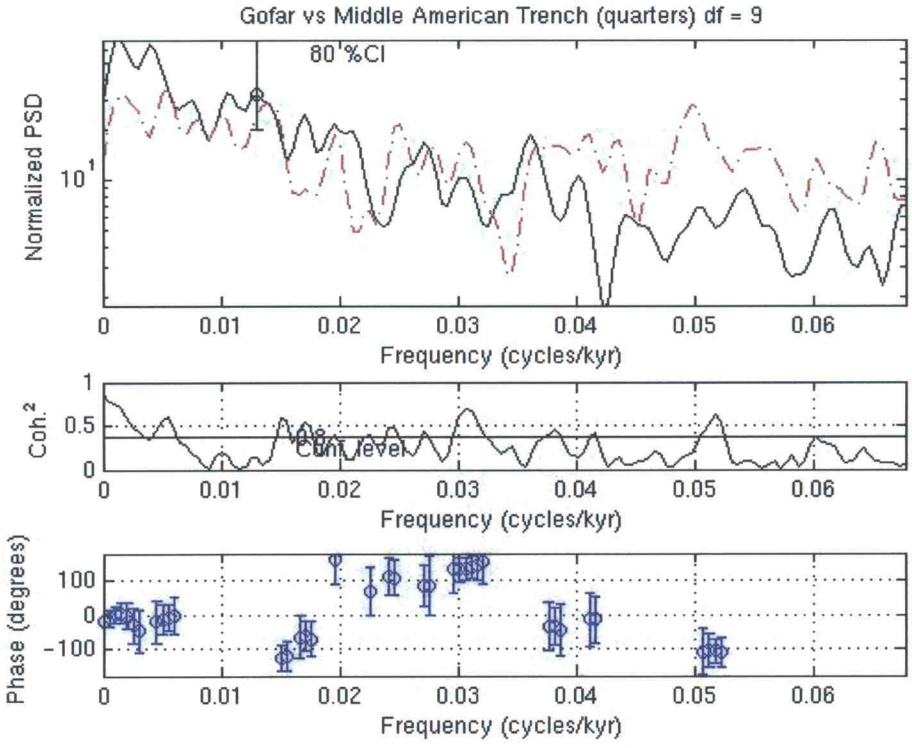
Gofar vs Middle American Trench (quarters) df = 9
80 %CI
Normalized PSD
Frequency (cycles/kyr)
Coh.²
95% Conf. level
Phase (degrees)

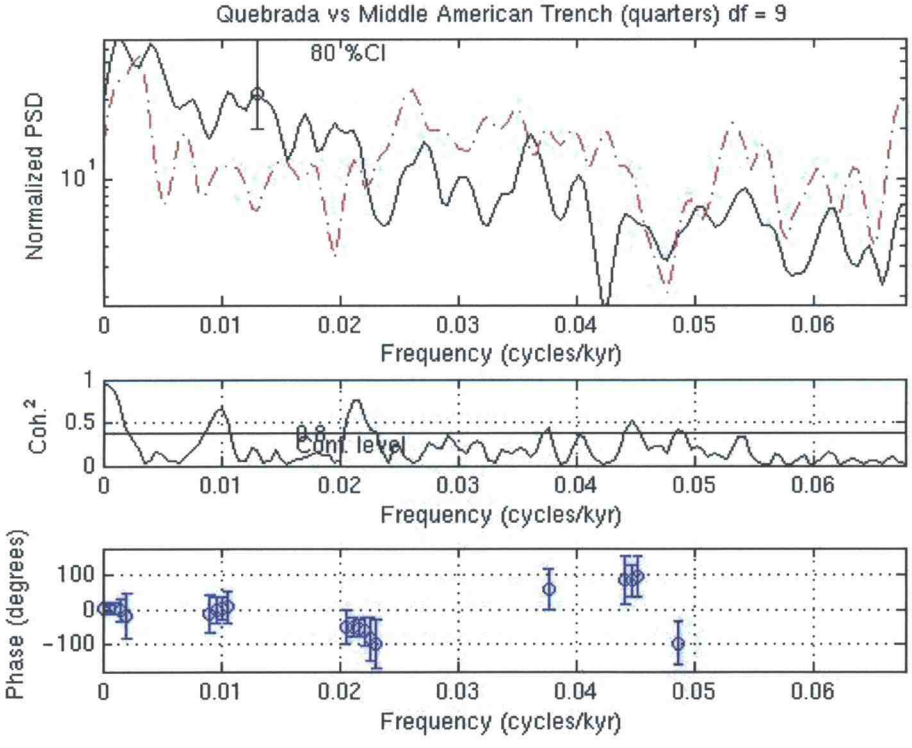
Quebrada vs Middle American Trench (quarters) df = 9
80 %CI
Normalized PSD
Frequency (cycles/kyr)
Coh.²
95% Conf. level
Phase (degrees)

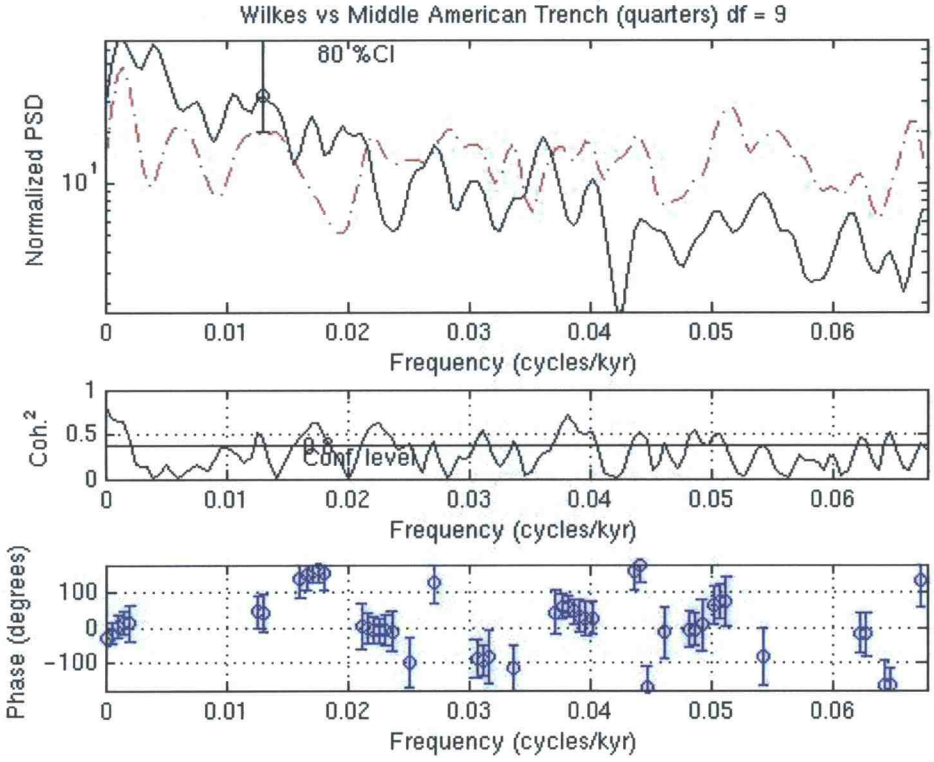
Wilkes vs Middle American Trench (quarters) df = 9
80 %CI
Normalized PSD
10^1
0
0.01
0.02
0.03
0.04
0.05
0.06
Frequency (cycles/kyr)
Coh.^2
1
0.5
0
95 % Conf level
Frequency (cycles/kyr)
Phase (degrees)
100
0
-100
Frequency (cycles/kyr)

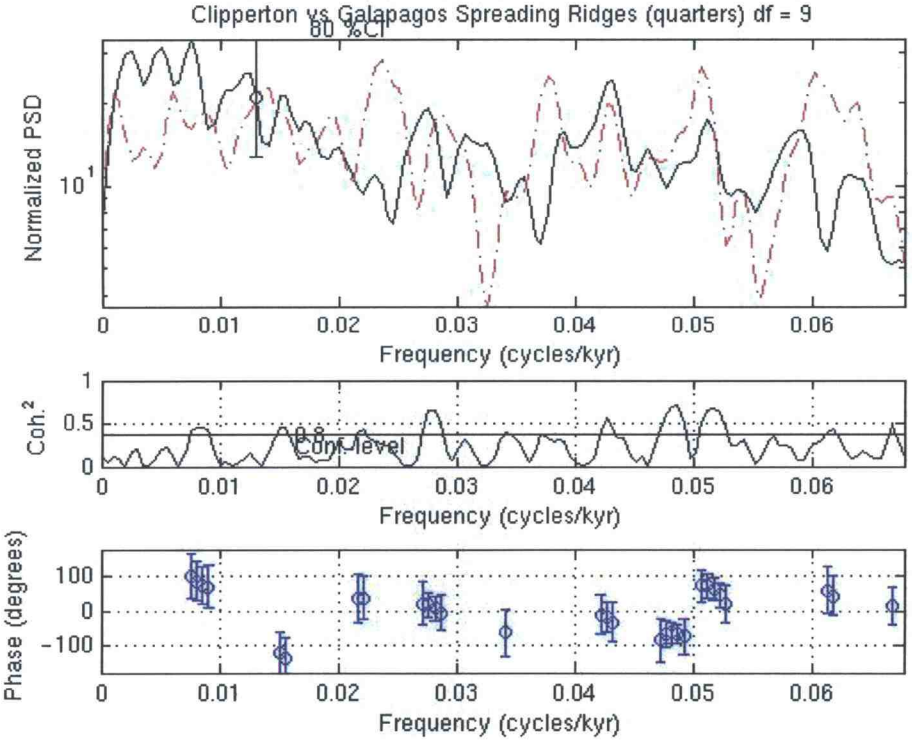
Clipperton vs Galapagos Spreading Ridges (quarters) df = 9
80 %CI
Normalized PSD
10^1
0
0.01
0.02
0.03
0.04
0.05
0.06
Frequency (cycles/kyr)
Coh.^2
1
0.5
0
95 % Conf level
Frequency (cycles/kyr)
Phase (degrees)
100
0
-100
Frequency (cycles/kyr)

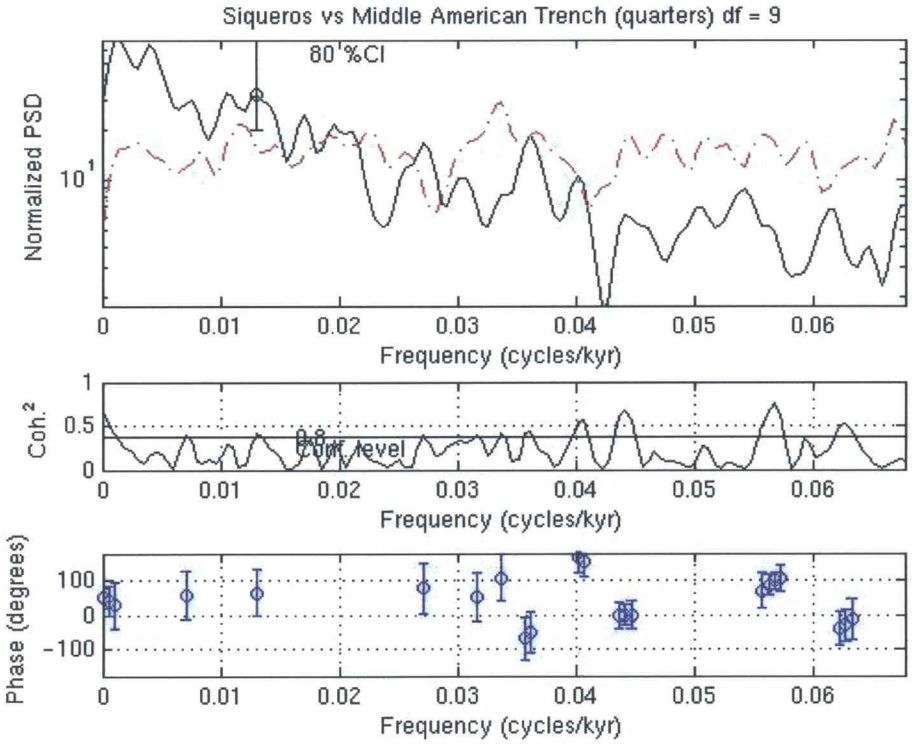
Siqueros vs Middle American Trench (quarters) df = 9
80 %CI
Normalized PSD
10^1
0 0.01 0.02 0.03 0.04 0.05 0.06
Frequency (cycles/kyr)
Coh.^2
1
0.5
0
0.8
Conf. level
0 0.01 0.02 0.03 0.04 0.05 0.06
Frequency (cycles/kyr)
Phase (degrees)
100
0
-100
0 0.01 0.02 0.03 0.04 0.05 0.06
Frequency (cycles/kyr)

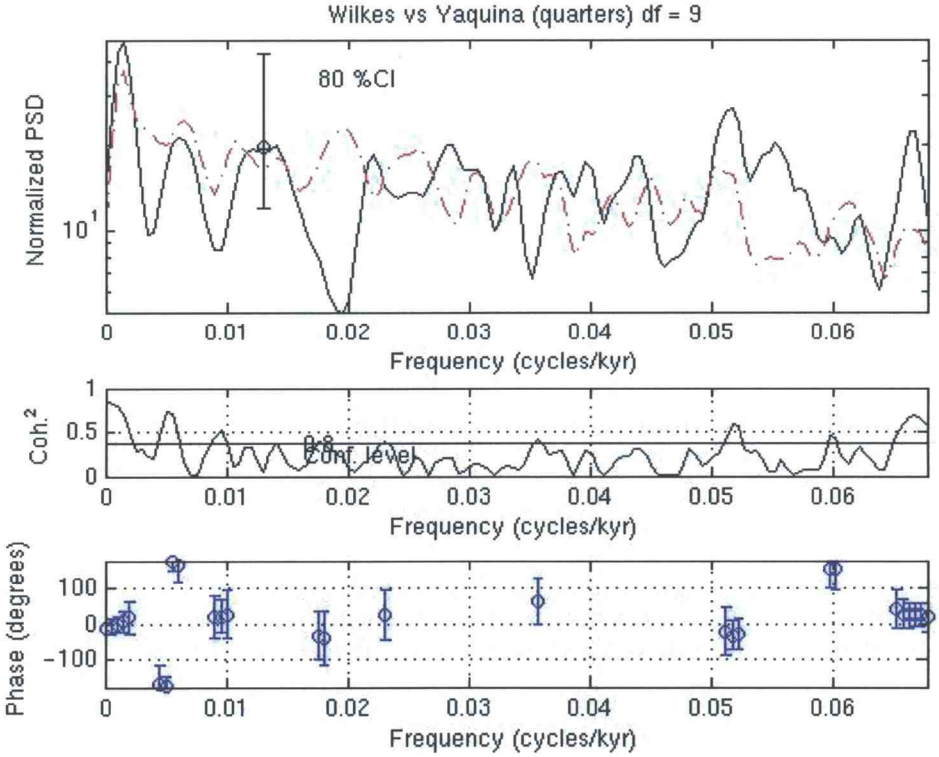
Wilkes vs Yaquina (quarters) df = 9
80 %CI
Normalized PSD
10^1
0 0.01 0.02 0.03 0.04 0.05 0.06
Frequency (cycles/kyr)
Coh.^2
1
0.5
0
0.8
Conf. level
0 0.01 0.02 0.03 0.04 0.05 0.06
Frequency (cycles/kyr)
Phase (degrees)
100
0
-100
0 0.01 0.02 0.03 0.04 0.05 0.06
Frequency (cycles/kyr)

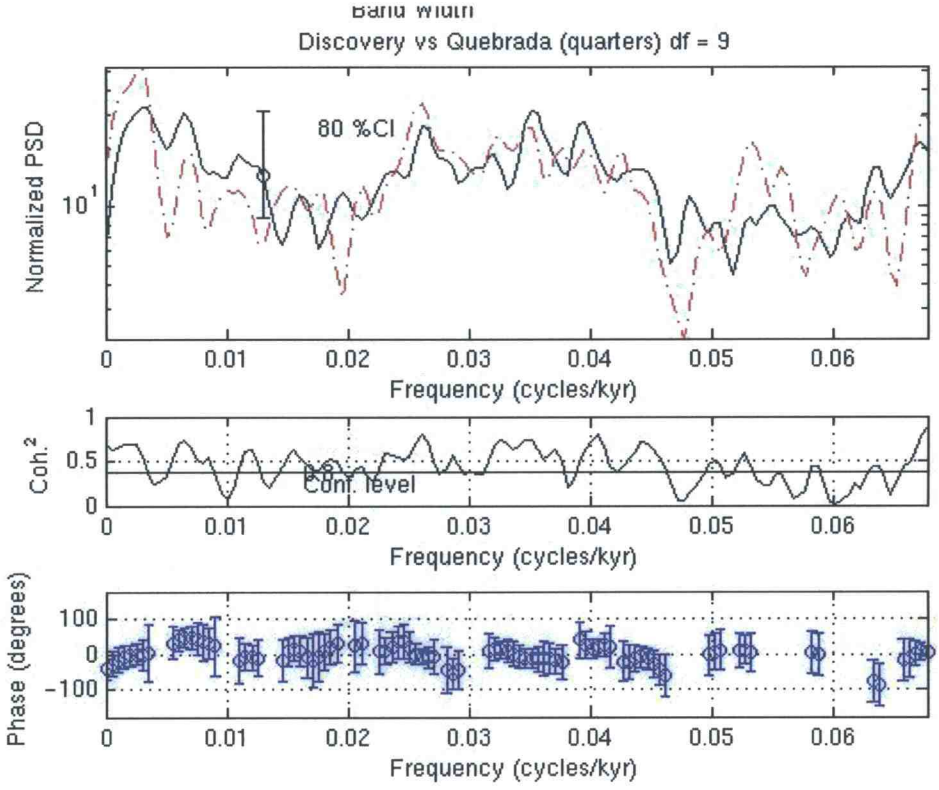
Band Width
Discovery vs Quebrada (quarters) df = 9
80 %CI
Normalized PSD
10^1
0
0.01
0.02
0.03
0.04
0.05
0.06
Frequency (cycles/kyr)
Coh.^{2}
1
0.5
0
95
Conf. level
Frequency (cycles/kyr)
Phase (degrees)
100
0
-100
Frequency (cycles/kyr)

4. Time-series cross-correlation analysis in the ocean tides time scale
4.1 Swarms in the Normal Faults
(Time lag = 1 hour)

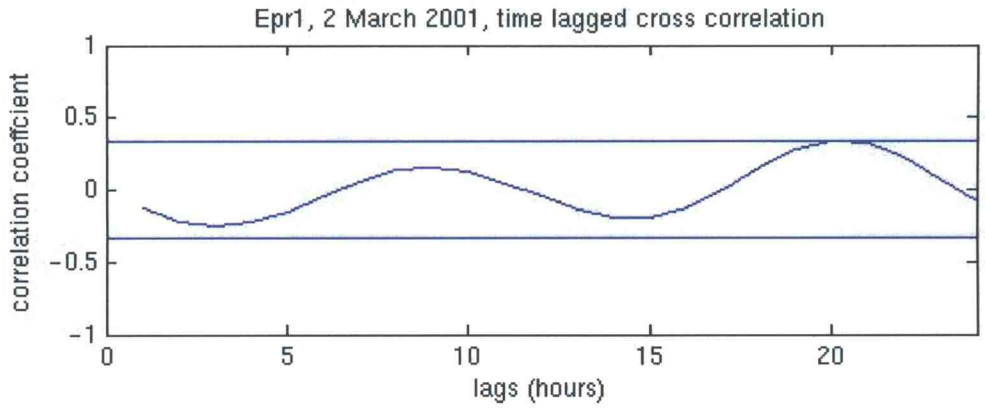

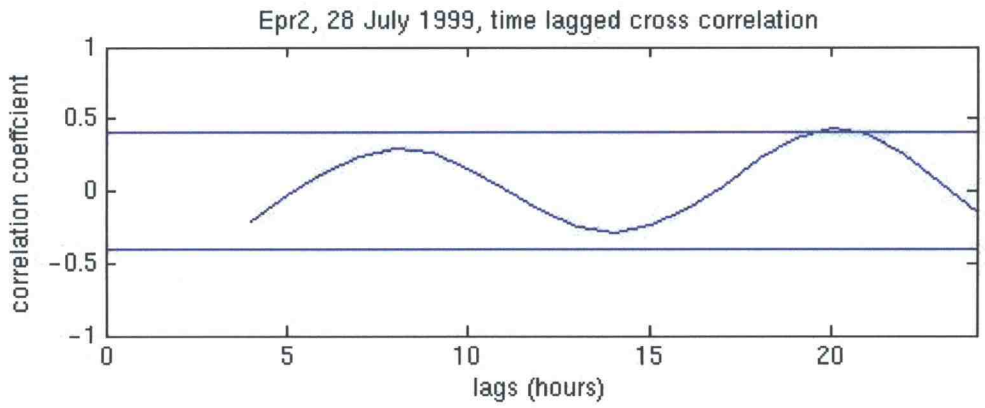

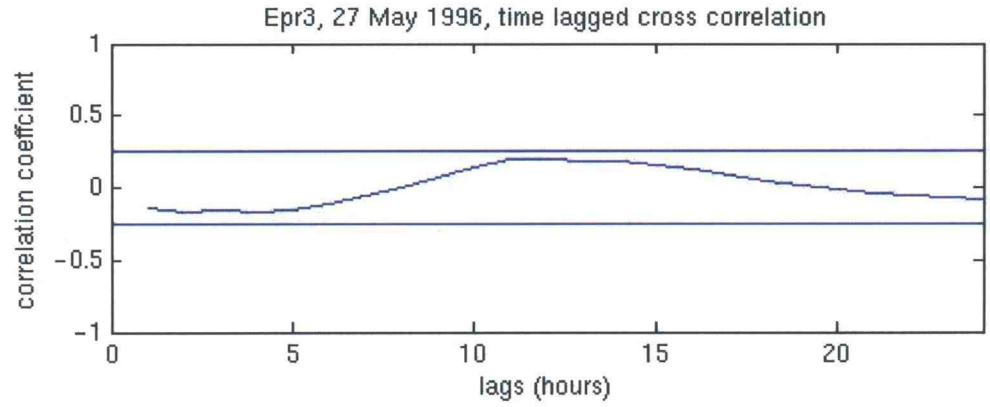
Epr3, 27 May 1996, time lagged cross correlation
correlation coeffcient
1
0.5
0
-0.5
-1
0
5
10
15
20
lags (hours)

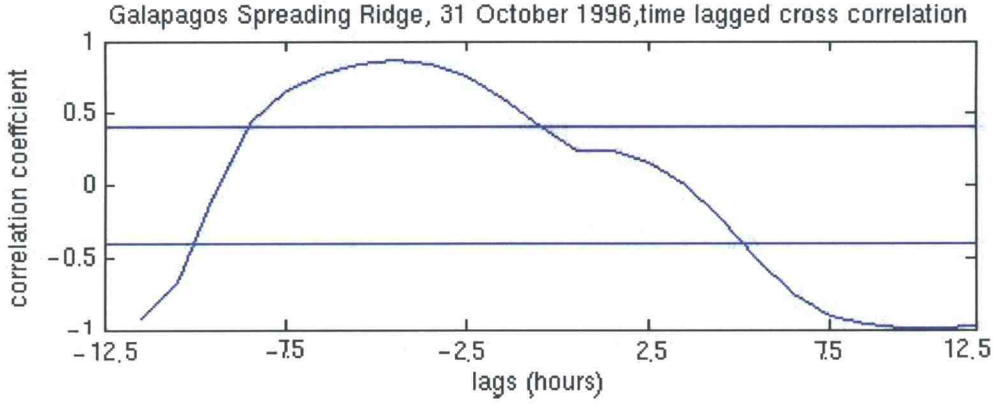
Galapagos Spreading Ridge, 31 October 1996,time lagged cross correlation
correlation coeffcient
1
0.5
0
-0.5
-1
-12.5
-7.5
-2.5
2.5
7.5
12.5
lags (hours)

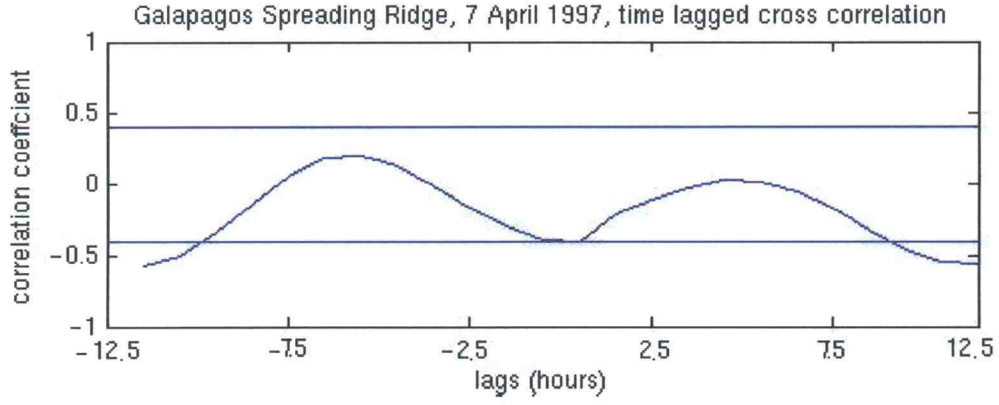
Galapagos Spreading Ridge, 7 April 1997, time lagged cross correlation
correlation coeffcient
1
0.5
0
-0.5
-1
-12.5
-7.5
-2.5
2.5
7.5
12.5
lags (hours)

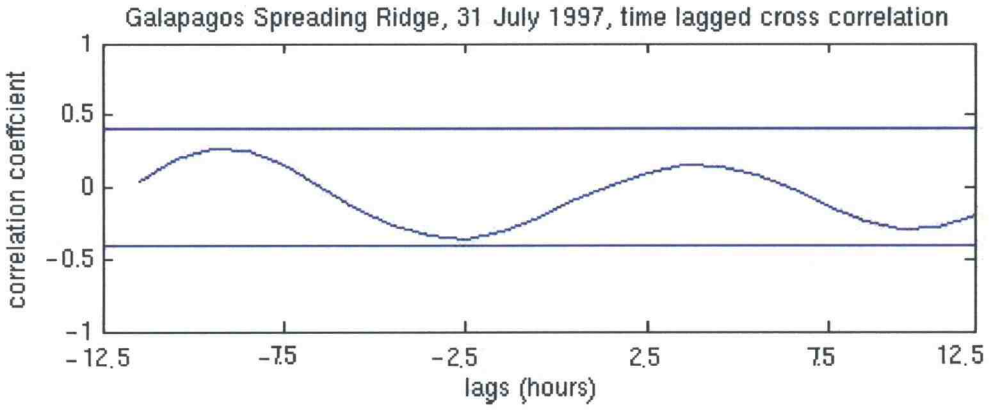
Galapagos Spreading Ridge, 31 July 1997, time lagged cross correlation
correlation coeffcient
1
0.5
0
-0.5
-1
-12.5
-7.5
-2.5
2.5
7.5
12.5
lags (hours)

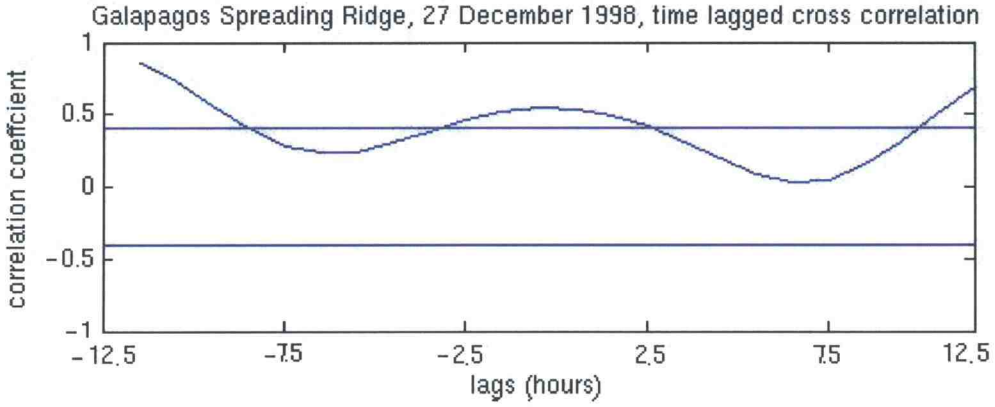
Galapagos Spreading Ridge, 27 December 1998, time lagged cross correlation
correlation coeffcient
1
0.5
0
-0.5
-1
-12.5
-7.5
-2.5
2.5
7.5
12.5
lags (hours)

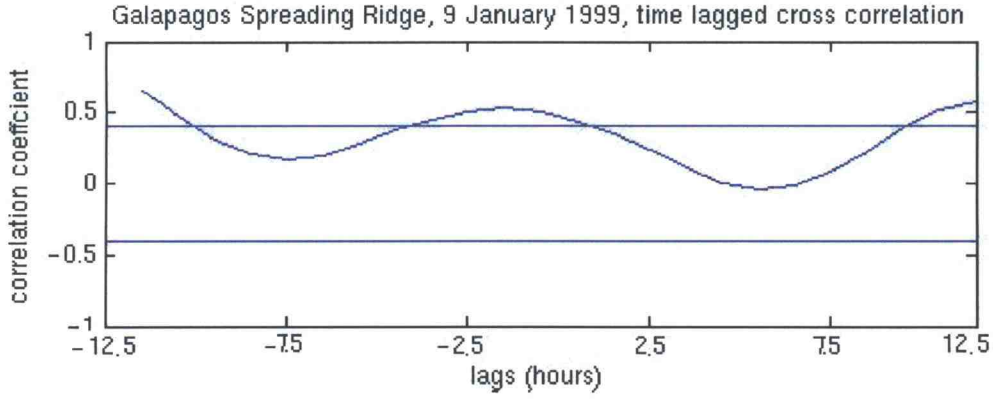
Galapagos Spreading Ridge, 9 January 1999, time lagged cross correlation
correlation coeffcient
1
0.5
0
-0.5
-1
-12.5
-7.5
-2.5
2.5
7.5
12.5
lags (hours)

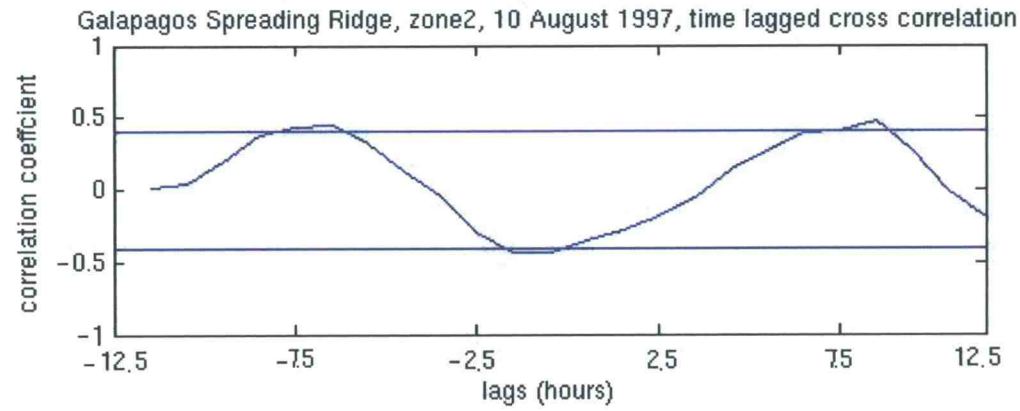
Galapagos Spreading Ridge, zone2, 10 August 1997, time lagged cross correlation
correlation coefficient
1
0.5
0
-0.5
-1
-12.5
-7.5
-2.5
2.5
7.5
12.5
lags (hours)

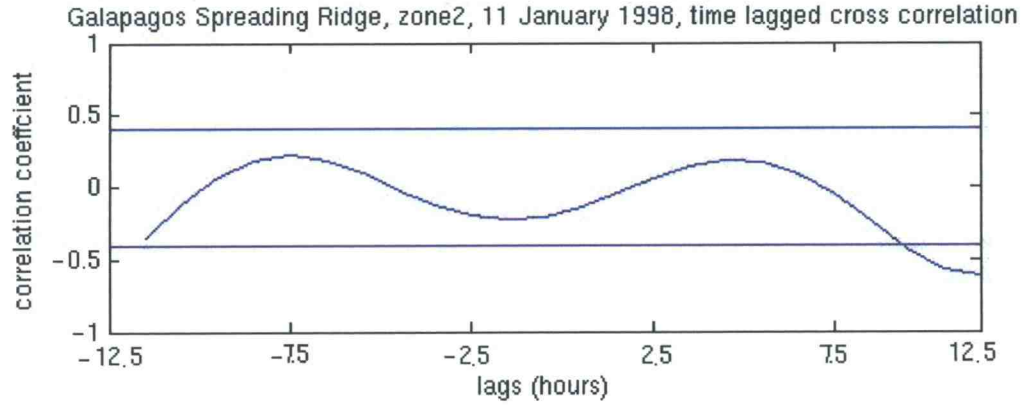
Galapagos Spreading Ridge, zone2, 11 January 1998, time lagged cross correlation
correlation coefficient
1
0.5
0
-0.5
-1
-12.5
-7.5
-2.5
2.5
7.5
12.5
lags (hours)

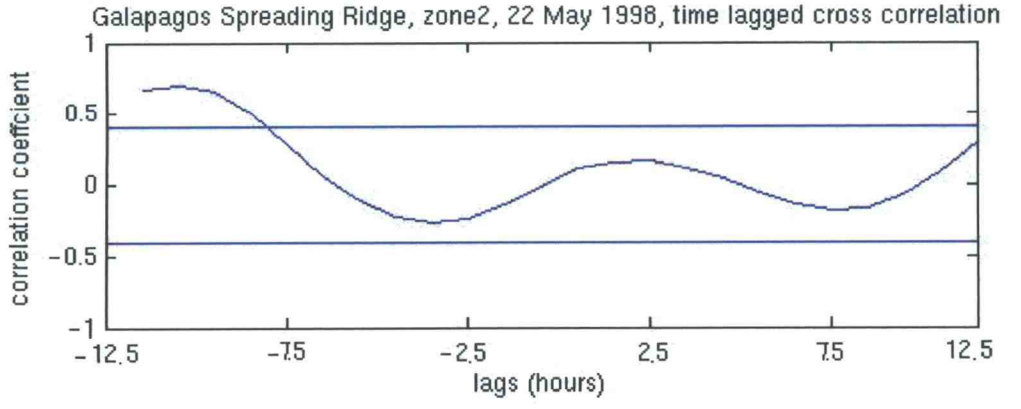
Galapagos Spreading Ridge, zone2, 22 May 1998, time lagged cross correlation
correlation coefficient
1
0.5
0
-0.5
-1
-12.5
-7.5
-2.5
2.5
7.5
12.5
lags (hours)

Galapagos Spreading Ridge, zone2, 30 Augost - 4 September 1998, time lagged cross correlation

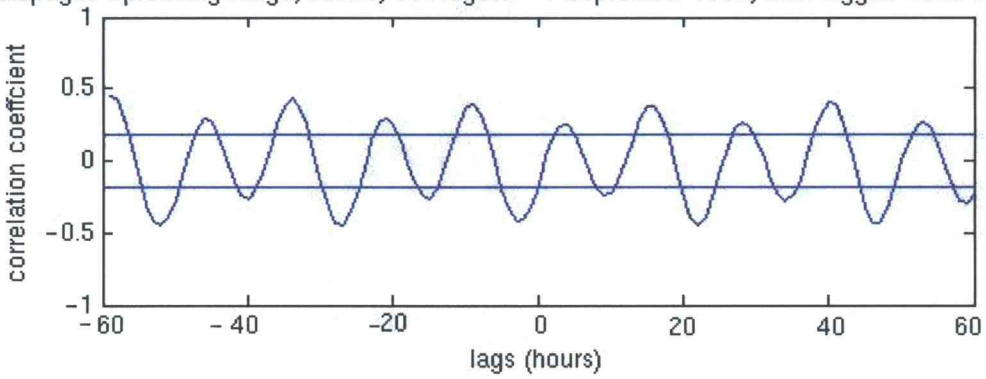

Galapagos Spreading Ridge, zone2, 22-23 September 1998, time lagged cross correlation

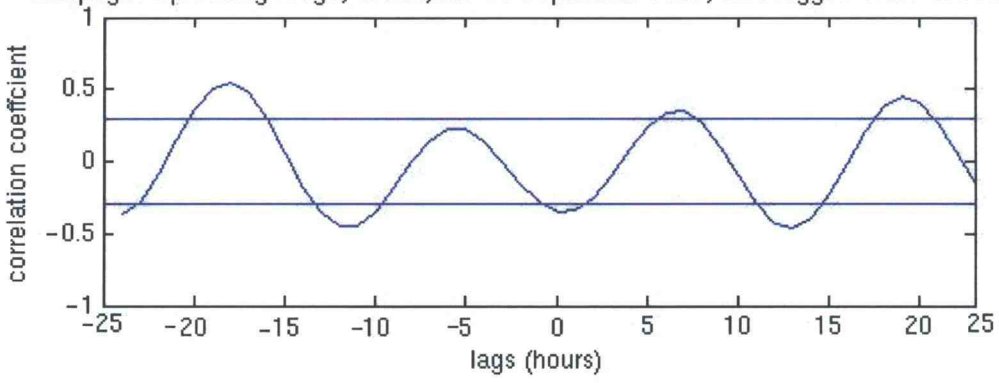

Galapagos Spreading Ridge, zone2, 16 September 1999, time lagged cross correlation

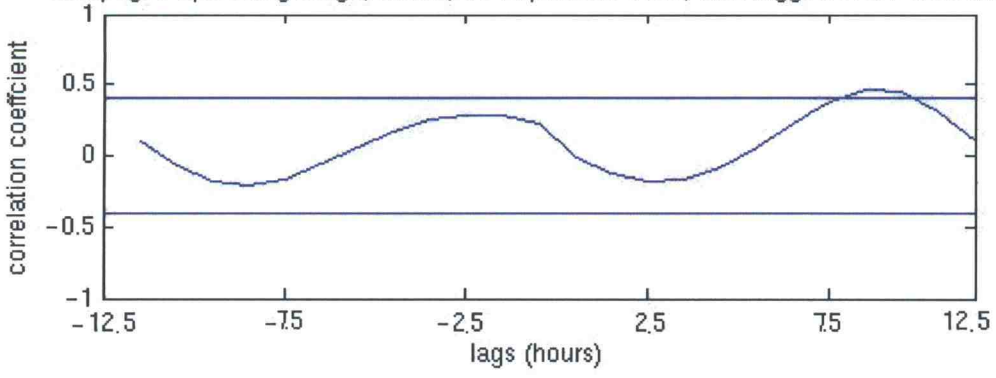

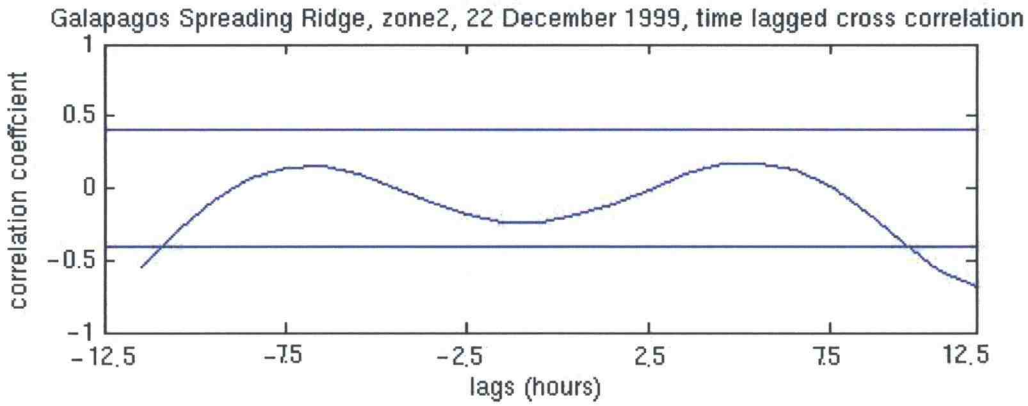

4.2 Swarms in the Transform Faults

(Time lag = 1 hour)

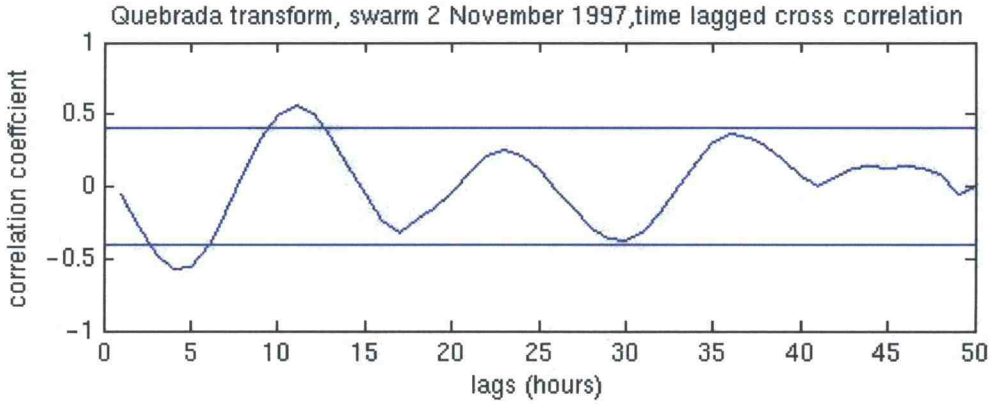

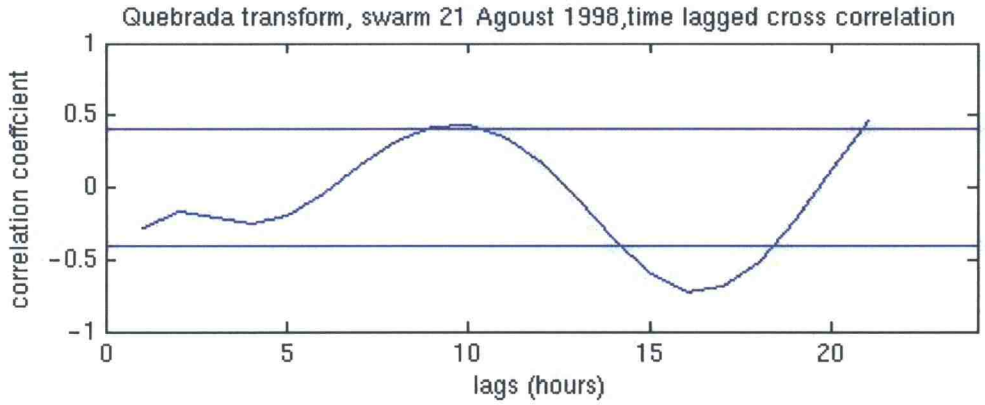
Quebrada transform, swarm 21 Agoust 1998,time lagged cross correlation
correlation coeffcient
1
0.5
0
-0.5
-1
0
5
10
15
20
lags (hours)

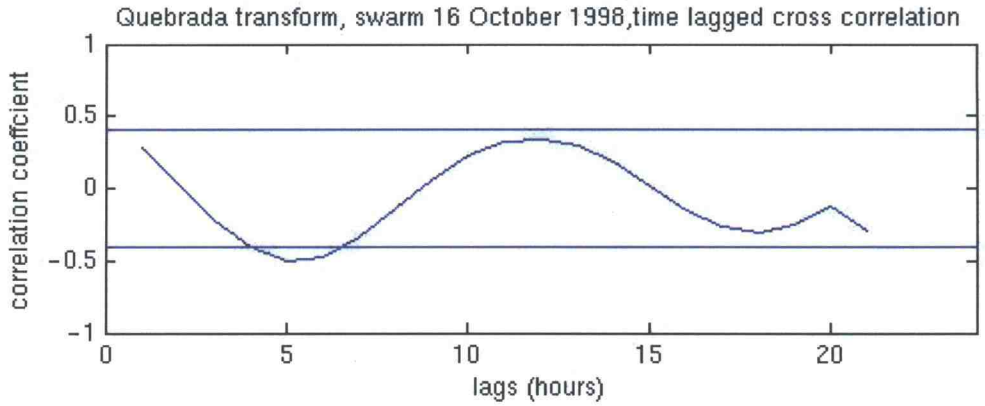
Quebrada transform, swarm 16 October 1998,time lagged cross correlation
correlation coeffcient
1
0.5
0
-0.5
-1
0
5
10
15
20
lags (hours)

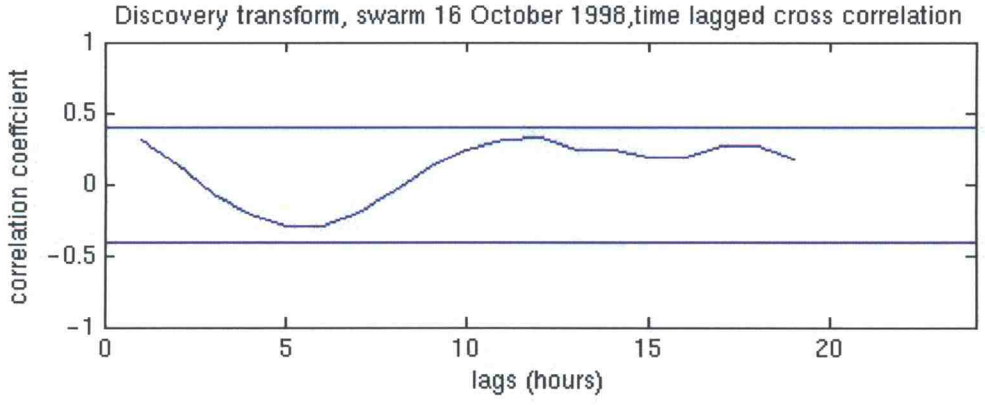
Discovery transform, swarm 16 October 1998,time lagged cross correlation
correlation coeffcient
1
0.5
0
-0.5
-1
0
5
10
15
20
lags (hours)

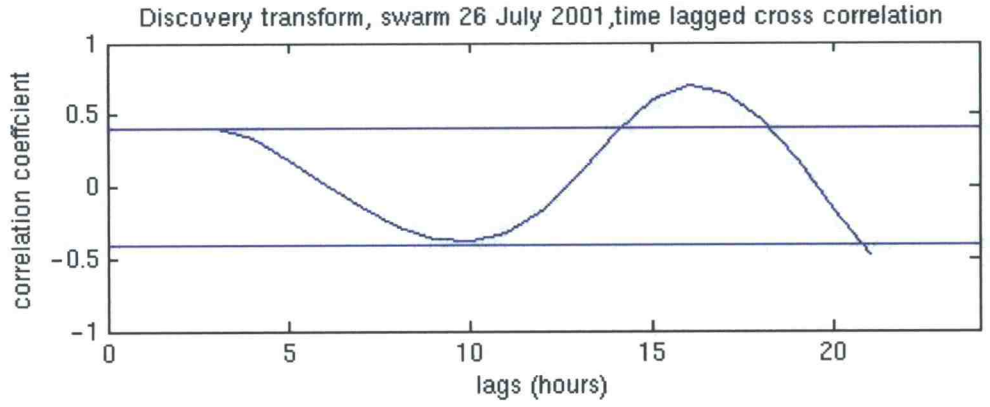
Discovery transform, swarm 26 July 2001,time lagged cross correlation
correlation coeffcient
1
0.5
0
-0.5
-1
0
5
10
15
20
lags (hours)

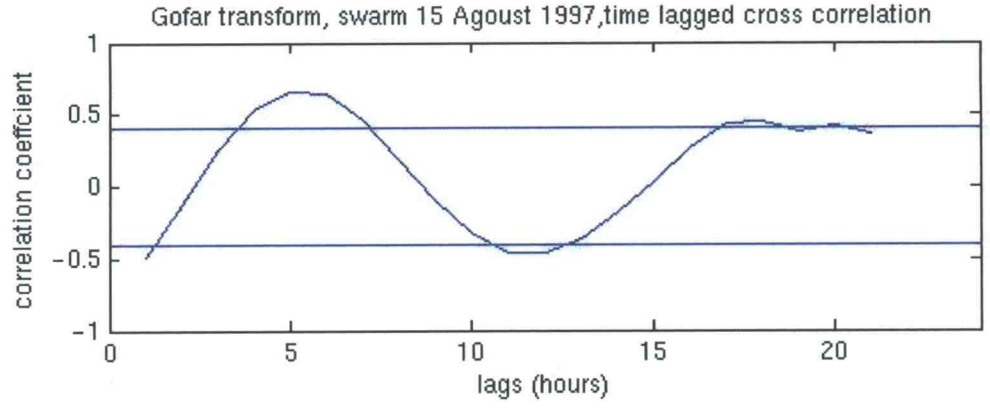
Gofar transform, swarm 15 Agoust 1997,time lagged cross correlation
correlation coeffcient
1
0.5
0
-0.5
-1
0
5
10
15
20
lags (hours)

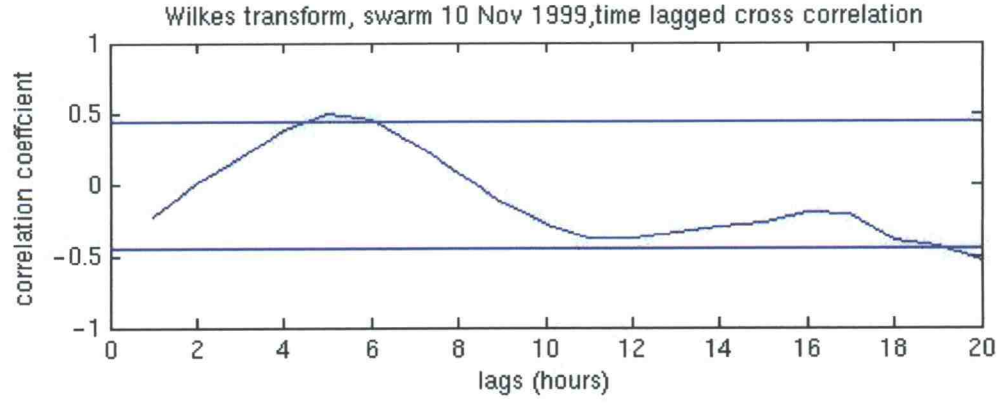
Wilkes transform, swarm 10 Nov 1999,time lagged cross correlation
correlation coeffcient
1
0.5
0
-0.5
-1
0
2
4
6
8
10
12
14
16
18
20
lags (hours)

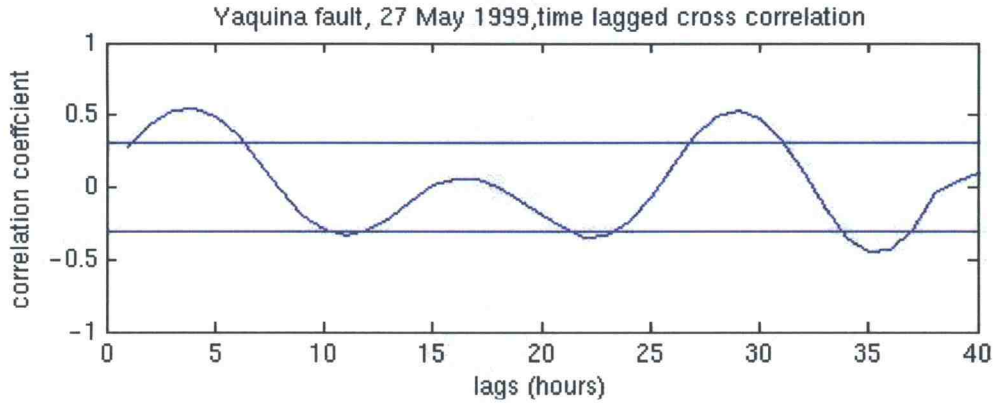
Yaquina fault, 27 May 1999,time lagged cross correlation
correlation coeffcient
1
0.5
0
−0.5
−1
0
5
10
15
20
25
30
35
40
lags (hours)

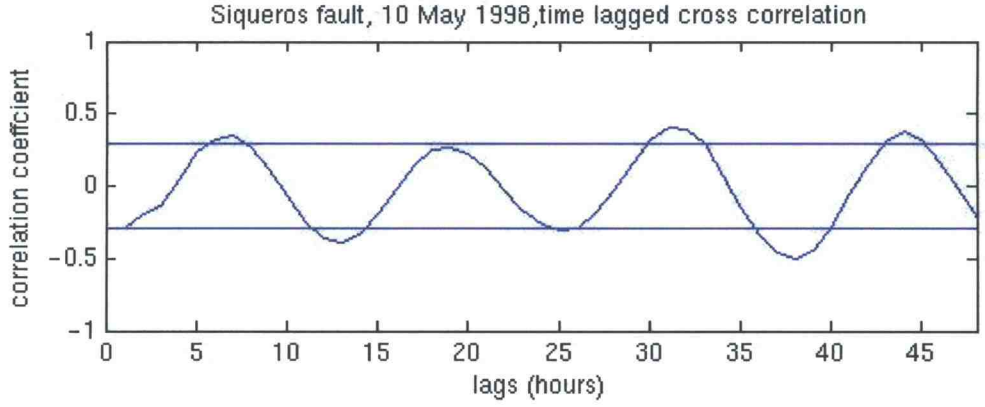
Siqueros fault, 10 May 1998,time lagged cross correlation
correlation coeffcient
1
0.5
0
−0.5
−1
0
5
10
15
20
25
30
35
40
45
lags (hours)

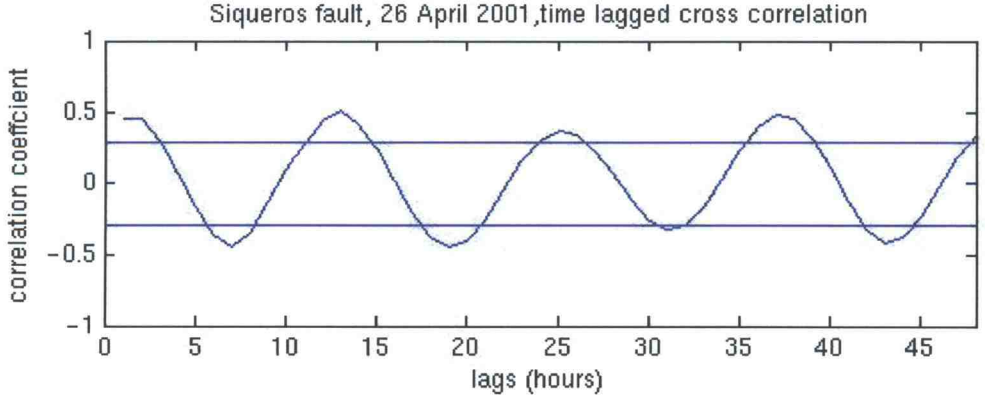
Siqueros fault, 26 April 2001,time lagged cross correlation
correlation coefficient
1
0.5
0
−0.5
−1
0
5
10
15
20
25
30
35
40
45
lags (hours)

8. APPENDIX 2

INTRODUCTION

This exercise consists of the first part of a research project that looked at possible triggering mechanisms for marine earthquakes. Earthquakes are used as an indicator of tectonic activity and the data were downloaded from the NOAA/Vents Program webpage (http://www.pmel.noaa.gov/vents). GIS is a powerful tool to select the data of interest, to make some first calculation, and to explore the characteristic of the data by doing a first descriptive statistics. GIS is a fast and user friendly tool to do these first operations, and it is extremely useful in the production of different maps regarding the data.

There are seven different short subchapters: the first two introduce the exercise and the last five explain step by step how to use GIS in such research.

1.1 What is GIS

An introduction to GIS, its components, its uses and its capabilities.

1.2 Obtaining the data

Explains why such data set was chosen for this research, and there are some basic explanations of plate tectonics. It then goes through the processes of obtaining the data from the NOAA webpage and how to move data from a text file into a GIS working station.

2.1 Displaying the data

Describes the first two layers we will be working with and how to change their look to make the map more user-friendly.

2.2 Data selection

Creates sub sets of the whole data set by creating a new feature, a layer running along the fault and by doing a buffer analysis (asking the software to select all those earthquakes that happened within a certain distance from the fault).

2.3 The attribute table

Explains what an attribute table is and how to explore the attribute table to obtain and store more information about your data. It then explains how to do add information to the attribute table and how to do some calculations between stored values.

2.4 The histograms

Explains what is a histogram, how to produce it and how to interpret it.

2.5 Geostatistical analysis

Shows other uses of the "geostatistical analyst" option. For example, it explains how to produce a normal or general Quantile Quantale Plot to compare and correlate data on different data sets.

At the end of this exercise the user should be able to import data from a text file into a GIS work station, display the data in different ways as more appropriate, explore the attribute table and use it to make calculation, and create and interpret histograms, normal and general QQPlots.

1.1 WHAT IS GIS

The Geographic Information System (GIS) is a computer system capable of linking geographic data shown in a map with other information stored in an attribute table. There are countless uses for GIS, including: agriculture, defence and intelligence, ecology and conservation, emergency management and public safety, environmental management, health care, education, real estate, mining, telecommunication and transportation.... For example, in this exercise, the GIS is able to store the data regarding the location of the earthquakes in the eastern tropical Pacific and to show it on a map. The data linked to each earthquake includes information regarding the magnitude and the timing of the events and all the calculation errors. In short, a GIS does not hold just a map or picture, it supports an entire database.

Using the information stored in the database, it is possible to use the GIS to perform spatial analysis. For example, it is possible do a query where the location of the strongest earthquakes on a fault is, when they occurred, how many earthquakes happened within a certain distance, and more.

The components of a GIS includes more than software. There are in fact other components that are necessary to have fully functional GIS system, which include:

People

A successful GIS user should be skilled in selecting and using tools from the GIS toolbox and should know well the data used. The GIS user should be able to create maps easily readable by the map user.

Hardware

There are many different kinds of computer, and GIS software can be purchased for any kind of computer. A fully functional GIS package is a "big" program and will need sufficient processing speed and RAM.

Software

The software is mainly a geographic database management system that is able to store geographic data, produce maps, and perform spatial analysis.

Data

Data can be both spatial and descriptive, for example, storing information about the location of the earthquake and attributes, such as the magnitude and the timing of the event.

The GIS software used in this exercise is called ArcGIS. The ArcGIS desktop includes different applications such as ArcMap, ArcCatalog and ArcToolbox. By using these applications in concert, different tasks, such as mapping, spatial analysis, data editing, can be performed.

In this exercise we will use both ArcMap and ArcCatalog. ArcMap is used for map-based tasks including cartography, map analysis, and editing. The ArcCatalog is use to organize and manage all GIS information such as maps, globes, data sets and models.

1.2 OBTAINING THE DATA

Why should we study earthquakes?

Earthquakes are indicators of tectonic activities. Earthquakes occur on the lithosphere when there is a rupture in the crust and they are an indicator of plate boundaries which include: spreading zones, strike-slip faults and subduction zones. ***Spreading zones*** are zones where plates move away from each other and new crust is being formed and have a shallower bathymetry given by the upwelling magma. They are characterized by shallow earthquakes with low magnitude. ***Compressional*** boundaries are areas where plates collide. In the ocean they create deep trenches and their earthquakes are found in several settings ranging from the very near surface to several hundred kilometres in depth, since the cold temperature of the subducting plate permits brittle failure down to as much as 700 km. Compressional boundaries host Earth's largest quakes, with some events on subduction zones in Alaska and Chile having exceeded a magnitude 9 on the Richter scale. ***Transforms faults*** are areas where plates mostly slide past each other laterally, producing less sinking or lifting of the ground than spreading or compressional environments. Earthquakes are shallow, running as deep as 25 km.

Plate tectonics links:

- http://www.seismo.unr.edu/ftp/pub/louie/class/100/plate-tectonics.html
- http://neic.usgs.gov/neis/plate_tectonics/rift_man.html
- http://volcano.und.nodak.edu/vwdocs/vwlessons/plate_tectonics/part12.html

From Excel to GIS

Data regarding earthquake events (time, magnitude and location and calculation errors) for the study area in the Eastern Tropical Pacific are available from the NOAA-PMEL catalogue, available on the VENTS website (http://www.pmel.noaa.gov/vents/data/index.html). Click on VentsGetPosit to retrieve the data. Change the latitude parameter to +20 and -20, and the longitude parameters to -70 and -120. Leave the other parameters as they are. These data ranges from May 1996 to November 2002 and were obtained by hydrophones able to monitor low level seismicity, by recording acoustic energy radiated into the water column by earthquakes and other sources (*T*-phases). Since the hydrophones are moored in the study site, sound energy from earthquakes is promptly recorded and it undergoes minimal attenuation. For this reason, the hydrophones are able to detect sound energy from the smallest earthquakes and the data has minimum location and timing errors.

- http://www.pmel.noaa.gov/vents/acoustics/bibliography.html

Create a new folder called "exercise" and save the data in it as a text file. You will use this folder as a container throughout all the exercise to keep the data together. The data includes 9 columns, each row being an earthquake. The first column indicates timing of the events, with the digits representing the year, the day, the hour, the minute and the second in the following order: YYYYDDDHHMMSSS. The second column tells how many hydrophones were able to detect the earthquakes (the more, the better). The third column lists the ID's of the recording hydrophones. Column 4 and 5 contain information on, respectively, the latitude and the longitude of the event, meanwhile the following three columns (column 6, 7 and 8), give an estimate of errors for latitude, longitude and source time. The last column, column 9, contains information about the level of acoustic energy recorded by the hydrophones (in decibels).

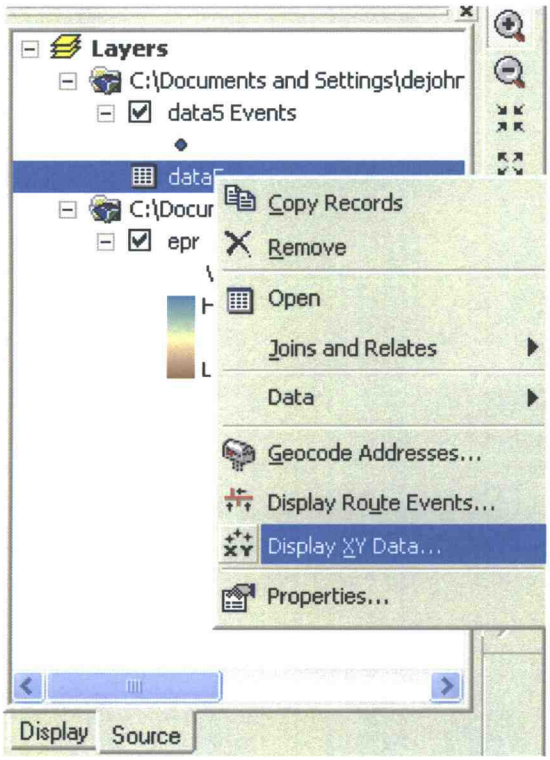

Open the .txt file in Excel, delete the first rows and the last row containing text and save the whole as a DBF 4 (dBASE IV) (*.dbf), in the save as type box. You should have around 33960 earthquakes recorded.

Now open ArcMap and click on the Add data bottom.

Navigate to the saved data and press OK. The data will appear in a table format in the Source lab of ArcMap. Right click on the imported data, and then "Display XY Data".
Select for the Longitude (N5) for the "X field" and Latitude for the "Y field". Then press "Edit" to define the coordinate system you want to use for the projection. Press "Import" and navigate to the coordinate system wanted. Choose the D_North_American_1927 datum, from
GCS_Assumed_Geographic_1.

If you are having problems going though these processes, you can download the previously georeferenced data from the "data.dbf" link.

2.1 DISPAYING THE DATA

A raster layer with the bathymetry of the studied area is also available in the "epr.lyr" link. Save it into the "exercise" folder and add it to the map using the Add Data botton.
Your data should now look like this:

On this map, each point represents an earthquake. Concentrated locations where many earthquakes are and some other areas where single earthquakes are present can be distinguished. In this research, I am only interested in earthquakes happening in spreading centers, transform faults and the subduction zone. By adding a background

picture of the seafloor topography, it is easier to distinguish the features I am interested in: spreading centers are correlated with ridges, transform fault with linear scarpes on the seafloor and subduction zone with deep trenches.

Let's look at only the EPR layer now by unchecking the box of the EPR_alldata. The dots representing the earthquakes will disappear and you will now be able to distinguish different features in the map: the coast of central and South America, where the Mid American Trench is, the spreading ridges and the scarpes of the transform fault.

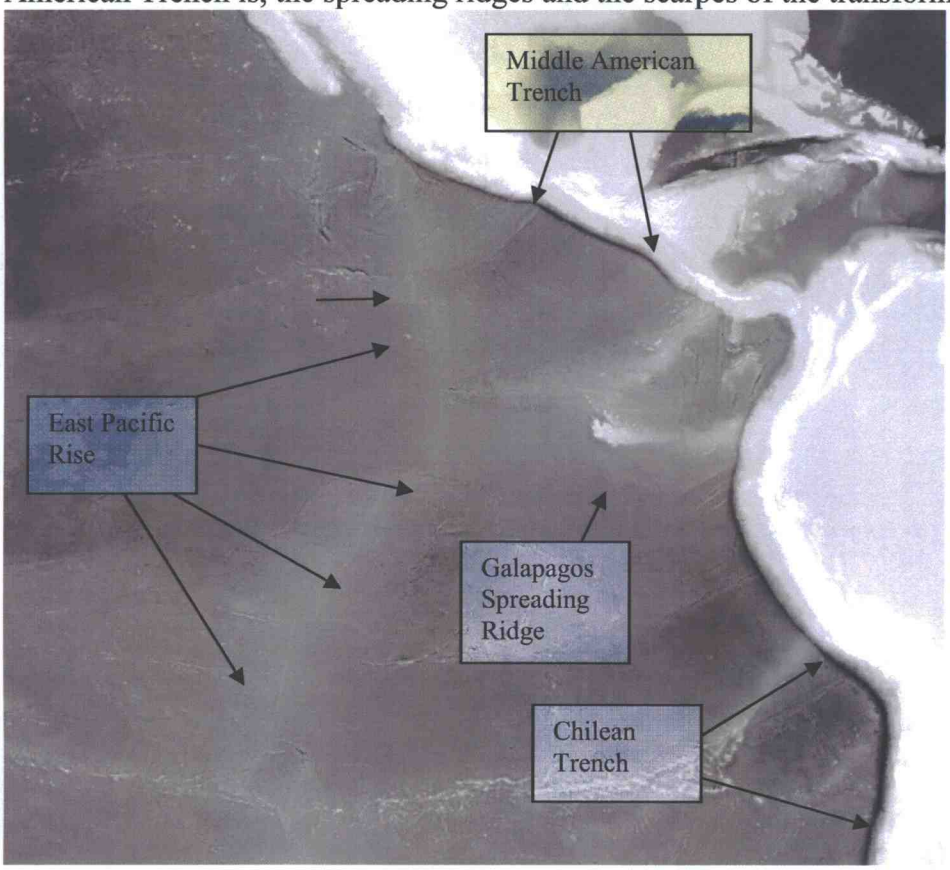

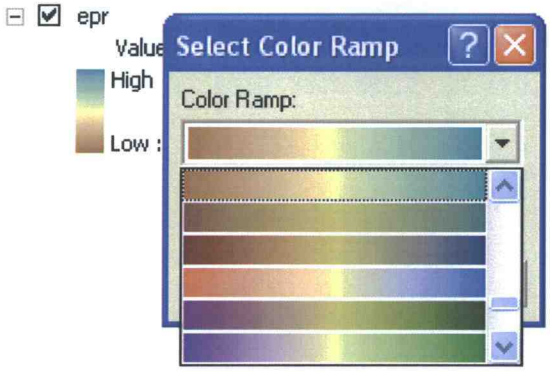

Maps have to be clear to be useful and informative, and sometimes it is necessary to make some changes to make them more easily interpretable. It is possible, for example, to change the colors of the bathymetry layer in order to make features such as rises, flanks, scarps and trenches stand out.

To change the colors in the layers of the

eastern Pacific, double click on the legend and then choose a different color ramp. It is also possible to invert the color by clicking in the opposite box.

This is an example of stretched symbology, but it is also possible to break different depths in different classes, by selecting the Classified field in the "Layer Properties" option (right click on the layer, then "Layer Properties").

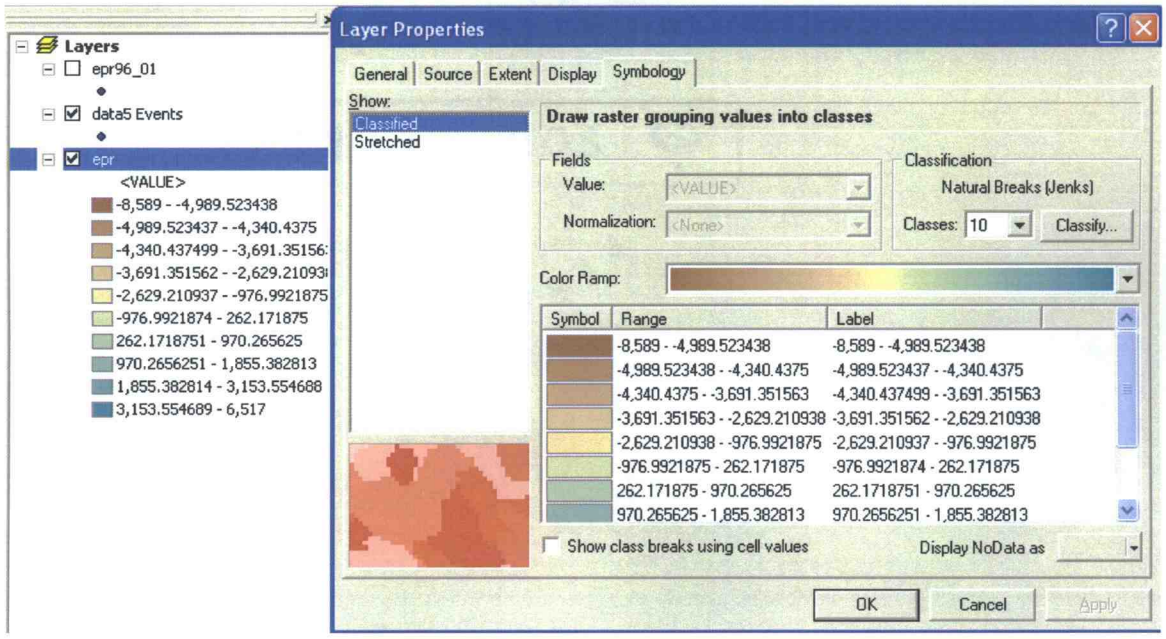

Choose an appropriate color ramp and choose how many classes you want from the "Classes" option. Click "Apply" and then "OK".

The next two figures represent the bathymetry layer as Stretched and as Classified in 10 different categories.

I find that displaying the data using a stretched ramp, more information regarding the bathymetry of the sea floor is maintained. It is possible to see a dark brown line representing the deeper middle American trench, where the Cocos Plate is subducted underneath the Middle American plate. Also, on the far right, it is possible to see part of the Chilean trench. Yellowish, lighter colored areas are the shallower part: this represents spreading centers, in this case the East Pacific Rise (EPR) running in the north-south direction, and the Galapagos Spreading Ridge, running east-west two degrees north of the equator.

Along the EPR, features such as strike-slip transform faults, where plates pass along each other, are clearly visible by zooming closer as shown in the figure above. The lines indicate higher areas with higher topography which are the Clipperton fault in the north and Siqueros fault the south. The scarves that the faults left on the crust as it moved away from the spreading center toward the Middle American subduction zone can also be seen.

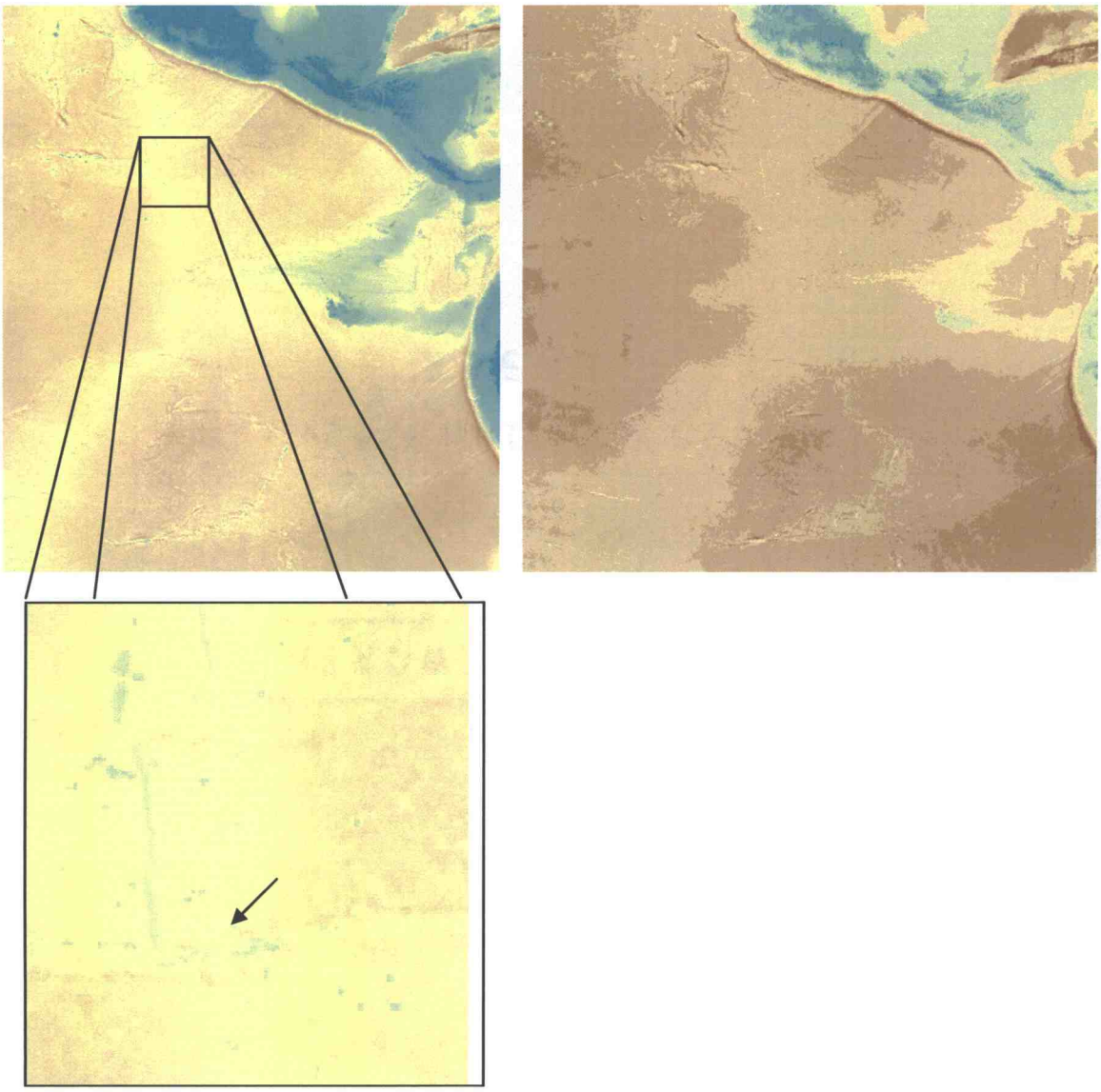

2.2 DATA SELECTION

The data clearly contain some errors in earthquake positioning. Moreover, we want to be able to divide the whole data set into smaller data sets to explore the seismicity in each fault. We will therefore create new subsets containing earthquakes for each fault by performing a buffer analysis. A buffer is a zone of a specified distance around a feature. In this case, it will be a zone where earthquakes happen at a determinate distance from a fault. After identifying this zone, the earthquakes will be selected and saved into a new layer.

Let's separate the earthquake on the Middle American Trench (MAT) from the whole data set. To do this, we will first create a new feature, a line what will run along the length of the MAT. Then we will operate a buffer analysis asking ArcMap to select all those earthquakes that happen in a buffer zone of 70 km from this line.

To create the line, we will temporarely leave ArcMap and use ArcCatalog. Click on the ArcCatalog icon and then navigate to the location where you are currently working. Right click on an empty space, the "New" and then "Shapefile".

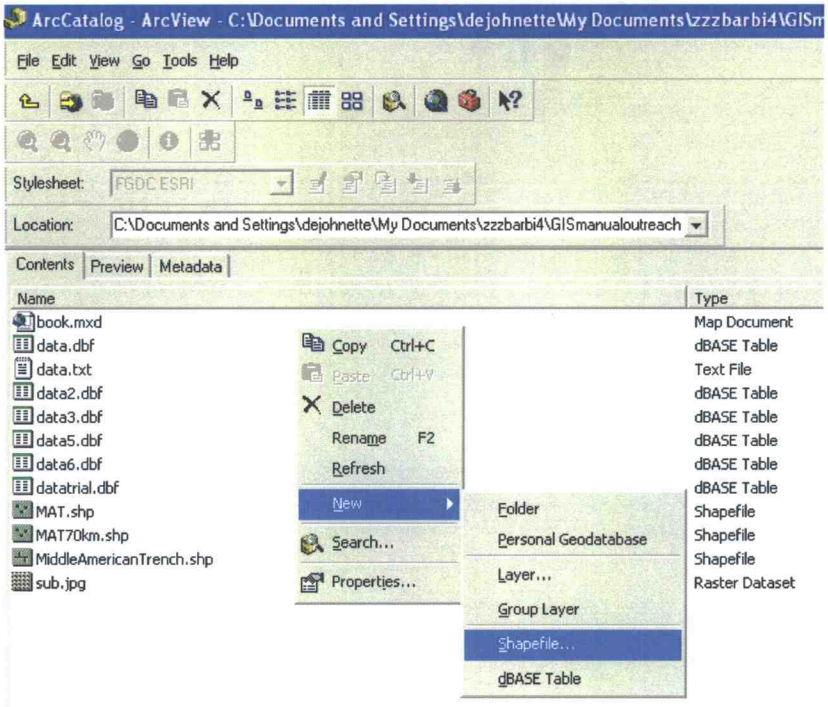

Choose an appropriate name for the new shapefile; choose "Polyline" in the feature type box. Click Edit and choose the same geographic projection as the one you used in the past for the other layers. You can do this just by clicking in "Import" and then select an already existing layer.

Create a new layer for each fault we will be looking, for example: Middle American Trench, Siqueros, Clipperton, Galapagos, Quebrada, Gofar, Discovery, Yaquina and Wilkes.

After the new lines have being created in ArcCatalog, return in ArcMap and add the new layers to the map. One by one, we will have to edit them so that they will fall on the corresponding faults.

Go to "Editor" and then "Start Editing". Select the area you are working and then click on "Start Editing". (If the "Editor" option is not available on your ArcMap screen, go to the "View" option in the Main Menu, then "Toolbar" and click next to the "Editor" option to make it appear in the ArcMap display).

Now, choose as "Target" the line you want to work in, for example the middle American trench; task is to "create new feature", and the on the left side select the way you want to draw the line.

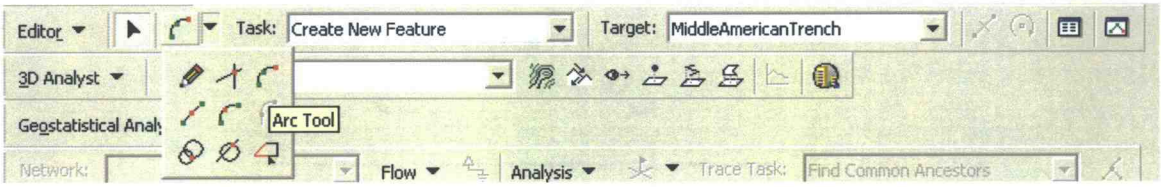

Using the bathymetry layer as a help to find the faults on the seafloor, trace a line as shown in the figure. When finished, go to "Editor", "Save Edits" and then "Close Edits". Repeat this process for all the other lines created.

Since earthquakes on the subduction zone happen in deeper depth toward the continent, I slightly move the line just drawn line inland.

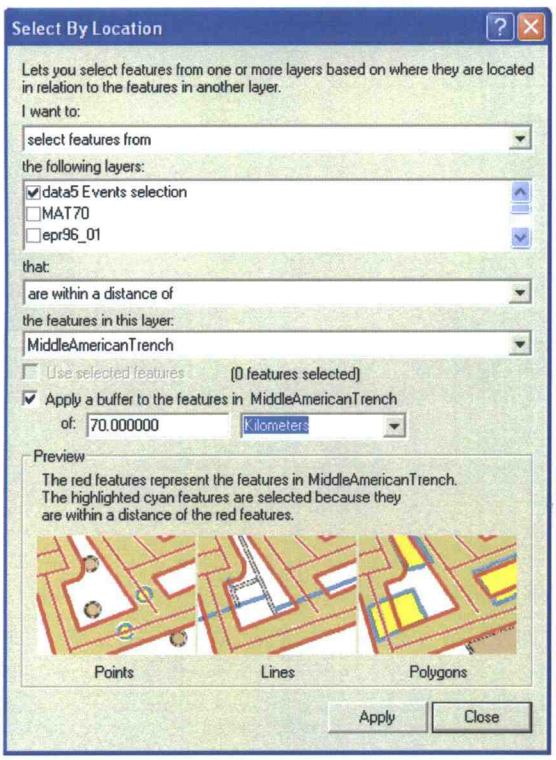

It is now possible to run the buffer analysis to select all those earthquakes from the whole dataset that happened within a certain distance from the middle American trench.

From the Main Menu click on "Selection" and then "Select by Location". In the dialog box, you want to "select features from" the layer where the whole dataset is (in my case it is called "data5 events"), that "are within a distance of" "the feature in this layer:". Choose the Middle American Trench, the line that you just edited. Lower in the box, I asked to apply a buffer of 70 km. Click "Apply".

The earthquakes selected will now be underlined in the map. To create a new layer from this selection, right click on the

whole dataset ("data5"), then "Selection" and then "Create layer from selected feature". The new layer will appear on top of all layers. Rename it in a new descriptive way, for example MAT70 (= Middle American Trench, 70 km buffer). To save this new layer, right click on the name, then "Data" and "Export Data". Save the new data with a different name, i.e. "EaMAT70.lyr".

Repeat the buffer analysis with all the other faults. At the end of this exercise, you should have 9 new layers, one for each fault, containing information on the earthquakes that happened between 1996 and 2002.

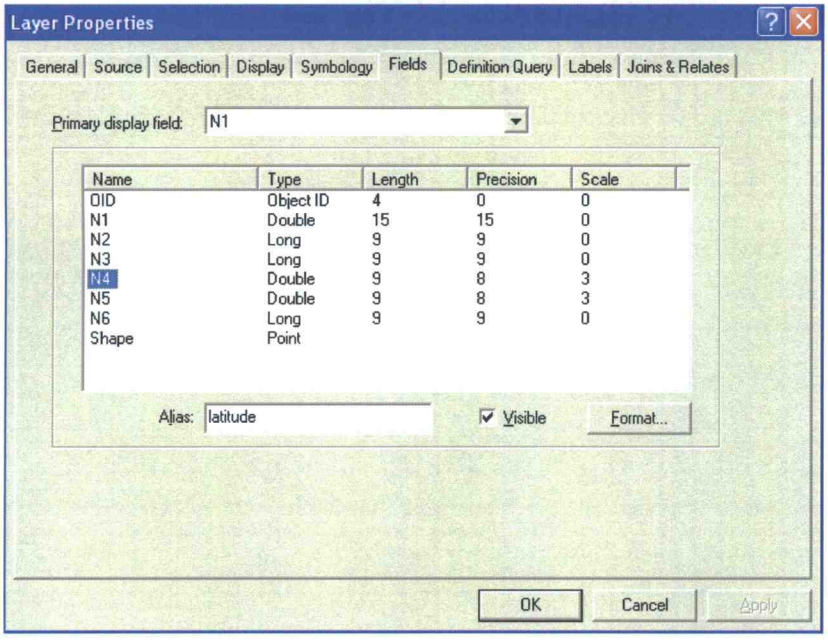

2.3 EXPLORING THE DATA: THE ATTRIBUTE TABLE

GIS can link the spatial data with information stored in attribute tables. Therefore, each point representing an earthquake on the map also contains tabular information stored as attributes in a linked file. For example, each earthquake has information about the latitude and the longitude it happened, and this information is used to project the event on the map. For each earthquake, the attribute table also stores information regarding the timing of the event and the sound pressure values in decibels.

To open the attribute table, right click on the data layers, and then select "Open Attribute Table". The attribute table should look like this:

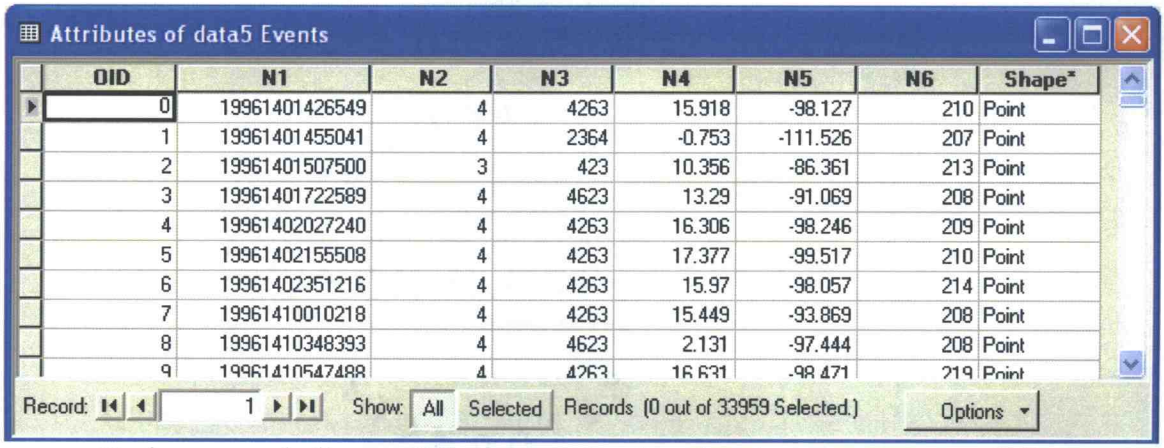

Attributes of data5 Events

OID	N1	N2	N3	N4	N5	N6	Shape*
0	19961401426549	4	4263	15.918	-98.127	210	Point
1	19961401455041	4	2364	-0.753	-111.526	207	Point
2	19961401507500	3	423	10.356	-86.361	213	Point
3	19961401722589	4	4623	13.29	-91.069	208	Point
4	19961402027240	4	4263	16.306	-98.246	209	Point
5	19961402155508	4	4263	17.377	-99.517	210	Point
6	19961402351216	4	4263	15.97	-98.057	214	Point
7	19961410010218	4	4263	15.449	-93.869	208	Point
8	19961410348393	4	4623	2.131	-97.444	208	Point
9	19961410547488	4	4263	16.631	-98.471	219	Point

Record: 1 Show: All Selected Records (0 out of 33959 Selected.) Options

Each row symbolizes a different event and each column represents a different field. "OID" or "Object Identification Number" gives a unique value for each earthquake. You can read in the lower part of the table that there are 33959 events in this table. Let's first change the name of the column to make the table more user-friendly.

To do this, again right click on the data layer, and this time select "Properties". There are several different tabs, select the one called "Fields".
The fields described are the same as in the attribute table. By underlining a field and adding a name in "Alias", the name will automatically change next time you open the attribute table. The column type indicate what kind of data is stored; "length" tells you how many digits the field can hold.

The "Layer Properties" contains information about the layer. This function is useful for many operations, therefore I suggest you explore the other tabs as well.

Earthquake data is recorded in sound pressure in decibels. It is possible to convert acoustic energy in body waves indicating the magnitude of the earthquakes by rearranging the formula developed by Fox et al (2001) for the eastern tropical Pacific:

$$SL = 7.84\ (Mb) + 195.83$$

where SL is the earthquake sound pressure in decibels and Mb is the value in body waves.

To do this, add a new field in the attribute table by clicking on "Options" and then "Add field". Choose an appropriate name such as "Magnitude" and change the "Type" into "Float". In the Field Properties box, choose a value of 9 for both the Precision and the Scale options. Click OK.

This will create a new column with 0 values in the attribute table.

To calculate the new values for magnitude, right click on the new column, and then select "Calculate Values". In the field calculator box, write the formula as given by Fox et al. (2001) in the empty box underneath "Magnitude =". Remember that "N6" is equal to the sounds level values given in decibel.

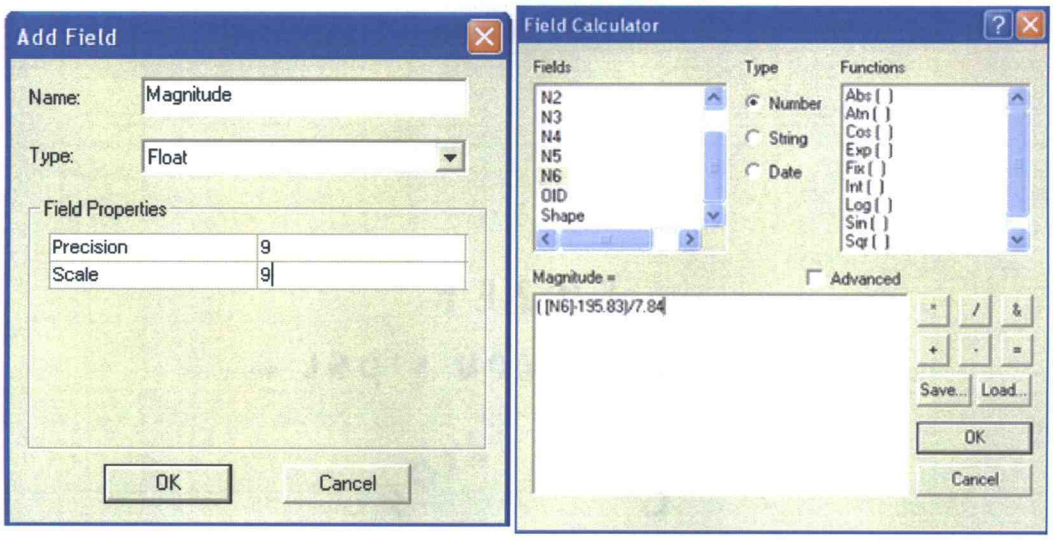

2.4 THE HISTOGRAMS

Statistically, GIS is able to produce a histogram for any of the subsets for any field present in the attribute table. The figure below is an example of a histogram created for the Siqueros transform fault to explore the range of earthquake magnitude. Information given includes the number of earthquakes in the particular dataset (1479), the smaller earthquake recorded (magnitude 0.7), the maximum earthquake recorded (magnitude 6.3), the mean and median seismicity (magnitude 2.3), the standard deviation (0.9), and the skewness and kurtosis of the histogram (1 and 3.9). By underlining the column containing information about earthquakes with the higher magnitude (from 5.7 to 6.2), it is possible to see simultaneously on the map where these earthquakes happened. This consists of a first description of the seismic structure of the fault. Now let's see how to do it.

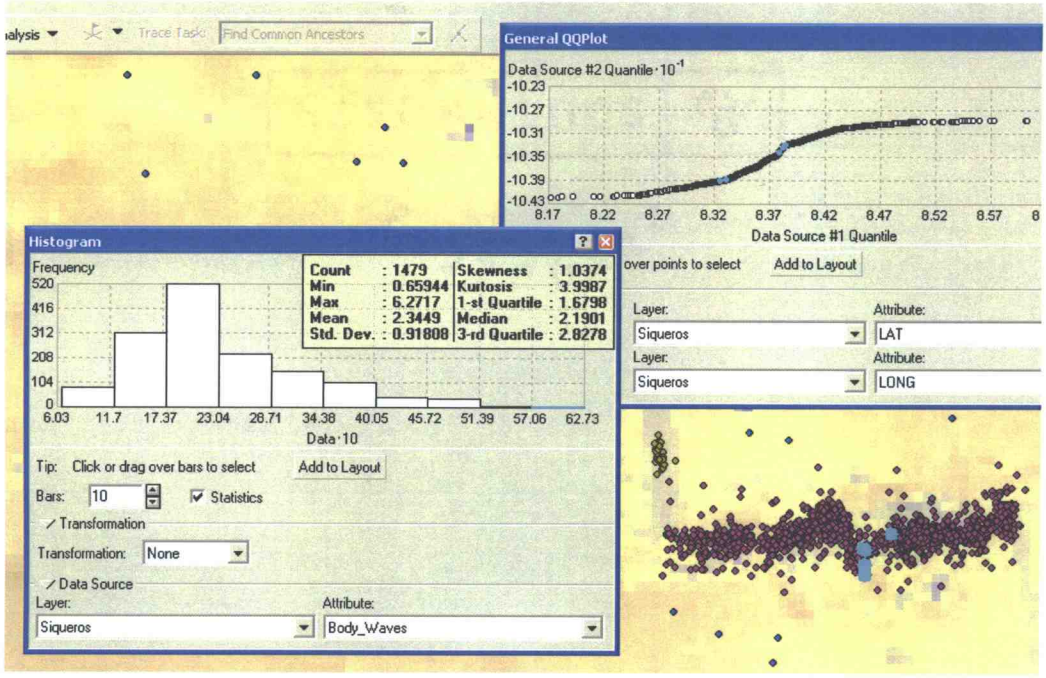

Creating and interpreting histograms

A histogram is bar graph that shows frequency data, sorting the data into categories. A histogram is used to graphically summarize and display the distribution of a process data set.

To create a histogram in ArcMap, go to the geostatistical analyst, and then explore data and then histogram.

Each bar of the histogram represents a category, in the case of figure 1, each bar describes how many earthquakes happened in Siqueros fault (layer used), for every 0.5 degrees of latitude (attribute used) (see the histogram figure).

By checking the "Statistics" box in the histograms, information regarding the count (how many earthquakes are present in this layer), the minimum and the maximum

values for the magnitude, the mean, the standard deviation, and the Skewness, Kurtosis, Median and 1st and 3rd quartile were appear the display box.

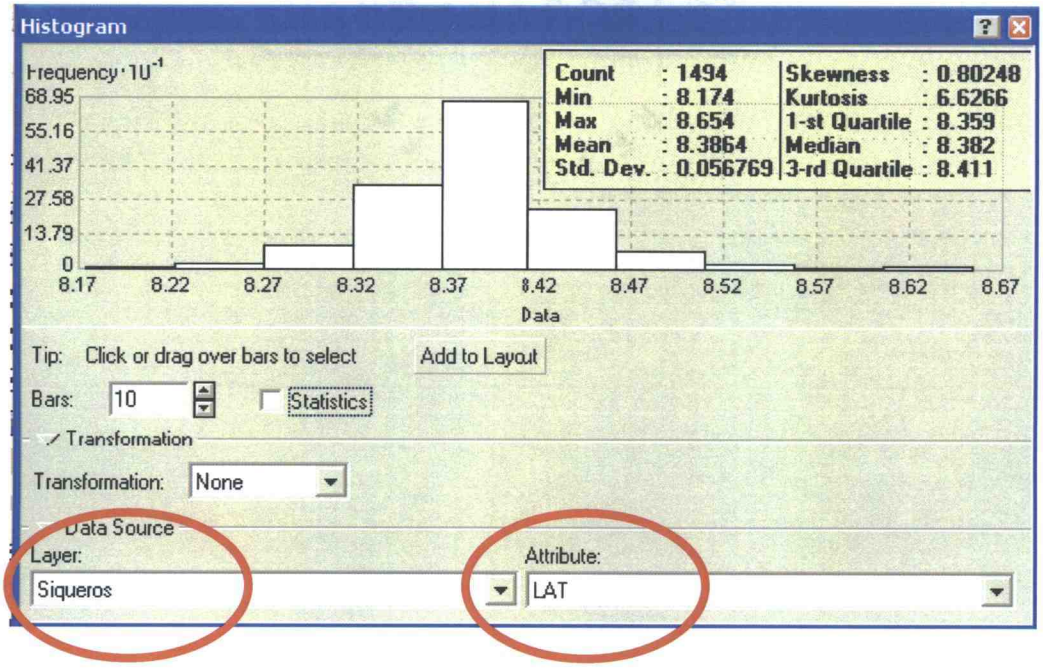

It is possible to create new histograms from different layers by selecting another fault in the "Data Source", "Layer" scroll down menu. All layers currently downloaded in the ArcMap will appear.

Similarly, it is possible to obtain histograms from any field in the attribute, just by selected the field wanted from the "Attribute" scroll down menu. All layers currently downloaded in the ArcMap will appear.

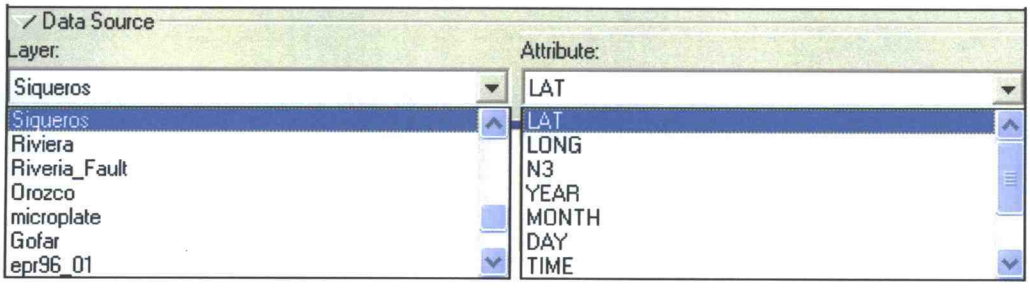

It is also possible to change the number of columns in the histograms by clicking in the up and down arrows next to "Bars" (red cicle in the histogram figure beneath): notice that the shape of the histograms slightly changed while the statistical values remained the same. Another function of the histogram allows the use of logarithmic and box-cox transformations of the attribute data (for more information, use the GIS desktop help).

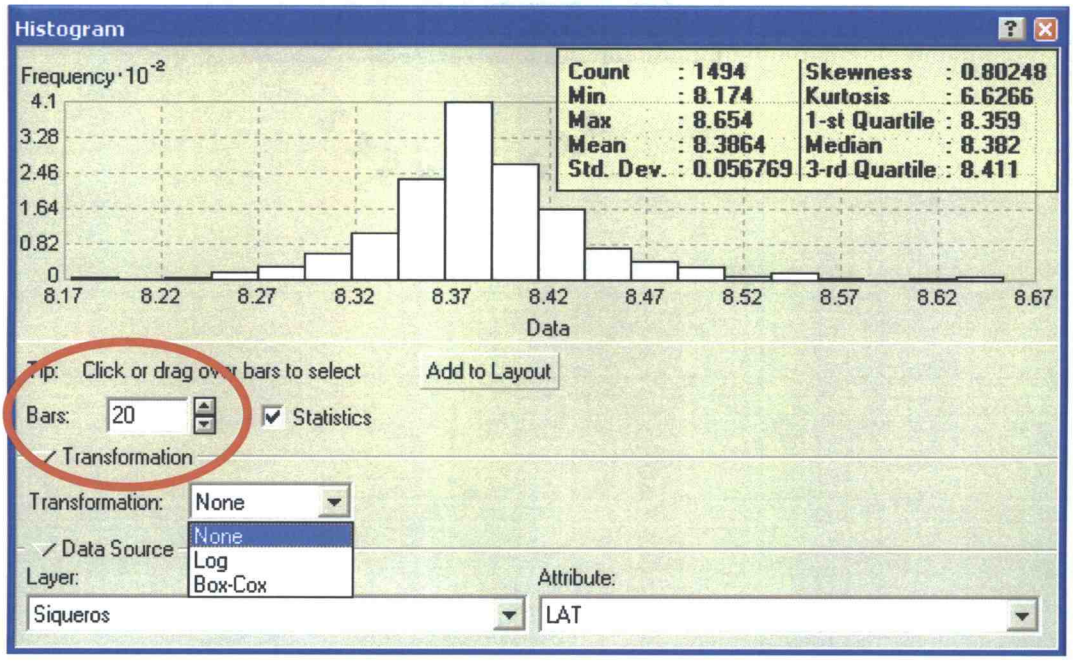

The function "Add to Layout" will add the graph to the layout view in order to create a map containing histograms. By right clicking on the histogram in the map, a set of operations to change the appearance of the graph will appear.

The main advantage of the histograms created in ArcMap is that the data are still connected to the attribute table and therefore it is possible to do statistical analysis, make changes and to see the results directly on the map. In fact, by selecting one or more columns, the underlined points in the histograms would also be underlined in the map.

For example, I want to see on the subduction zone where earthquakes of magnitude 6.03 and greater happen. I will first have to underline the last two columns in my 10 bars histograms, and then I will be able to see the results also on the map in ArcMap. If I want to investigate in what year these events occurred, a new histogram keeping the previously selected attributes will appear when I change the attribute in the histogram window from "magnitude" to "year" (see figure beneath).

The results show that earthquakes with larger magnitude occur throughout the subduction zone without preference for a specific zone and throughout the six years the dataset includes.

To clear the selection, just click in any empty space outside the columns.

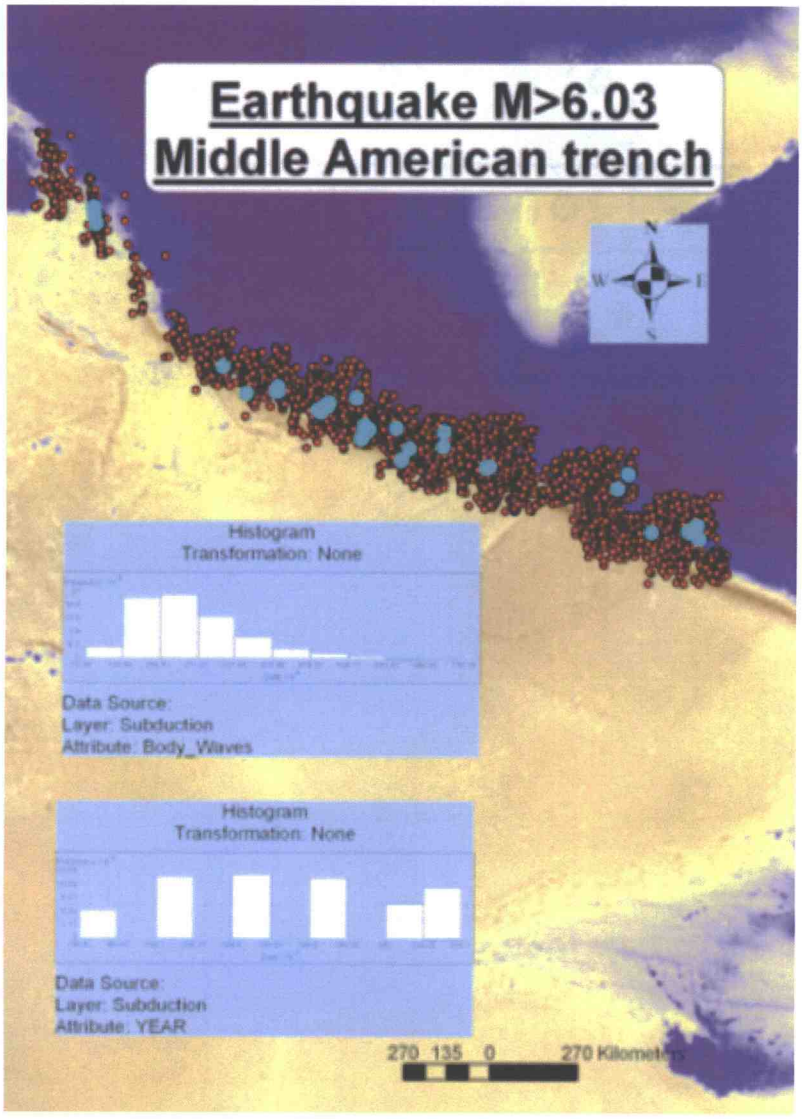
Earthquake M>6.03
Middle American trench
N
W
E
S
Histogram
Transformation: None
Data Source:
Layer: Subduction
Attribute: Body_Waves
Histogram
Transformation: None
Data Source:
Layer: Subduction
Attribute: YEAR
270 135 0 270 Kilometers

2.5 GEOSTATISTICAL ANALYST

The geostatistical analyst is also able to calculate normal and general quantile-quantile (QQ) plots. This is a graphical technique for determining if two data sets come from populations with a common distribution. A 45-degree reference line is also plotted and if the two sets come from a population with the same distribution, the points should fall approximately along this reference line. The greater the departure from this reference line, the greater the evidence for the conclusion that the two data sets have come from populations with different distributions. To create a Normal QQPlot, click on "Geostatistical Analyst", then "Explore Data", and then "Normal QQPlot".

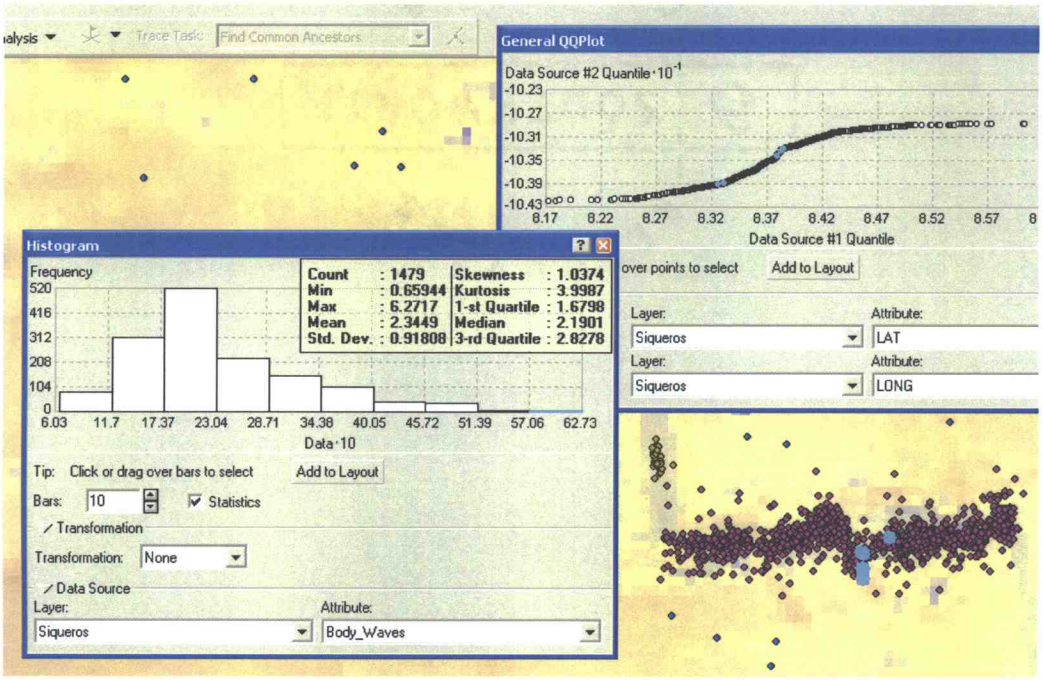

The figure beneath represents other examples of QQ plots in which the magnitude of events for Discovery and Clipperton, and for Discovery and Quebrada transform faults were compared to each other. As the graphs show, Discovery is more related to Quebrada than it is to Clipperton. In a normal QQ plot, the straight line represents what our data would look like if it were perfectly normally distributed: the closer the squares are to the line, the more normally distributed our data looks.

A semivariogram, a covariance, or a cross-covariance cloud depict all possible pairs of points for a range of lag distances. Therefore, it is useful to find data points that may represent an error, as it is shown in the figure for the Clipperton fault. By underlining those values furthest from the average, the correspondent points on the map are

highlighted; then by looking at the histogram, it is possible to see what magnitude they were and how they may have affected your dataset. It is now possible to proceed to manual elimination of the irrelevant data. Datasets with hundreds or thousands of samples should be restricted to smaller domains, to avoid overcrowding the variogram/covariance cloud diagram (GIS default set at 300 points).